THE MAGNETIZATION AND SUSCEPTIBILITY OF CuAu(Fe)

by

JAMES B. HADDAD

A dissertation submitted to the Graduate Faculty in Physics in partial fulfillment of the requirements for the degree of Doctor of Philosophy, The City University of New York.

1974

This manuscript has been read and accepted for the Graduate Faculty in Physics in satisfaction of the dissertation requirement for the degree of Doctor of Philosophy.

5/8/74
date

Myriam P. Sarachik
Chairman of Examining Committee

5/8/74
date

Marvin H. Millman
Executive Officer

Professor Arthur Paskin

Professor Joel Gersten

Professor Frederick W. Smith

Professor Samuel Williamson

The City University of New York

ACKNOWLEDGEMENTS

The author would like to acknowledge the efforts of his mentor Professor Myriam P. Sarachik. Her guidance, assistance, discussion, and enthusiastic support were most valuable and were greatly appreciated.

Further, the author wishes to acknowledge many valuable discussions with Dr. Frederick W. Smith.

Dr. Gordon Knapp was most helpful in assisting with the design of the apparatus. The entire staff of the City College machine shop assisted in the construction of the equipment. Especial thanks go to Mr. Jack Giampietro who did most of the machine work and actual construction.

The author would like to thank Dr. Randy Caton, Mr. Jerold Touger, and Mr. Jing-cheng Liu, for their assistance in making samples and for helpful discussions. Mr. Randy Fenstermacher very kindly assisted in the programming of the PDP-8 and in performing the least squares fits.

TABLE OF CONTENTS

I. INTRODUCTION

When small amounts of 3d transition metals are dissolved in some metallic hosts, the excess susceptibility due to the impurity exhibits Curie law behavior at high temperatures. This strongly temperature-dependent susceptibility is attributed to the presence of a local moment on the impurity atom. The formation of a moment depends on both solute and solvent, for instance, Fe has a magnetic moment in Cu or Au, while Fe in Al does not. [1] A classic example is that of Fe dissolved in Mo-Nb host alloys. As Nb is added to the Mo(Fe) system, the magnetic moment on the Fe appears to decrease continuously until there is no moment in host alloys with more than 60 atomic % Nb. [2] The theoretical work of Friedel [3] and Anderson [4] provides a qualitative understanding of this behavior. In fact, the theory has successfully predicted which of the 3d metals will form local moments in various simple metal hosts. [3]

The formation of a local moment is associated with strong changes in many other physical properties of the alloy. For instance, there is a peak in the excess specific heat, a peak in the thermo-electric power, and a minimum in the electrical resistance. [1] The minimum in the electrical resistance is of particular historical importance. The source of the resistance minimum had been a problem of

long standing until Kondo [5] treated the scattering of the host conduction electrons by the spin localized on the impurity site using the second Born approximation. This calculation successfully explained the source of the resistance minimum, but raised a new problem. There is a temperature (the Kondo temperature, T_K) below which calculations using perturbation theory diverge.[1] Various techniques have been applied to investigate the low temperature behavior of the Anderson and Kondo models. Early treatments of the problem associated the divergence with the formation of a nonmagnetic ground state in which the conduction electrons of the host material form an electron cloud in the vicinity of the impurity atom.[6] This electron cloud has a net spin polarization anti-parallel to the impurity spin and thus tends to reduce the effective local moment. More recent treatments indicate that the ground state is nonmagnetic, but dispense with the idea of the spin compensated state.[7] (There is still experimental interest in the search for conclusive proof of the existence or nonexistence of the spin polarized electron cloud.)[8]

The properties of these alloys have been the subject of a great deal of theoretical and experimental work. The main body of theoretical work has dealt with the single impurity

problem and neglects interactions between impurities. The comparison of theory and experiment is complicated by the possible presence of impurity-impurity interaction effects. For instance, many experimental results on the CuFe system were used as evidence for the formation of the "quasi-bound" state. [9-16] But the situation has been confused by recent susceptibility measurements, which indicate that interactions between impurities are important in CuFe even for concentrations as low as several ppm. [17]

The theories cited so far ascribe the continuous decrease of the magnetic moment of Fe atoms in the Mo Nb systems to a continuous change of the spin and moment of all the Fe atoms as the host composition is varied.

An alternative description of the MoNb (Fe) system was proposed by Jaccarino and Walker [18]. They pointed out that the variation of the magnetic moment can also be explained by assuming that Fe atoms with two or more Nb near neighbors are nonmagnetic and those with fewer than two Nb near neighbors have full magnetic moments characteristic of the Mo (Fe) system. The apparent decrease in the magnetic moment as the Nb content of the host is increased is thus due to a decrease in the number of Fe atoms which are fully magnetic. This model adequately describes the results of experiments on several other ternary alloy systems.

In particular, experimental support for this point of view has been obtained for MoNb (Co) alloys. [19, 20]

On the other hand, measurements of the resistance, [21] specific heat, [22] and magnetoresistance [23] of Fe impurities dissolved in CuAu hosts show behavior which is consistent with the continuous model, rather than the localized Jaccarino-Walker point of view. These results indicate that there are no differences in the behavior of Fe atoms in a CuAu host due to local variations in the CuAu composition. A further important conclusion of these experiments is that the Kondo temperature decreases rapidly as Au is added to the CuFe system.

We present here the results of magnetization and susceptibility measurements of Fe in several CuAu hosts and in pure Au. Since this type of measurement is more sensitive to local environment effects than measurements of the specific heat and resistivity, we can provide more convincing evidence for the validity of the continuous model for this system. More importantly, we have observed the effect of varying T_K from near 15 K to about 1 K on susceptibility measurements in the temperature range 1.5 to 120 K. There is no agreement on the theoretically predicted form for the susceptibility near T_K and this study

will indicate the experimental behavior. In addition, we have observed the effects of addition of Au to the CuFe system on the pairs of ferromagnetically-coupled Fe atoms, which have been observed in CuFe. [17]

Before presenting the results, their analyses and interpretation, a more extensive introduction will be presented for those not familiar with the single impurity problem. Section II, which reviews the theory, contains a qualitative discussion of local moment formation and the resistance minimum. Since there are several good reviews[1, 6, 24-26] of this problem, our discussion will be brief. Several formulas for the susceptibility in the range of temperature from slightly below T_K to high temperatures will be presented, since comparisons between our data and these formulas will be made. A brief discussion of methods used in the two-impurity problem will then be presented.

Section III will review some previous experimental results for Fe in Cu and in Au, as well as for Fe in CuAu host alloys. The main purpose of this section is to contrast the behavior of Fe in CuAu with its behavior in other systems which fit the Jaccarino-Walker model.

The results and analysis of our measurements will be presented in Section IV. Later sections describe the

construction and operation of the apparatus built to perform these measurements, and further experimental details.

II. THEORY

A) The dilute impurity problem - a brief historical review

There are several good reviews of the magnetic impurity problem, [1, 6, 24-26] so this section will be limited to a brief historical outline of the main developments of the theory. A useful idea in the understanding of local moment formation is the concept of the virtual bound state. Following a qualitative discussion of local moment formation, the work of Kondo on the resistance minimum problem will be mentioned, and the path taken by more sophisticated approaches to the problem will be indicated. There is general agreement on the behavior of the magnetic susceptibility for temperatures slightly below T_K to very high temperatures. These formulas will be presented in this section and later will be used in discussion of our data. Recent progress on the low temperature behavior of the impurity - conduction electron system will be mentioned, followed by a discussion of attempts to treat interactions between impurities.

It is possible to get a qualitative understanding of local moment formation using the concept of the "virtual bound state".

Friedel [3] treats the impurity in a metal as a spherical potential which scatters the conduction electrons. Since the impurity charge must be screened, the screening charge has to be equal to the excess charge on the impurity. This

leads to a condition on the phase shifts which can be used to check the correctness of the potential assumed for the impurity. The Friedel sum rule is $Z = \frac{1}{\pi} \sum_{\sigma} \sum_{l} (2l+1) \eta_{l\sigma}(E_F)$, where Z is the excess charge of the impurity, (2l + 1) is the degeneracy of the angular momentum state l, and $\eta_{l\sigma}(E_F)$ is the phase shift evaluated at the Fermi energy.

The d-levels associated with the transition metal impurity have an energy which falls within the conduction band of the host. This leads to resonance behavior in the l = 2 phase shift. The physical interpretation is that in the free atom the potential is deep enough to bind the d-states, but in the host the screened potential is no longer deep enough to bind these states. The d-state is pushed into the continuum where it interacts strongly with the continuum states and is broadened. Although the d-state is no longer bound, it is useful to think of a virtual bound state with some width Δ, and energy E_o, which is localized near the impurity site.

In some cases, the impurity has a magnetic moment. This corresponds to the virtual bound state being split into separate states for spin up and spin down, which are not equally occupied. From data on atomic spectra, Friedel was able to estimate the energy involved in the splitting,

compare it with expected values of Δ , and successfully account for the existence of a magnetic moment for several transition metals in several simple hosts.

P.W. Anderson [4] did a self-consistent Hartree-Fock calculation to investigate the conditions necessary for the presence or absence of localized moments on solute ions. His Hamiltonian can be written as $H = H_{of} + H_{od} + H_{corr} + H_{sd}$. H_{of} is the unperturbed energy of the free electrons, $H_{of} = \sum_{k,\sigma} \epsilon_k n_{k\sigma}$, $n_{k\sigma} = C^*_{k\sigma} C_{k\sigma}$, where $n_{k\sigma}$ is the number operator for electrons of momentum k and spin σ , and $C^*_{k\sigma}$ and $C_{k\sigma}$ are the creation and destruction operators for the corresponding states. H_{od} is the unperturbed energy of the impurity d states, $H_{od} = E(n_{d+} + n_{d-})$. $H_{corr} = U\, n_{d\uparrow}\, n_{d\downarrow}$ is the repulsive energy among the d functions. The last term, $H_{sd} = \sum_{k,\sigma} V_{dk} \left(C^*_{k\sigma} C_{d\sigma} + C^*_{d\sigma} C_{k\sigma}\right)$, is the s-d interaction term, which represents the interaction between the localized state and the conduction electron states.

Anderson solved this Hamiltonian in the Hartree-Fock approximation and found a sharp transition between the magnetic state and the nonmagnetic state, depending on the density of states of free electrons, V_{dk}, and V. In the Hartree-Fock approximation the d-states are broadened and shifted in energy. The width of the virtual state, Δ ,

depends on the s-d interaction and the density of free electron states, $\Delta = \pi \langle V^2 \rangle_{av.} \rho(\epsilon)$. The states are centered about the energies $E_\sigma = E + U\langle n_{d,-\sigma} \rangle$.

Integration of the density of states leads to a pair of formulas for the occupation of the virtual states, in which the spin down and spin up occupation are coupled. Anderson uses this pair of equations to derive a condition for the formation of a local moment.

A more physical picture of the criterion for magnetism is given by Van den Berg [27], who credits Stoner [28], with the first application of the idea. Starting with virtual bound states for each spin equally occupied, a small splitting, ΔE, of the up and down spin states, leads to a magnetic moment by transferring δn electrons from one spin state to the other. The gain in kinetic energy will be $\delta n \Delta E$. The change in potential energy will be

$$\Delta U\langle n_\uparrow \rangle\langle n_\downarrow \rangle = U\langle n + \delta n \rangle\langle n - \delta n \rangle - U\langle n \rangle^2 = -U(\delta n)^2$$

If the energy is lowered by the splitting, the moment formed will be stable. The change in energy is ΔK.E. + ΔP.E. or $\delta n [\Delta E - U \delta n]$. Since $\delta n = \rho(\epsilon) \Delta E$, the change in energy is $\Delta E(1 - U\rho)$. The maximum value for ρ is $1/\pi\Delta$, and the condition for magnetism is $U\rho > 1$ or $\frac{U}{\pi\Delta} > 1$.

Although the calculations give a qualitative understanding of the formation of a local moment, further work was needed since the Hartree-Fock approximation breaks down in the region $U/\pi\Delta > 1$. As Schrieffer [29] points out, in this $U/\pi\Delta > 1$ "the interaction time $\tau_U = \frac{\hbar}{U}$ is less than the time, $\tau_\Delta = \frac{\hbar}{\Delta}$ required for electrons to hop on or off the impurity into the band." Hartree-Fock theory fails because an electron on the impurity interacts with the electrons nearby at that instant, and does not see an average potential through interaction with all the electrons, as assumed by Hartree-Fock. It is a true many-body problem because previous electron-impurity encounters affect what the conduction electron sees. Thus the Hartree-Fock theory applies only in the nonmagnetic limit $U < \Delta$, and the conditions found by Anderson are modified when further correlations are included in the calculations.

A concurrent approach to the problem was, as Kondo did, to assume the existence of a local moment, $\vec{S}$, and to calculate its effect on the physical properties via the exchange Hamiltonian $J\vec{S}.\vec{s}$, where J is the exchange integral, $\vec{S}$ is the spin of the electrons localized on the impurity site, and $\vec{s}$ is the spin of a conduction electron.

Several authors have attempted to show a correspondence between this form and the Anderson Hamiltonian. Kondo [30] treated spin-flip scattering of the conduction electrons using the Anderson Hamiltonian in second order, assuming the localized state to be singly occupied. The matrix

elements found for this scattering correspond to the matrix elements found for spin-flip scattering, when the Hamiltonian $J\,\vec{S}.\vec{s}$ is used and if $\frac{J}{2N} = -\frac{|V|^2 U}{(U+E)(-E)}$. If there is a local moment $E < 0$ and $(U + E) > 0$, so that J is negative. Schrieffer and Wolff [31] obtained a similar result by applying a canonical transformation to the Anderson Hamiltonian. More recently Schotte [32] has compared the free energies calculated for the two models. His results for J are 1/2 the values found by Schrieffer and Wolff and in general there are additional terms in the quantities under comparison, which "indicate that the Kondo and the Anderson models are not that intimately connected."[32]

Experimentally, it had been observed that in those alloys where the impurity has a well-defined magnetic moment, there is a minimum in the resistance as a function of temperature. [33] An explanation for this behavior was obtained by Kondo [5] when he calculated the conduction electron scattering probability using the s-d Hamiltonian ($J\vec{S}.\vec{s}$) in the second Born approximation. (The scattering in the first Born approximation does not lead to a temperature dependent resistivity.) Kondo found that there was a term in the impurity resistivity which varies as lnT. Similar terms were subsequently found in perturbation theory calculations of other physical properties, such as spin relaxation time, susceptibility, and free energy. [25]

Application of more sophisticated techniques such as many body perturbation theory [34], double time Green's functions,[35] or dispersion theory, [36, 37] suggests that the divergence in perturbation theory is associated with the formation of a "non-magnetic" ground state. This state forms below a characteristic temperature $T_K \cong T_F e^{-N/|J|\rho(0)}$, where T_F is the Fermi temperature and $\rho(0)$ is the density of states at the Fermi energy. This "Kondo" or so-called spin-compensated state is characterized by a spin polarization of the conduction electrons near the impurity, which opposes the impurity spin. At T = 0 it is expected, according to this view, that the impurity moment is completely canceled by the spin polarization cloud.

More recent work has shown an equivalence between the ground state of the Kondo problem and the thermodynamics of a one-dimensional classical Coulomb gas. [38, 39] A similar equivalence to the one-dimensional Coulomb gas has also been shown for the Anderson model. [32, 40] Anderson et al. [41] developed a scaling theory comparing the resonant level model (Anderson model with U and E_o = 0) with the antiferromagnetic s-d model. The solutions of the s-d model are qualitatively the same as the solutions of the resonant level model, which is soluble. [42] Although there are only a few calculations of physical properties using these

techniques, Anderson et al. [41] find that the ground state does behave like a true bound singlet, as originally conjectured by Nagaoka. [35]

B) Single Impurity Susceptibility

The most commonly used expression for the impurity susceptibility above T_K is (1) $\chi = \frac{C}{T}\left[1 - \frac{1}{\ln(T/T_K)}\right]$, [43,44]

where C includes the usual factors in the Curie constant. Since this expression isderived using perturbation theory, it is not expected to be valid near or below T_K and in fact gives unphysical results for $T/T_K < 10$. In the range of T/T_K between 7 and 100 this expression is closely approximated by a Curie-Weiss law with $\Theta = 4.5\ T_K$.

More recent calculations in the temperature range from slightly below T_K to higher temperatures lead to (2)

$$\chi = \frac{S(S+1)}{3kT}(\mu_B g)^2 c N\left\{1 - \frac{1}{(S+\frac{1}{2})}\left[\frac{1}{2} - \frac{1}{\pi}\operatorname{arc\,tg}\left(\frac{\ln \frac{T}{T_K}}{\pi(S+\frac{1}{2})}\right)\right]\right\}.$$

This expression was derived by C.S. Ting, [45] who used a Green's function diagrammatic approach introduced by Abrikosov [34] to examine the graphs which generate the free energy in Suhl's theory [36, 37], and by Brenig et al. [46] who used the "heavy impurity model". [47] These calculations are expected to be valid in the vicinity of T_K as well as at higher

temperatures. The leading terms of this expression are in agreement with expression 1.

Theoretical predictions of the behavior of the susceptibility below T_K have differed widely in the past. At low temperatures the inverse susceptibility calculated for the resonant level model [42] behaves as $\chi_{RL}^{-1} \approx a + bT^2$, and according to the scaling theory, the susceptibility of the s-d model should have the same qualitative behavior. [41, 42] The calculations of Schotte and Schotte [42] show that the static magnetic spin susceptibility is finite at T =0 (a point which has been debated at length) and exhibits Curie-Weiss like behavior for high temperatures, with a Neél point of about 1/3 T_K.

Götze and Schlottman [48] calculated the susceptibility near the Kondo temperature and compared their results with the numerical calculations of Schotte and Schotte [42] and formula 2. From well below T_K to 6 T_K, the range of the graph they show, their results are in agreement with the calculations of Schotte and Schotte, but differ significantly from formula 2. Another comparison between formula 2 and the low temperature results is made in an article by Anderson and Yuval. [49] They also indicate that formula 2 does not agree with the low temperature calculations in the vicinity of T_K.

It is generally acknowledged that over limited ranges of temperature the susceptibility is described by a Curie-

Weiss law, [6, 49] with the Curie constant and Θ dependent on the range of T/T_K. The value of Θ is usually taken as a measure of T_K. The calculations mentioned above agree with this conclusion, although there are some problems. If in the vicinity of T_K, χ follows a Curie-Weiss law with $\Theta \approx 1/3\ T_K$, measurements on CuFe, which indicate that $\Theta \approx 30$ K, would show that T_K is near 90 K. This is much higher than the commonly accepted values. Another problem is that formula 2, which is expected to be valid from slightly below T_K to higher temperatures, (this is the temperature range of our data) does not agree with the low temperature calculations which are expected to be valid. Thus, there is no firm theoretical relationship between Θ and T_K.

C) Interactions

It has become increasingly clear that many experimental results which were obtained in the 1960's, and which were ascribed to the behavior of single impurities, were in fact complicated by the presence of impurity-impurity interactions. A major thrust of recent research activity and interest is to study these interaction effects and how they modify the single impurity behavior.

Several methods have been used to investigate the effect of interactions between impurities. The first method to be discussed involves the generalization of the Anderson Hamiltonian to the case of more than one impurity. To illustrate

the parameters introduced in such a generalization, the Hamiltonian used by Alexander and Anderson [50] will be discussed. They treated the case of two similar impurities in a simple host. The Hamiltonian can be separated into 3 terms. The first is just the single impurity Hamiltonian generalized to the case of two impurities without considering any interaction. $H_1 = H_f + E_o \sum_\sigma (n_1^\sigma + n_2^\sigma) + U(n_1^\uparrow n_1^\downarrow + n_2^\uparrow n_2^\downarrow)$, where E_0 is the self-energy of the localized states in the absence of interactions and U is the Coulomb repulsion between two electrons in a localized state. The second term describes an interaction between the impurities through direct transfer of charge between the two impurities. $H_2 = \sum_\sigma \left(V_{12} C_1^{\sigma *} C_2^\sigma + V_{21} C_2^{\sigma *} C_1^\sigma \right)$, where c_i and c_i^* are, respectively, the annihilation and creation operators for a d electron at site i with spin σ, and V_{12} is the transfer integral between the two d states. The dependence on the spatial separation of the impurities is contained in V_{12} and the direct interaction is expected to be of short range. The third term in the Hamiltonian is the interaction of each impurity with the conduction electrons, $H_3 = \sum_{ik,\sigma} \left(V_{ki} C_k^{\sigma *} C_i^\sigma + V_{ik} C_i^{\sigma *} C_k^\sigma \right)$. This is the same interaction as discussed for the single impurity, but now that there are two impurities there is an indirect interaction between the impurities through the conduction

electrons. The spatial separation of the impurities enters through the phase relationship between the V_{ik}, ie. $V_{1k} = e^{i\vec{k}\cdot\vec{r}} V_{2k}$.

Several authors have treated generalizations of this Hamiltonian (References 50 through 53 are not a complete listing.) These authors use the Hartree-Fock approximation to solve the Hamiltonian. There is agreement that the direct interaction is antiferromagnetic for atoms with half-filled d-shells. This has been put forth as the qualitative explanation for the antiferromagnetism of Cr and Mn as opposed to the ferromagnetism of Fe, Co and Ni.[53] Kim [51] has generalized the above theory to the case of many impurities, which are not necessarily the same. One of the problems he investigated is the modification of the condition for magnetism caused by the local environment. These results are of limited usefulness, however, since they do not provide expressions for physical properties which can be used for comparison with experiment.

Another approach is to consider the coupling of the impurities through the RKKY interaction. [54,55] A magnetic impurity interacting with the conduction electrons through the s-d Hamiltonian, $H = J \vec{S}.\vec{s}$, causes a spin polarization of the conduction electrons. Another impurity will be influenced by the spin polarization of the conduction electron, resulting in an indirect interaction between the

two impurities. The form of this interaction is calculated in the lowest order of perturbation theory to be

$$6\pi z J^2 \left[\frac{\cos 2k_F R}{(2k_F R)^3} - \frac{\sin 2k_F R}{(2k_F R)^4} \right] \vec{S}_1 \cdot \vec{S}_2 .$$

For large separations the interaction is oscillatory and falls off as R^{-3}, and is therefore not expected to lead to long-range order. [24] One approach to the problem is to assume that the impurities are randomly distributed and that the effect of the other impurities can be treated as an effective field. The effective field is described by a distribution function $p(H,T)$ which gives the probability of an impurity experiencing a given field. If the function p (H, T) is known, properties of the system can be calculated by taking suitable averages. Several calculations of this type have been performed. All of these, however, make the approximation of replacing $\vec{S}_1 \cdot \vec{S}_2$ with $S_{1z} S_{2z}$. [56, 57, 58]

There is a more general treatment based on dimensional considerations, which was suggested by Blandin. The discussion presented here is from Souletie and Tournier. [59] The same spatial distribution of impurities which represents an alloy of concentration c can be used to represent an alloy of concentration c', by imagining the unit of distance changed from r to r', where $cr^3 = c'r'^3$ follows since the total number of impurities is unchanged. Since the RKKY interaction and the effective field, H_i, vary as R^{-3} for large values of R, H_i/c will vary as $(CR^3)^{-1}$ and be independent of concentration. The magnetic moment which appears in the effective field is a

function of H/T, where H includes the external field. The moment can also be rewritten as a function of (H/c)/(T/c). Since $P(H,T) = \frac{dN}{dH} = \frac{dN}{d(H/c)} \times \frac{1}{c}$, these considerations show that $cp\ (H, T) = f\ (\frac{H}{c}, \frac{T}{c})$, where p(H, T) is the field distribution function introduced above.

There are some immediate results from these arguments. At low temperature and fields, the field-distribution function is inversely proportional to concentration. The specific heat (if a linear function of T) and the susceptibility due to RKKY effects at low temperatures should then be independent of concentration, and the ratio of the two depends only on the impurity spin. The experimental results at all temperatures where the RKKY interaction is dominant should obey scaling laws. For instance, the susceptibility plotted as a function of T/c should be independent of concentration. There is a maximum in the susceptibility as a function of temperature and the scaling theory predicts that in agreement with experimental observation, the temperature of the maximum should be proportional to concentration. In order to actually calculate the temperature dependence of the physical properties using this theory, or even to predict broad features such as the maximum in the susceptibility, it is necessary to determine p(H,T).

Since our measurements were made on dilute samples, we expect that the dominant effect will be due to single impurities and not to RKKY coupling between the impurities. There have been attempts to study the effects of interactions in this concentration region. Several authors [60] have attempted to extend the methods used in calculations for the single impurity problem to the case where several impurities are present. They found no essential modification of the single impurity effect. Tsay and Klein [61] attribute this to the fact that the RKKY interaction only enters in orders higher than those considered in these calculations. Tsay and Klein try to get around this difficulty by explicitly including an interaction of the RKKY form in their Hamiltonian. Their main result is that there is a change in the Kondo temperature due to the interaction, and thus each impurity has a Kondo temperature depending upon the impurity site. There are at the moment no explicit formulas for the susceptibility which can be compared with experimental results and which include the effects of interactions in this concentration region.

III. EXPERIMENTAL REVIEW

A. Summary

This review will be limited to experiments relevant to an understanding of our CuAu(Fe) data. These include susceptibility measurements on dilute concentrations of Fe in Cu and Au, experiments done on the CuAu(Fe) system, and some discussion of MoNb(Co). The MoNb(Co) system is reviewed because it is typical of alloys which are best treated by the Jaccarino-Walker model. This is in contrast with CuAu(Fe) which does not seem to exhibit effects due to variations in the local near-neighbor environment of the impurity. More detailed reviews of the experimental situation are contained in references 1, 6, 26 and 62.

CuFe is one of the most extensively studied of the dilute magnetic systems. Due to its high T_K (16K) [62], measurements can be easily made for $T \ll T_K$, where the compensation of themagnetic moment is expected to occur. The measured behavior below TK of the magnetization [15], NMR [12-14], magnetoresistance [16], Mössbauer effect,[11] and susceptibility [9, 10] has been interpreted as being due to this spin compensation. Many recent measurements[17, 63] indicate the presence of interactions between Fe impurities, even at very low concentrations, which would complicate the interpretation of these earlier experiments.

The magnetization measurements of Tholence and Tournier [17] have demonstrated the importance of interactions in the CuFe system. They found that even at low concentrations the magnetization and susceptibility were not linear functions of concentration, as one would expect for impurities acting singly. Using values of the concentration found from the high field susceptibility, they separated the magnetization into two contributions, $M = M_1C + M_2C^2$. The term linear in concentration was attributed to single impurities; while the second term was attributed to pairs of ferromagnetically coupled Fe atoms.

Following the work of Tholence and Tournier, several other investigators have separated their magnetization and susceptibility data into two terms. If it is assumed that the alloys are random and that the impurity behavior depends on the number of impurities occupying z sites surrounding a central impurity, the concentration of pairs and single impurities can be calculated as functions of z and the nominal Fe concentration. Using the calculated concentrations, Franz and Sellmyer [63] have separated their CuFe magnetization data into a term due to single impurities and a term due to pairs. In the limit of low concentration their analysis is the same as that used by Tholence and Tournier. Ekström and Myers [64] have used the difference in temperature dependence of the single impurity and pair susceptibilities to achieve

a similar separation. Their susceptibility data were fit by the expression $\chi_{imp} = \chi_o + \frac{C_1}{T+\theta_1} + \frac{C_2}{T+\theta_2}$. The temperature independent term, χ_o , and the first Curie-Weiss term were attributed to the single impurities, while the second Curie-Weiss term was attributed to pairs for which θ was found to be near 1K.

Fe-Fe interactions have also been observed in specific heat,[65] low field magnetoresistance,[66] Mössbauer, [67, 68] and other magnetization [69] measurements on the CuFe system. The Mossbauer results are particularly interesting since they show the same relationship between the pair and single impurity concentrations as the magnetization measurements.

The source of the pairs is not understood. Two possible explanations are: direct coupling between near neighbor Fe atoms, or a longer range indirect coupling through the RKKY interaction. The concentration of pairs is too large to be due to nearest neighbor Fe atoms if the distribution of impurity atoms is random. Thus, if the pairs are due to a short range interaction between near neighbor Fe impurities, there must be metallurgical effects which lead to an excess number of such near neighbor Fe atoms. This possibility is supported by the fact that the concentration of pairs depends sensitively on sample preparation. The concentration of pairs is sensitive to heat treatment, and alloys which have

been cold worked (a process which should randomize the alloy) have a lower concentration of pairs. [63] On the other hand, for a particular method of sample preparation, the concentration of pairs is usually found to be a quadratic function of the impurity concentration. Although this does not rule out metallurgical clustering, it would be easier to explain this behavior in terms of a long range interaction.

Using the different temperature and concentration dependences of the pairs, the single impurity term can be separated from the pair term. For the temperature range 1.4 to 40 K, Tholence and Tournier [17] have found the single impurity susceptibility to fit a Curie-Weiss law. The effective moment is 3.4 μ_B corresponding to a spin S=1.3, and the Weiss temperature, Θ , is 29 K. Ekström and Myers[64] measured χ over a much wider temperature range and found deviations from the Curie-Weiss law at temperatures above 50 K. They fit their data to a temperature independent term and a Curie-Weiss law. Their results for the Curie constant and the Weiss temperature are consistent with those of Tholence and Tournier. The constant term is included to compensate for the deviation from Curie-Weiss behavior and at present has no theoretical justification.

The AuFe system is interesting for a study of interaction effects as well as for a study of single impurity behavior.

Iron is readily soluble in Au, so the system can be studied over a wide range of concentrations. It is found that behavior characteristics of either ferromagnetic or antiferromagnetic interactions can be found as the concentration, temperature, and magnetic field are varied. [70] Past experiments are not sufficient to determine the nature of the interactions or the concentration at which single impurity behavior is dominant. Since T_K is near 0.2 K, [71] it is difficult to investigate behavior below T_K. However, there are several theoretical expressions for the susceptibility and magnetization, which are expected to be valid for T greater than T_K, and it would be interesting to compare data in the single impurity region with these expressions.

Borg and Kitchens [70] have published the results of magnetization measurements of AuFe alloys with Fe concentrations between 500 ppm and 12.5 atomic % and a review of Mössbauer measurements on the same system. As the concentration is varied there is a large variation of the magnetization per impurity. At a field of 33 kG and a temperature of 1.35 K there is a minimum in the magnetization per impurity near 1 atomic %. Using the magnitude of the hyperfine splitting as a measure of the impurity moment indicates that the moment on the impurity is a weak function of concentration. Borg and Kitchens suggest that this behavior indicates that the exchange

coupling between Fe atoms is ferromagnetic for small separations and antiferromagnetic for larger separations. An ordering temperature, T_o, is also deduced from the Mössbauer measurements. The concentration dependence of T_o for concentrations from 100 ppm to near 15 atomic % is described by the formula 11.6 $c^{0.45}$. Cannella et al. [72] find sharp peaks in the low field susceptibility in AuFe samples in the concentration range 1 to 22 atomic %. For concentrations below 13 atomic % the temperatures of the peak are very near T_o as measured from Mössbauer results.

On the other hand, Souletie and Tournier [59] claim that both the specific heat and susceptibility fit the scaling relations characteristic of the RKKY interaction, in the concentration range 1000 ppm to 8 atomic %. There is a maximum in the susceptibility at a temperature T_m which is proportional to the concentration. [73] Well below T_m the specific heat is a linear function of temperature and both the specific heat and the susceptibility are independent of the concentration. This conflicts with the results presented by Borg and Kitchens [70] and Cannella [72] et al. where the concentration dependence of T_o is not linear and is thus not the expected behavior if the RKKY is the dominant interaction.

As the concentration is reduced below 1000 ppm, deviations from the scaling laws are observed. [73] For concentrations below 100 ppm the susceptibility due to the Fe impurities is a linear function of Fe concentration, except for some deviations at temperatures well below 1 K, which have been attributed to pairs of ferromagnetically coupled Fe atoms. The linear concentration dependence of the susceptibility below 100 ppm has been taken as evidence that single impurity behavior dominates in this concentration region and that the deviations from the scaling laws for concentrations below 1000 ppm are due to the increasing importance of single impurities. There is some doubt about this conclusion, since the Mossbauer measurements [70] indicate an ordering temperature near 1 K for 100 ppm of Fe in Au, and it might thus be expected that interactions would be important for concentrations below 100 ppm.

If a wide range of temperatures is considered, the susceptibility is not adequately described by a Curie-Weiss law. Hurd [74] fit his data for samples in the concentration range 6 to 220 ppm to a single Curie-Weiss law over the temperature range from 6 to 300 K. There is no obvious deviation from a linear concentration dependence for the susceptibility. His values of Θ = 10 K and $\mu_{eff} = 3.68\ \mu_B$ differ substantially from the values Θ = 0.5 K and $\mu_{eff} = 3.25\ \mu_B$ found from Curie-Weiss fits of data for concentrations below 100 ppm over the temperature range

0.05 to 5 K. [73] Hurd [75] has also fit his susceptibility data to one of the commonly used expressions for the susceptibility when T is greater than T_K i.e. $\chi = \frac{\mu_e^2}{3kT}\left[1 - \ln\frac{T}{T_K}\right]$. [43,44] The value found for T_K is 1.0 K, which is much larger than the value of 0.1 K found from fitting the low temperature data to this expression. This indicates that this expression will not fit the data over the entire range of temperature. (It should be mentioned that Loram et al. [76] imply that their AuFe results fit the perturbation theory prediction.)

A similar behavior is found for CuFe, [74] where Hurd has found a value for T_K from fits to this expression, which is much lower than the accepted values. Hoeve et al. [77] tried to fit their high temperature CuFe data (300 - 770 K) to this expression and to

$$\chi = \frac{\mu_e^2}{3kT}\left\{1 - \frac{2}{\pi(2S+1)}\left[\frac{\pi}{2} - \operatorname{arc\,tg}\left(\frac{2\ln\frac{T}{T_K}}{\pi(2S+1)}\right)\right]\right\}$$ [45,46]

and find values for the effective moment and T_K which differ from the accepted values.

These results point up the lack of a reliable theoretical prediction of the temperature dependence of the susceptibility over the range of temperature from T_K to higher temperatures As discussed previously, the AuFe results deviated from the perturbation theory result and many analyses of CuFe data

have added a temperature independent term to compensate for deviations from a Curie-Weiss law. Several authors have discussed the possibility that the experimental results are not typical of single impurities, but instead are affected by interactions between impurities [78, 79] or a change in the host susceptibility due to alloying. [64] There is no definite proof that the observed behavior is not due to single impurities and no definite statement can be made without further theoretical and experimental work.

A more detailed review of the magnetization and susceptibility experiments on CuFe and AuFe is presented in sections B and C of this chapter. This summary will be concluded with a discussion of the ternary alloy systems CuAu(Fe) and MoNb(Co).

The Kondo temperature defines the temperature scale for properties of the single impurity problem. If different alloy systems could be completely characterized by specifying a different Kondo temperature T_K for each, then the single impurity properties or parameters should be universal functions of T/T_K. As demonstrated by resistivity[21] and specific heat [22] measurements, Fe in CuAu hosts approximates this behavior. The resistivity measurements lie on the same curve when plotted as functions of T/T_K, and T_K is found

to decrease as the Au content of the host is increased. By using values of T_K which decrease with increasing host Au content, the specific heat measurements can also be fitted to a univeral function of T/T_K. Measurements of the magnetoresistance [23] and the Hall coefficient [80] have also been interpreted in terms of a T_K, which decreases with increasing Au content.

There is a striking contrast between the behavior of CuAu(Fe) and that of MoNb(Co), which is typical of alloys described by the local Jaccarino-Walker model. Susceptibility measurements [20] show that the average magnetic moment decreases continuously as the Nb content of the host is increased, but there is very little change in the temperature dependence of the susceptibility.

In addition, the change in resistivity due to the addition of Co to MoNb hosts with 0, 10 and 20 atomic % Nb shows the characteristic knee associated with the formation of a Kondo state, but there is no appreciable change in the temperature at which the knee occurs [20]. This indicates that the Kondo temperature is unchanged by the addition of Nb to the MoNb host.

The Jaccarino-Walker model [18] explains these results in terms of a decrease in the number of magnetic Co atoms

as the Nb composition is increased. In this model a Co impurity is either magnetic or nonmagnetic depending on the number of Nb near neighbors. As the Nb composition of the host is increased, the number of such non-magnetic Co atoms increases and the average moment decreases. Those Co atoms which are magnetic remain typical of the MoCo system, and the temperature dependence of the resistivity remains the same, although the magnitude varies. This picture is verified by measurements of the Co ^{59} MNR. [19] As Nb is added to the host, a resonance due to nonmagnetic Co atoms appears and the intensity of this nonmagnetic site resonance increases relative to that of the magnetic site.

Susceptibility measurements on the CuAu(Fe) system should shed further light on the role of local environment effects in this system. In the CuAu(Fe) system one would expect extreme local effects to manifest themselves in terms of two different kinds of Fe atoms. However, in contrast to the MoNb(Co) system where the Co atoms are either magnetic (characteristic of MoCo) or nonmagnetic (characteristic of NbCo) the Fe atoms would have two different moments and Kondo temperatures, characteristic of CuFe and AuFe, depending on the detailed near neighbor environment of each Fe atom. Thus, if extreme local effects of this kind play a role, it should be possible to separate the single impurity

susceptibility into a Curie-Weiss term with a Θ typical of AuFe and another such term with a Θ typical of CuFe. The susceptibility measurement of Ekström and Meyers [64] on a CuAu(Fe) alloy with 10 atomic % Au is more consistent with this model than with the continuous model, which characterizes the system in terms of the impurity spin, S, and a Kondo temperature which decreases as the host Au content is increased. On the other hand, our attempts at such a separation have failed to give any reasonable fit. In fact, any admixture of a Curie-Weiss term with a Θ_{AuFe} worsens the fit obtained to the data with a small temperature independent term and a Curie-Weiss term (behavior consistent with the continuous model). We conclude that a local model of this kind is inappropriate for this system, in agreement with similar conclusions drawn from resistivity and specific heat measurements.

B. CuFe

Table I summarizes the results of susceptibility measurements on CuFe, which are discussed in this section.

Hurd [74] performed susceptibility measurements on a series of CuFe alloys with Fe concentrations less than 200 ppm in the temperature range 6-300°K. Using the method of least

squares the impurity susceptibility was fitted to a Curie-Weiss law. He found average values for the Curie temperature and effective moment (32 ± 2^{o}K and 3.68 μ_B). The plots of χ^{-1} as a function of T deviate from the Curie-Weiss law at T less than 10 K and at temperatures above 100^{o} K. The low temperature deviation was first attributed to the formation of a spin compensated state [81], but was later found to be due to spurious effects associated with helium exchange gas. [75] The data was also fitted to an expression for χ above T_K derived by Scalapino [10], and T_K and effective moment were parameters which were determined from the fit. The value of T_K found from these fits, 3.8K, is much smaller than the usually accepted value.

Daybell and Steyert [9, 10] performed susceptibility measurements at temperatures as low as 40 millidegrees. In an early publication [9] the data of a 110 ppm sample was represented as $\chi_{Fe} = \left[\frac{2.52}{T+14} + \frac{.168}{T+.045}\right] \times 10^{-8} \quad \frac{emu}{gm \ ppm \ Fe}$.

Further work indicated an anomalous field effect.[10] For fields above 1 kilogauss, χ was independent of temperature (for $T < 0.2$ K) but at lower fields χ could be fitted to a $T^{-\frac{1}{2}}$ dependence. At the time there was a prediction by Anderson that χ would have the $T^{-\frac{1}{2}}$ behavior, but this term has since been attributed to superparamagnetic clusters of Fe atoms.[1, 14]

From the theoretically predicted value as $T \to 0$ of $\frac{\mu_e^2}{3k T_K}$ and Hurd's value of μ_{eff}, a Kondo temperature of about 15 K can be deduced. [1, 10]

Chaikin and Jensen [82] made measurements in the temperature region between Hurd's measurements and those of Daybell and Steyert. Their measurements showed a gradual change in χ from $C/(T + 32)$ behavior to $C_2/(T + 16)$ as the temperature was decreased.

In all of these papers it was assumed that the Fe concentrations were sufficiently dilute that impurity-impurity interactions could be neglected. Tholence and Tournier [17] performed measurements on a series of CuFe alloys with Fe concentrations from 11-600 ppm and found that the susceptibility and magnetization were not linear functions of concentration. The concentration dependence of the initial susceptibility ($\chi_1 C + \chi_2 C^2$) and the behavior of the high field susceptibility (linear in concentration), indicated that there were at least two types of contributions to the magnetic behavior. Using values of the concentrations found from the high field susceptibility, they separated the magnetization into two contributions, $M = M_1 c + M_2 c^2$. This separation worked for concentrations less than 400 ppm and yielded initial susceptibilities for the two terms which could be fitted

to a Curie-Weiss law ($\Theta_1 = 2.9 \pm 1$ K, $\mu_{1\,eff} = 3.4\ \mu_B$, $\Theta_2 < 5$K) Since M_2 could be saturated, the combination of the Curie constant and the saturation magnetization could be used to calculate the effective moment and the concentration of moments associated with the quadratic term. The spin associated with the second term was nearly double the spin for an Fe impurity in Cu, which suggested that the quadratic term was the result of pairs of ferromagnetically coupled Fe atoms. The concentrations of pairs, $130c^2$ pairs (c in at.fr.) per atom of alloy, is much larger than the concentration of near neighbor Fe atoms expected in a random alloy.

Additional evidence in support of this picture is found in the magnetization measurements (H up to 100 K G) of Franz and Sellmyer.[63] Since the range of concentrations (450 to 6000 ppm Fe) was much wider than that used by Tholence and Tournier, the expressions used in the analysis are more complicated. If a pair is formed when any of z sites in the neighborhood of an Fe atom are occupied by another Fe atom, then the concentration of single impurities is $C(1-C)^z$ and the concentration of pairs is $\frac{1}{2}zC^2\ (1-C)^{z-1}$. Assuming that only pairs and single impurities are present, $M = NC\ (1-C)^z\ M_1 + \frac{1}{2}\ z\ C^2\ N\ (1-C)^{z-1}\ M_2$. The method of analysis was essentially to find M_1, M_2 and z using a computer fit. In the limit of low concentration the analysis

is the same as that used by Tholence and Tournier. Qualitatively the results are similar to those of Tholence and Tournier, but $\frac{1}{2}z$, the concentration of pairs, is less. For annealed samples $\frac{1}{2}z = 65$ while for unannealed samples $\frac{1}{2}z = 85$. Both of these numbers are appreciably less than the 130 found by Tholence and Tournier. Hirschkoff et al.[69] performed low temperature measurements (0.010 - 0.40 K) on 6 concentrations between 102 and 478 ppm in fields between 1 and 200 gauss. The magnetization was a quadratic function of concentration with behavior dependent on whether T was above or below an ordering temperature which depended on concentration and field. This behavior was interpreted in terms of two types of interactions involving pairs. One involves the interaction between elements of the pair and between the pair and its environment. It is estimated that Fe atoms must be within a volume of 10^3 Å^3 to form a pair. The second type of interaction is between pairs and causes ordering for low fields, at essentially field-independent temperatures.

Mishra and Beck[83] have analyzed the data of Tholence and Tournier[17] and of Hirschkoff et al.[69] for samples in the range of 110 ppm. They performed a least squares fit of the data to $\sigma = \chi_0 H + \mu_1 C_1 B\left(\mu_1 \frac{\mu_1 H}{T-\Theta_1}\right) + \mu_2 C_2 B\left(\frac{\mu_2 \mu_2 H}{T-\Theta_2}\right) + \ldots$

Here the magnetization, σ, is expressed as the sum of a

term corresponding to the temperature and field independent susceptibility, χ_o , and of three Brillouin terms, which are functions of the dipole moments $\mu_i = g S_i$, the dipole concentrations c_i , and characteristic temperatures θ_i , representing either interactions between the dipoles or a Kondo or local spin fluctuation temperature. It is assumed that $g \neq 2$, but the spin is not restricted to half integer values. The analysis agrees with the conclusion of Tholence and Tournier, that most of their observed magnetization was due to single impurities and pairs. There is disagreement, however, on the values of θ and the concentrations of dipoles. (See table I) There is no evidence of a decrease in the size of the dipole moments as the temperature is decreased.

Analysis of the data of Hirschkoff et al. indicates that χ_o is much larger and that all of the temperature dependent magnetization is due to dipoles larger than pairs. Extrapolation of the susceptibility of the single impurities and pairs from the data of Tholence and Tournier, indicates that the increase in χ_o is due to the single impurities and pairs which, because of the large values of θ , behave as if they were independent of temperature. This would suggest that the single impurity term follows the same Curie-Weiss law above and below the Kondo temperature.

Ekström and Myers [64] have published the results of susceptibility measurements on four alloys with concentrations between 100 and 300 ppm in the temperature range 1.7 - 300° K. Their data is accurately represented by the expression $\chi = \chi_0 + \frac{C_1}{T+\Theta_1} + \frac{C_2}{T+\Theta_2}$. ($\Theta_1 \approx 26$ K , Θ_2 is less than 5 K but concentration dependent). They have noted a contribution due to iron clusters, which was subtracted from the data before fitting to the above expression. The behavior of the various terms as the concentration is varied indicates that the first two terms are due to single impurities, while the second term is due to pairs. The value of Θ_1 is less than the values found by Hurd [74] and Tholence and Tournier. [17] The values of C_2 do not obey the concentration dependence expected from the work of Tholence and Tournier, and Θ_2 also varies with concentration instead of being constant.

The results indicate that the susceptibility of a single Fe impurity follows a Curie-Weiss law with Θ = 29 K and an effective moment of 3.4 μ_B , which corresponds to a spin S = 1.3. Data at temperatures below T_K could also be fit with the same Curie-Weiss law, although the data can probably be fit with other laws. As the temperature is increased above 50 K deviations from this Curie-Weiss law become evident. Ekström and Myers fit these deviations

by adding a temperature independent term to the susceptibility. Hoeve and Ostenburg [76] performed measurements from 300-770 K which can be used to show that χ_o is at most 5.4×10^{-4} emu/mole Fe. This is about $\frac{1}{2}$ the value found by Ekstrom and Myers, and about 1/5 the value found by Mishra and Beck.

There is conclusive evidence that there are interactions between impurities, even at these low concentrations. Mössbauer measurements on CuFe alloys by Window[67] and by Campbell, Clark, and Liddell [68] also show evidence of interactions, which were attributed to clustering of the Fe atoms. The spectra for alloys in the concentration range 500-20,000 ppm Fe, were analyzed in terms of separate doublets originating from Fe atoms with different numbers of Fe neighbors. The results of Window do not show any extra lines at the lowest concentration, but he states that it is possible that as much as 5% of the Fe may be in pairs. Campbell et al. see an extra doublet at concentrations as low as 200 ppm. The fractional area of this doublet showed a regular increase as the concentration was increased.

There are two possible explanations for this extra term, which is attributed to pairs of Fe impurities. The pairs might be due to pairs of nearest neighbor Fe atoms, or Fe atoms could interact over a longer range to form pairs in a random alloy. In the former case, the pair term could be used

as a measure of the degree of clustering. Campbell et. al. have analyzed their data in this fashion and found that the degree of clustering increases as the concentration is decreased. Their data is not inconsistent with the view that the pairs are due to Fe atoms which are further apart than near neighbors in a random alloy. In this case the concentration of pairs would be proportional to c^2 [63]. This explanation put forth by Tholence and Tournier [17], and Hirschkoff et al. [69] indicates that an Fe impurity behaves as a pair if there is another Fe atom within a radius of 10 Å . Ekström and Myers [64] do not find the Curie constant of the pair term to be proportional to c^2, so their data does not fit this random alloy interpretation. It is not clear which view point is correct (possibly a combination of both), but it is difficult to reconcile the regular dependence of the magnetization on concentration, found by Tholence and Tournier and by Franz and Sellmyer with the idea of a large number nearest neighbor due to clustering, which would be expected to cause irregular variations in the magnetization as the concentration is varied. There is also evidence for pairs of Fe impurities in measurements of the resistivity [66] and specific heat, [65] but they do not shed any light on this question.

C. AuFe

Table II contains the relevant information for the studies of magnetic properties to be discussed. These were chosen as the most recent studies in the low concentration range and contain references to earlier work. Hurd [74] performed measurements of the initial susceptibility in the temperature range 6-300 K on samples with concentrations below 220 ppm. The data was fitted to a Curie-Weiss law, but there are systematic deviations from this behavior at temperatures above 150 K. The Curie temperature and effective moment are independent of concentration. (Average values are listed in table II.) This same data was also fitted to the perturbation theory expression for χ [43] and T_K was found to be 1.0 K. [75]

Loram et al. [76] measured susceptibility and magnetization for three samples with Fe concentration below 100 ppm. Their data fit a Curie-Weiss law in the temperature range 1.5-4.2 K. and comparison with the expected behavior due to the Kondo effect gave T_K - 0.10 K. Using the perturbation theory results for the average electron spin and the average impurity spin, they found an expression for $g\mu_B$ as a function of field and temperature, which was used to fit their magnetization data to a Brillouin function.

Tholence and Tournier [73] have studied ordering in this system by measuring initial susceptibility and magnetization in the temperature range 0.05 - 5 K as the concentration was varied from 26 to 5000 ppm Fe. There is a maximum in the susceptibility which occurs at a temperature T_m = 800 c. At concentrations below 100 ppm the susceptibility is a linear function of concentration, which fits a Curie-Weiss law with Θ = 0.4 K and an effective moment of 3.25 μ_B. At low temperatures there are deviations from this Curie-Weiss law, which vary with concentration and were interpreted as pairs of interacting Fe atoms.

IV. Magnetization and Susceptibility of CuAu(Fe)

A. Introduction

Before presenting the results of our magnetization and susceptibility measurements on the CuAu(Fe) system, some of the points made in the previous sections will be summarized.

1) Resistivity,[21] specific heat [22] and magnetoresistance [23] measurements show that T_K decreases as Au is added to CuFe alloys. This contrasts with the behavior observed for several other ternary alloy systems (Fe in MoNb, Co in RhPd and MoNb) which is more consistent with a localized model proposed by Jaccarino and Walker. [18-20] In these alloys it appears that the properties of the magnetic impurities depend on their local environment in the host. For instance Co atoms in MoNb hosts are either magnetic or nonmagnetic depending on the number of near neighbor Mo atoms. The temperature dependence of properties due to the magnetic impurities are the same, but the number of magnetic impurities decreases as the Nb concentration is increased. There is a susceptibility measurement on Fe in $Cu_{0.9}Au_{0.1}$ which indicates that T_K is very near the value of T_K for Fe in Cu.[64] This result is consistent with the Jaccarino-Walker model rather than the continuous model, which describes the other measurements on the same system.

2) Studies of the magnetization of Fe in Cu have shown that even at very low Fe concentrations there are contributions

to the magnetization and suceptibility due to pairs of ferromagnetically coupled Fe atoms.[17] Even at relatively high temperatures the susceptibility is not a linear function of concentration. On the other hand, for Fe concentrations less than 100 ppm, the susceptibility of AuFe is a linear function of concentration.[73] For higher concentrations the effects of the RKKY interaction become more important.

To investigate the variation of T_K with host composition, local environment effects, and the behavior of the pair contribution as Au is added to CuFe, we have measured the magnetization of Fe in several CuAu hosts.

B. Experimental Procedure

Magnetization measurements were performed on a series of CuAu(Fe) alloys. For hosts with 5, 9, 17, 20 and 100 atomic % Au, a series of samples with Fe concentrations less than 500 ppm was studied. The samples were in the form of 1 gram buttons prepared from five nines starting materials by melting in an argon atmosphere arc furnace. Except for the AuFe alloys, samples were annealed for 8 days at 830 C and rapidly quenched in iced brine. The AuFe samples were annealed for 1 day at 900 C. All samples were stored in liquid nitrogen. The magnetization was measured using the Faraday method at several temperatures between 1.4 and 122 K. Fields up to

50 kG were obtained using a superconducting solenoid and a separate superconducting coil was used to provide a gradient of 480 gauss/ cm. A Cahn electrobalance with a sensitivity of 2μ grams was used to measure the force. The sensitivity of the apparatus is enhanced by the capability of reversing the gradient polarity. More details of the experimental apparatus and sample preparation are contained in sections V and VI of this thesis.

C. Superparamagnetic Clusters

Figure 1 is a plot of the impurity magnetization as a function of field for 325 ppm Fe in a $Cu_{0.95}Au_{0.05}$ host at 77 K. These data are typical of the behavior found for samples containing Cu at temperatures above 44 K. For 5 kG and above the magnetization is a linear function of field, while there is curvature below 5 kG. Similar curvature has been observed in CuFe alloys and attributed to superparamagnetic clusters of Fe atoms. [1, 14, 64, 82] The linearity above 5 kG indicates that the magnetization of the clusters is saturated by a field of less than 5 kG. The saturation magnetization of the clusters, M_c, is found by extending the linear portion of the curve to zero field. M_c is found to be nearly the same for all temperatures above 44 K and is assumed to be the same at lower temperatures. Correction for these clusters was made

by subtracting M_c from all data for 5 kG and above. These clusters were not observed in the AuFe alloys.

A more detailed discussion of the behavior of M_c is presented in section VII C.. Tables 3, 4, 5, 6 and 7 present the magnetization data after this correction has been made. The susceptibility was deduced from the magnetization as described in section VII D. Tables 3, 4, 5, 6 and 7 also present the susceptibility.

D. Interactions

Figure 2 presents the impurity magnetization per mole of Fe impurity at 40 kG and 1.4 K for each of the CuAu hosts as a function of nominal Fe concentration. If the alloys are dilute enough for single impurity behavior to dominate, it is expected that the impurity magnetization will be a linear function of concentration and these curves will be horizontal straight lines. It is clear from this figure that there are interactions between the Fe impurities. For the hosts with 5 and 9 atomic % Au, the concentration dependence is similar to the behavior observed for alloys of CuFe,[17] where the positive slope is attributed to the magnetization of pairs of ferromagnetically coupled Fe atoms. For the alloys with 17 and 20 atomic per cent Au, the slope is much smaller, and for AuFe the impurity magnetization per mole Fe decreases as the

Fe concentrations is increased. A similar decrease has been observed previously in AuFe [70, 73] and several other alloy system, [63, 84] where it can be attributed to the effects of the RKKY interaction. [85]

Since the behavior of the Cu-rich alloys is similar to that observed for CuFe, it is expected that the magnetization and susceptibility can be separated into a term due to single impurities and a term due to pairs of ferromagnetically coupled Fe atoms. The two methods of analysis applied to the data are reviewed briefly here and discussed in detail in section VII E.

The first method is similar to that used by Tholence and Tournier [17] to analyze their CuFe magnetization data. If the pair magnetization is saturated at high fields and low temperatures, the high field susceptibility will be a linear function of the single impurity concentration, $\chi_{H.F.} = a n_s$. Once the constant, a, is determined, this relationship can be used to find n_s . For low concentrations n_s is within several per cent of c_{nom}, and only a small error is introduced by setting $n_s = c_{nom}$ for one sample and solving for the constant, a. (See Tables 8-11 for values of n_s. The explanation of these Tables is in Section VII E.) The magnetization is then expanded as a function of the single impurity concentration, $M = M_o + M_1 n_s + M_2 n_s^2$. The coefficient M_o is the host magnetization, M_1 is the single impurity magnetization, and the coefficient of the quadratic term M_2, is the

product of the pair magnetization and a constant relating the concentration of pairs to the square of the single impurity concentration. (See Equ 9 on pg.128) From the magnetizations found in this way, a susceptibility for each term can be determined. The saturation magnetization and the temperature dependence of the susceptibility yield information about the magnitude of the spin and the concentration of the pairs. Similar information is not obtained for the single impurity term, since 50 kG is not a large enough field to saturate the single impurity magnetization at these temperatures.

The second analysis is based on the difference in temperature dependence expected for the pair and single impurity susceptibility. As applied by Ekström and Myers [64] to CuFe, the single impurity susceptibility is approximated by a temperature independent term, χ_o plus a Curie-Weiss term, while the pair susceptibility is described by a Curie-Weiss term. The method consists then of fitting the susceptibility to the expression, $\chi_{imp.} = \chi_o + \frac{C_s}{T+\theta_s} + \frac{C_p}{T+\theta_p}$, to determine χ_o, C_s, θ_s, C_p , and θ_p . This type of analysis has also been applied to other alloy systems [84, 86]. If local environment effects are present, the different Curie-Weiss terms are associated with impurities in regions of different host composition.

Both analyses yield expressions for the temperature dependence of the single impurity susceptibility and the pair

susceptibility. If the pair model is appropriate, the Curie constants and values of Θ should be in substantial agreement.

There are difficulties with both analyses. The concentration of pairs is less than 10 ppm in a sample with 400 ppm of Fe. Without a significant difference in behavior of the pairs and single impurities it is obviously difficult to separate the effects of the small number of pairs from the effects of the much greater number of single impurities. For CuFe there is a substantial difference in the temperature dependence of the two contributions, but as the Au content of the alloys is increased, the temperature dependence of the single impurities and the pairs become more alike (that is Θ_S approaches Θ_P). In determining the single impurity concentration from the high field susceptibility a systematic error in the concentrations is introduced if the pair magnetization is not saturated. The effect of this error is to make M_2 proportional to $(M_p - bM_s)$, where b increases as the behavior of single impurities and pairs become more similar. (See section VII E)

This possible systematic error was the motivation for performing two different analyses. On the other hand, as the Au content is increased and the Kondo temperature decreases, the representation of the single impurity susceptibility by $\chi_o + \frac{C_s}{T+\theta_s}$ is not as good as for the

CuFe alloys. These points are discussed in more detail in Section VII E. In the rest of this section, we will discuss the effects of interactions in each of the alloy sets studied.

D.1. $Cu_{0.95}Au_{0.05}$ and $Cu_{0.91}Au_{0.09}$

The magnetization of these alloys is very well described by $M = M_o + M_1 n_s + M_2 n_s^2$. The coefficients determined by fitting the magnetization to this expression using the method of least squares are listed in Tables 12 through 20. Figures 3 and 4 for the host with 5 atomic % Au and Figs. 5 and 6 for the host with 9 atomic % Au show how well this expression describes the magnetization, as well as indicating the temperature and field dependence of the coefficients M_1 and M_2. The plots are of $(M-M_H)/n_s$ as a function of n_s, where M_H is the magnetization of the nominally pure sample at 77 K after subtracting the magnetization due to the estimated Fe content of this sample. In Figs. 4 and 6 the field is maintained at 40 kG and data for several temperatures are plotted, while in Figs. 3 and 5 the temperature is 1.38 K and the field is varied. The plots are very good straight lines, which indicates that $M = M_o + M_1 n_s + M_2 n_s^2$ does describe the magnetization. The slope of the line is M_2 and the intercept is M_1. From the curves it can be seen that M_1 and M_2 increase as the field

is increased or as the temperature is decreased. This is consistent with the behavior expected if these coefficients are related to magnetizations due to single impurities and to pairs of ferromagnetically coupled Fe atoms.

The error bars shown have been found using the methods described in section VII E . Most of this calculated error is due to the uncertainty in n_s. In most cases the uncertainty due to the possible errors in the impurity magnetization is less than the size of the data points. Due to the uncertainty in n_s, it is impossible to rule out the presence in M of higher order terms in n_s.

The figures for the alloy with 9 atomic % Au clearly show another feature of our data. The samples with Fe concentration above 250 ppm clearly fit on a different straight line than the one for the lower concentration samples. The high concentration samples and the low concentration samples were made and heat-treated in two separate batches. Similar behavior was found whenever several sets of samples were made, even if the same masters were used. This effect is possibly due to slight differences in the heat treatment of the alloys.

As further illustration of the behavior of M_1 and M_2, these coefficients are plotted as a function of field for several values of the temperature. Figures 7 through 10 show once again that these coefficients, which we intend to

associate with the magnetization of single impurities and pairs, have the expected field and temperature dependence. The error bars have been estimated using plots similar to Figs. 3 through 6. The uncertainty in the coefficients is found from the slope and intercept of the straight lines with the largest and smallest slope consistent with the uncertainty in the impurity magnetization. Uncertainties in the value of n_s, which would cause a similar shift in the slope and intercept at all values of field and temperature, have been neglected. Note that there is considerable curvature in the plots of M_2 at low temperatures, while the plots of M_1 are nearly linear. This difference in behavior is important to the separation of the two terms. (Note that the manner in which n_s was determined forces M_2 to saturate at 50 kG and 1.38 K.)

The susceptibilities χ_0, χ_1 and χ_2 can be found by estimating the limit as $H \to 0$ of $\frac{M_0}{H}$, $\frac{M_1}{H}$ and $\frac{M_2}{H}$. An alternate method is to find the total susceptibility χ, from the limit as $H \longrightarrow 0$ of $\frac{M}{H}$ and then expand χ as a function of n_s,

i.e. $\chi = \chi_0 + \chi_1 n_s + \chi_2 n_s^2$.

Both of these methods were used and the results are shown in Tables 12 through 20. Except at the lowest temperatures

where the nonlinear field dependence of the magnetization affects the determination of χ , the results are in substantial agreement. The uncertainty in χ_1 and χ_2 can be estimated from the uncertainty in the coefficients M_1 and M_2 mentioned in the preceding paragraph.

The single impurity susceptibility is adequately represented by a temperature independent term plus a Curie-Weiss term. This is shown in Figs. 11 and 12 where the susceptibility per mole of impurity is plotted as a function of $1/(T+\Theta_S)$. Values of Θ_S, χ_0, and C_S were found by fitting to the expression $\chi_S = \chi_0 + \frac{C_S}{T+\Theta_S}$ using the method of least squares. These values are listed in Tables 21 and 22 along with values found using other analyses. A more detailed discussion of the single impurity susceptibility will be presented later.

Figures 13 and 14 show χ_2^{-1} for the alloys with 5 and 9 atomic % Au as a function of temperature. The data have been fitted to a Curie-Weiss law using the method of least squares. The values of C_2 and Θ_2 found from this analysis are listed in Tables 21 and 22 and the Curie-Weiss law which is the best fit is shown in the figures. The differences between the calculated and experimental values of χ_2 are always less than the estimated error in the experimental values, although there appears to be a systematic difference for the alloy with 9 atomic % Au. (These deviations along with the slight peak in M_2 as a function of field at 1.4 K, are possible indications that there is a systematic error in n_s, which causes an

admixture of the single impurity susceptibility in χ_2 . This point will be discussed in more detail in section D2. Using the Curie constant and the saturation magnetization, the spin and the concentration of pairs has been calculated (assuming $g \doteq 2$). These values are listed in Table 23. The values found for the spin are close to 3, which indicates that this term is in fact due to pairs of ferromagnetically coupled Fe atoms. The indicated errors are due to the uncertainty inthe Curie constant and the saturation magnetization caused by the uncertainty in the impurity magnetization.

The total impurity susceptibility for each sample has also been fit to the full expression $\chi = \chi_0 + \frac{C_S}{T+\Theta_S} + \frac{C_P}{T+\Theta_P}$, using the method of least squares. The results of these fits are listed in Tables 21 and 22. Two sets of values are listed: for one set Θ_S and Θ_P were assumed to be known from the previous analysis; while for the other, all five coefficients $\chi_0, C_S, \Theta_S, C_P$ and Θ_P were allowed to vary. The results indicate, in agreement with the previous analysis, that there are two types of magnetic impurity, one with relatively high Θ which we associated with single impurities and one with Θ less than 5 K which we associated with pairs of ferromagnetically

coupled Fe atoms. Furthermore the higher Θ value is significantly less than the Θ for CuFe and decreases as the Au content of the host is increased. This differs from the results of Ekström and Myers,[64] who found no significant differences in the corresponding values of Θ as the Au content of the host is increased.

The results of these fits for the alloy with 9 atomic % Au are in very good agreement with the results of our previous analysis. A glance at Table 22 shows that even when all five coefficients are allowed to vary, χ_o and C_s are linear functions of concentration, while C_p is proportional to c^2. We have not estimated the uncertainty in the coefficients, but the numerical agreement of the coefficients with those found in the previous analysis is very good. Notice that the difference in the two sets of samples made at different times is not apparent in this analysis.

The situation for the alloys with 5 atomic % Au is not as clear. If Θ_s and Θ_p are assumed known from the previous analysis, there is also good agreement between the values found for the other coefficients. However, there appears to be a small systematic variation in χ_o and C_s (aside from the linear concentration dependence expected) as the Fe concentration is varied. Furthermore, if all five coefficients

are allowed to vary the behavior of the "pair" term changes significantly. A significant improvement in the fits is obtained for values of Θ_p which vary systematically with Fe concentration and for a C_p which varies less rapidly than c^2. It is possible that the fitting procedure separates out a low Θ term, which, since its concentration dependence is between c and c^2, probably includes a portion of the linear (single impurity) term. There are other possible causes for this effect, which, as described above, was not found for the alloy with 9 atomic % Au. However, it is interesting to note that similar behavior was in fact found for the CuFe system by Ekström and Myers.[64]

D. 2. Fe in $Cu_{0.83}Au_{0.17}$

The magnetization of these alloys is also fit by the expression $M = M_o + M_1 n_s + M_2 n_s^2$. However, it is not quite as clear as for the more Cu-rich alloys that the coefficients correspond to the magnetizations of single impurities and pairs of ferromagnetically coupled Fe atoms.

The suitability of the above expression for the concentration dependence of the magnetization is illustrated in Figs. 15 and 16. The impurity magnetization per unit single impurity concentration is plotted as a function of the single impurity concentration for various fields at a temperature of 1.38 K in Fig. 15, and for various temperatures with a 40 kG field in Fig. 16. Just as for the alloys with 5 and 9 atomic % Au, these plots are very good straight lines, but for comparable values of field and temperature the slope of these curves for

the 17 atomic % Au alloy is much smaller. Note that as in the case of the 9 atomic % Au host, the data points for two batches of samples lie on two separate straight lines.

The coefficients M_o, M_1, M_2, χ_o, χ_1 and χ_2 were found by fitting the magnetization and susceptibility to an expression with the above form. The results of these fits are listed in Tables 24 through 29. In Figs. 17 and 18 the coefficients M_1 and M_2 are plotted as functions of field for several values of temperature. The plots of M_1 for low temperatures show more curvature than the corresponding plots for the alloys with less Au, but the most notable features are the maxima in the plots of M_2 at 1.38 and 4.2 K. Similar behavior is also discernible in the plot of M_2 at 1.38 K for the $Cu_{0.91}Au_{0.09}$ alloys but in a less dramatic form. This effect is probably caused by a systematic error in the determination of the single impurity concentrations. As discussed in Section VII E, the effect of such an error is to couple the single impurity and pair magnetizations in the coefficient of the quadratic term. As the Au content of the host is increased, M_1 decreases and the coupling of the pair and single impurity magnetizations in M_2 become much more important. Similar behavior in an even more pronounced form can be demonstrated in the 9 atomic % Au alloys if the expansion is carried out using the nominal Fe concentration instead of the single impurity concentration.

χ_2 has been fit to a Curie-Weiss law. Figure 19 shows the inverse of this susceptibility as a function of temperature. The susceptibility decreases systematically below the Curie-Weiss law at higher temperatures. This is similar to the behavior found for the alloy with 9 atomic % Au and could also be due to the effects of systematic errors in the concentration. If it is assumed that this term is due to pairs of ferromagnetically coupled Fe atoms with a spin of 3, the Curie constant of 2.52 x 10^{-12} c^2 emu K / gm is consistent with a concentration of pairs equal to 36 c^2 pairs / atom of alloy.

Figure 20 shows the results of a least squares fit of the single impurity susceptibility to $\chi_o + \frac{C_s}{T+\theta_s}$, a temperature independent term plus a Curie-Weiss term. The single impurity susceptibility is plotted as a function of $1/(T + 3.3)$, where 3.3 K is the value of θ_s which minimized the sum of the squares of the deviations. There are systematic deviations from this expression at the higher temperatures. It is not clear whether the deviations are caused by errors incurred in separating the terms or whether they are caused by the failure of this expression to approximate the temperature dependence of the true single impurity susceptibility.

Table 30 lists the values of χ_o, C_s, θ_s, C_p and θ_p found by fitting the susceptibility of each sample to the full

expression $\chi_o + \frac{C_s}{T+\theta_s} + \frac{C_p}{T+\theta_p}$. If the single impurity susceptibility is adequately represented by $\chi_o + \frac{C_s}{T+\theta_s}$, this analysis should separate the single impurity and pair susceptibilities. There is a wide difference between the values found from this analysis and those found from the previous analysis. For instance θ_s is 5 times larger than the previous value and C_p is from 5 to 10 times larger than the previous value. If the values of C_p are correct and are due to pairs of ferromagnetically coupled Fe atoms, the concentration of pairs would be near 300 c^2 pairs per atom of alloy. The concentration dependence of χ_o , C_s and C_p is shown more clearly in Figure 21. C_p is almost a linear function of concentration, besides being much larger than expected. C_s is nearly linear in concentration, but does have a small quadratic dependence in addition. It is clear that in this case it is impossible to attribute one term to single impurities and the other to pairs of ferromagnetically coupled Fe atoms. Since the term which would be attributed to the pairs has a strong admixture of linear concentration dependence, it is reasonable to suspect that this portion of the "pair" term is in fact not due to pairs, but serves the function, rather, of correcting for the fact that the linear term is not adequately described by a simple form $\chi_o + \frac{C_s}{T+\theta_s}$.

D. 3. Fe in $Cu_{0.8}Au_{0.2}$

The concentration dependence of the impurity magnetization of these alloys is shown in Figs. 22 and 23. No clear deviation from linear concentration dependence is evident in these figures. The samples were made in three different sets and it is possible that there is a slight concentration dependence, which is obscured by the difference in different batches of samples. (One set includes up to 212 ppm, the 525 is separate, and the 260 and 304 make up the third set.) Because of this, no attempt was made to fit the magnetization to the form $M = M_o + M_1 + n_s + M_2 n_s^2$.

The susceptibility of each sample has been fit to the expression $\chi_o + \frac{C_1}{T+\Theta_1} + \frac{C_2}{T+\Theta_2}$. The values of χ_o, C_1, Θ_1, C_2 and Θ_2, which minimize the sum of the squares of the deviations are listed in Table 31. Figure 24 shows χ_o, C_1, and C_2 as functions of concentration. All of these coefficients are nearly linear functions of concentration, so that no term can be associated with pairs of ferromagnetically coupled Fe atoms.

D. 4. AuFe

The analysis of the AuFe data is not as straightforward as the analysis for the other alloys. When the magnetization is assumed to be due to pairs and single impurities, it is possible to relate the concentrations to the high field

susceptibility. But, as shown in Fig. 2, the behavior of the AuFe alloys is not consistent with the behavior expected if there are only pairs of ferromagnetically coupled Fe atoms and single impurities. In fact, a similar decrease of the magnetization per impurity as the concentration is increased has previously been observed [70, 73] in AuFe alloys and can be attributed to the effects of the RKKY interaction. [85] Under these circumstances the high field susceptibility would not be expected to be a linear function of concentration. Because of the uncertainty in the concentrations, we have analysed the data in several ways. Before describing the details of these analyses we present a summary of the main conclusions.

1. For Fe concentrations above 60 ppm the magnetization per impurity at temperatures below 10 K decreases as the Fe concentration is increased. This behavior is clearly shown in Figs. 25 through 27.

2. The temperature dependence of the impurity susceptibility per impurity is not strongly affected by variation of the concentration in the range studied.

3. The magnetization per impurity and the temperature dependence of the susceptibility are in good agreement with previous measurements.

4. The uncertainty in the Fe concentrations does not allow an accurate comparison with the scaling relations

expected if the RKKY interaction effects dominate or a definite statement about the behavior of the magnetization per impurity for concentrations below 60 ppm.

The results of one analysis are shown in Figs. 25, 26, and 27, where the impurity magnetization per ppm of Fe impurity is plotted as a function of concentration for various combinations of H and T. The impurity magnetization has been found by subtracting the magnetization of a nominally pure sample from the magnetization of a sample containing Fe. The plots show this impurity magnetization divided by the nominal Fe concentration. As the concentration of Fe is increased the magnetization per impurity clearly decreases, and this behavior is more pronounced as the field is increased and as the temperature is decreased. Except for the 60 ppm sample, it appears that at 10 K and above, the magnetization appears to scale with Fe concentration.

The above analysis is complicated by the presence of approximately 10 ppm of Fe in the nominally pure sample. The presence of the Fe is clear from the temperature and field dependence of the magnetization. At 1.38 K there is a substantial difference between the magnetization of the nominally pure sample and the magnetization expected for pure Au. All the samples were made from the same materials

and in the same way, so it is not unreasonable to assume that there is an additional 10 ppm of Fe in each sample. In this case, the actual concentration is the nominal concentration + 10, but the difference in concentration between the sample with Fe and the nominally pure sample would still be the nominal concentration. The above analysis will give correct results for large concentrations, and in cases where the magnetization is a linear function of the concentration. However, where the magnetization decreases as the concentration increases, the above analysis will overestimate the decrease for the low concentrations.

In Figs. 25 through 27 the error due to the uncertainty in the impurity magnetization is in most cases less than the size of the data points. The major uncertainty is in the concentrations. Instead of estimating this uncertainty, we have analysed the data using concentrations found in three other ways.

1) Using the method applied to the alloys containing Cu, n_s was found from the high field susceptibility and M_H was estimated from the data for the nominally pure sample.
2) Concentrations were found by assuming that the magnetization at one field and one high temperature (77 K) is a linear function of concentration.
3) Susceptibility data above 44 K was fit to a Curie-Weiss law. The concentrations were determined by assuming

that the Curie constant is a linear function of concentration.

All analyses give values of $\Delta M/c$ which decrease (for concentrations above 60 ppm) as the concentration is increased, although there is disagreement in the numerical results.

A similar decrease in the magnetization per impurity with increasing Fe concentration has been observed previously. The data of Tholence and Tournier [73] at 0.05 K for the concentration range 26 to 10,000 ppm clearly show such a decrease. It is difficult to make a comparison with their data because of the low temperature. However, we can compare our results with those of Borg and Kitchens.[70] They present magnetization data on concentrations from 500 ppm to 12.5 atomic %. At 33 kG and 1.35 K the magnetization per Fe atom decreases from 1.2 μ_B for 500 ppm to 0.5 μ_B for 1 atomic %. After the concentration is raised above 2 at %, the magnetization per Fe atom begins to increase. When our data for the magnetization per atom at 30 kG and 1.38 K is expressed in these units we find a decrease from 1.84 μ_B to 1.53 μ_B as the Fe concentration is increased from 60 to 400 ppm. We also agree that the decrease is greater as the field is increased. However, if our data is extrapolated to 500 ppm the magnetization will be about 20% larger than that found by Borg and Kitchens.

In Figs. 28 and 29 we show $c/\Delta\chi$ as a function of temperature. In this case, $\Delta\chi$ is the difference between the susceptibilities of the sample with Fe and the nominally pure sample and c is the nominal concentration. Figure 28 is for the entire temperature range 1.38 to 120 K, while Fig. 29 is an enlargement of the portion below 10 K.

For the temperatures above 10 K there is no clear concentration dependence in Fig. 28. The three high concentration samples (185, 288 and 395 ppm) are represented by a single point. The data points for the 61 ppm sample differ by a large enough amount at some temperatures to warrant a separate symbol, although the differences are less than the estimated uncertainty in the measurements. The error bars shown for the 61 ppm sample are due to the uncertainty in $\Delta\chi$. At lower temperatures the uncertainty in all data points is less than the size of the data points.

The data between 44 and 133 K is adequately described by a Curie-Weiss law. The intercept corresponds to Θ = 10.5 K and the Curie constant is 2.0 emu K/ mole Fe, which corresponds to an effective moment of 4.0 μ_B . This compares favorably with the results of Hurd [74] who found Θ = 9.8 K and an effective moment of 3.75 μ_B, from susceptibility measurements between 6 and 300 K. The difference in the values of the effective moment could be accounted for if our concentrations were 13% below the actual value. This is

similar to the previously mentioned difference between our magnetization values and those of Borg and Kitchens.

At the lower temperatures there is a concentration dependence, which can be seen in Fig. 29 where the segment of the data below 10 K is shown in more detail. Except for the 395 ppm sample at 4.2 and 9.46 K, $\Delta\chi/c$ decreases as the concentration is increased. Where no error bars are shown, the uncertainty due to errors in the determination of the impurity susceptibility is less than the size of the data points. In Table 32 we have listed the values of and the effective moment found by numerically fitting the 1.38 and 4.2 K points to a Curie-Weiss law (including uncertainties due to errors in the impurity susceptibility). The uncertainties in this procedure are too large to detect any variation of the effective moment. Although it is not clear from the figure, it appears that Θ increases as the concentration is increased. The effective moment is 3.2 μ_B and Θ increases from 0.7 $\pm$ 0.06 K to 0.88 $\pm$ .04 K as the concentration is increased from 61 to 400 ppm. These values also agree with previous measurements on the AuFe system. Loram et al. [76] find Θ = 0.5K and μ_{eff} = 3.1 $\pm$ 0.15 μ_B for samples with less than 100 ppm in the temperature range 1.5 to 4.2 K. Tholence and Tournier [73] found that Θ varies linearly with concentration. From their expression we deduce that Θ should vary from

0.45 to 0.7 K as the concentration is varied from 61 to 400 ppm. They also find an effective moment of 3.2 μ_B . The agreement of our values for the effective moment with other low temperature values is a possible indication that our values of the concentration are also in agreement.

The decrease of the magnetization per impurity as the concentration is increased above 61 ppm is an indication that the behavior of these alloys is affected by the RKKY interaction. Tholence and Tournier [73] concluded from their susceptibility and magnetization measurements that the behavior below 100 ppm is dominated by single impurity effects. In an effort to shed further light on the behavior of samples with less than 100 ppm, we have attempted another analysis of the data for our nominally pure samples, which actually contain on the order of 10 to 15 ppm of Fe.

As mentioned earlier, it appears that the data from 44 to 133 K fit a Curie-Weiss law with $\Theta = 10.5$ K with a Curie constant which is a linear function of concentration and thus the concentrations can be determined from the Curie constants. The procedure is to plot the susceptibility for each sample as a function of $1/(T + 10.5)$ and to extrapolate the data to the intercept at $1/(T + 10.5) = 0$ which then gives the host susceptibility. It should be pointed out that in the absence of data at very high temperatures, this may give a

very approximate measure only (See ref. 78). Table 33 lists the values of the host susceptibility, the Curie constant, and values of the concentration found from the Curie constant assuming that C = 2.0 emu K/ mole Fe. As the concentration is increased there is a slight increase in the host susceptibility as given by the intercept. Thisvariation indicates that there is some deviation from the assumed Curie-Weiss law with $\Theta = 10.5$ K and forcing the intercepts to be -14.38×10^{-8} emu/gm causes a substantial change in the Curie constant and the concentrations. These values of the concentration are also listed.

Using the values of the concentration and the host magnetization from this analysis, values of $\Delta M/C$ for the low concentration samples can be found, but the errors in the concentrations are too large to permit any conclusion about the concentration dependence for concentrations less than 61 ppm. At all fields and temperatures the values for $\Delta M/C$ for the low concentration samples are smaller than the values found for the 61 ppm sample. This is the opposite of the concentration dependence found above 61 ppm, but if the possible errors in the low concentrations are considered, it is possible that the behavior above 61 ppm continues to lower concentrations or it is possible that $\Delta M/C$ is independent of concentration below 61 ppm.

The impurity susceptibility per impurity, $\Delta\chi/c$, was also found in the same fashion. Values for the effective moment and Θ found by fitting the 1.38 and 4.2 K data points to a Curie-Weiss law are listed in Table 32. The effective moment is sensitive to the uncertainty in the concentrations, but the values of Θ are unaffected by these uncertainties. The values of Θ are similar to those found for the higher concentration samples and it is clear that there is no strong change in the temperature dependence of the impurity susceptibility as the concentration is varied in the range of 10 to 400 ppm.

D. 5. Summary

Table 23 summarizes the parameters for the pairs of ferromagnetically coupled Fe atoms in CuAu hosts. For the alloys with 5 and 9 atomic % Au, we feel reasonably confident that the procedures used to separate the pair and single impurity terms were successful and that the values for the concentrations of pairs are reasonably accurate. The discussion presented section D 2 indicates that the separated pair magnetization for the 17 atomic % Au host does not have the expected field dependence at 1.38 K. Although there is definitely a pair term present, the unexpected field dependence indicates that we have not accurately separated the pair and

single impurity terms and that the numbers presented in the table are only estimates. For the alloy with 20 atomic % Au the concentration dependence of the magnetization is too small to attempt to separate two terms. This may be an indication that there are no interactions present, but a similar result is possible if the difference between the pair and single impurity magnetizations is small.

Tholence and Tournier [17] have suggested that whenever two Fe atoms are within some critical distance, they are coupled through the RKKY interaction to form a pair. From their CuFe susceptibility data they estimate this critical distance to be near 12 Å. Assuming that the mean free path is inversely proportional to the resistivity, estimates of the mean free path in Cu [87], and resistivity measurements on CuAu alloys, [88] indicate that alloying of Au into Cu will not decrease the mean free path to this critical distance. It would thus be expected that the concentration of pairs would remain constant as the host Au content is varied. The apparent decrease in the pair concentration for the 20 atomic % Au alloys would indicate that this is not the correct explanation. Franz and Sellmyer [63] have put forth stronger arguments against this model.

Our magnetization measurements on the AuFe system clearly show the influence of the RKKY interaction in the

decrease of the magnetization per impurity as the concentration is increased above 60 ppm. The concentrations of our samples are not accurate enough to determine if this behavior continues to lower concentrations, but we have not observed any strong concentration dependence in $\Delta\chi/c$ and in the following section will use the susceptibility of the 61 ppm sample as representative of our AuFe alloys.

E. Single Impurity Susceptibility

Our data for the single impurity susceptibility is plotted in Fig. 34 as a function of the temperature. The susceptibility shown for the alloys with 5, 9, and 17 atomic % Au was derived from the single impurity magnetization found in sections D 1 and D 2. For the alloys with 20 and 100 atomic % Au, the impurity susceptibility was found by subtracting the susceptibility of a nominally pure sample from the total susceptibility of a sample with about 50 ppm nominal Fe concentration. The impurity susceptibility was divided by the nominal Fe concentration. As indicated in section D 4, the concentration dependence of the AuFe susceptibility is slight and does not seriously affect the shape of the curve shown in Fig. 34.

If a straight line is drawn through the low temperature points, the intercept is less negative as the Au content of the host is increased. It is generally acknowledged that Θ is related to T_K [6, 49, 62] (the relationship depending upon the range of T/T_K), and we interpret this decrease in Θ as indicating a decrease in T_K as the host Au content is increased. For CuFe Θ = 29 K[17], while for our alloys with 5 and 9 atomic % Au Θ = 15.5 and 8.4, respectively. These values indicate that the data for these alloys cover comparable ranges of T/T_K, thus the relationship between T_K and Θ would also be expected to be similar. In Table 34 we list values of Θ/Θ_{CuFe} derived from the present data, and values of $T_K/T_{K_{CuFe}}$ found by Loram et al.[21] and by Delinger et al.[22] Although it is not clear that the data for the $Cu_{0.83}Au_{0.17}$ alloys are in the same range of T/T_K as the alloys with lower Au content, Θ/Θ_{CuFe} for this alloy has also been included in the table along with the values for T_K from resistivity measurements by Star et al.[89] For all of these alloys there is a similarity between the decrease in Θ and the decrease in T_K, as the host Au content is increased.

It is apparent from Fig. 34 that over the range of temperature shown, a Curie-Weiss law will not adequately describe the susceptibility of any of the alloys. For the alloy with 5 atomic % Au, a Curie-Weiss law appears to fit the

data from 1.4 to 44 K, but above this temprature deviations from Curie-Weiss behavior become apparent. As the Au content of the host is increased, there is a decrease in the temperature at which the deviations from the low temperature Curie-Weiss law become noticeable. This is the type of behavior which would be expected if these deviations were characteristic of the s-d model and if the susceptibility of the alloys were to scale with T_K.

Several calculations [43-46] of the susceptibility above T_K have the form $\chi = \frac{C}{T} f(T/T_K)$, so that if the Curie constant (a function of the impurity spin) is independent of the host Au content, χT should be a universal function of T/T_K. Figure 35 is a plot of $\frac{\chi T}{C}$ as a function of T/T', where the values of χ/C are the same as those used for Fig.34 and T' is proportional to the Kondo temperatures found from resistivity measurements.[21, 90]. Although the curves lie near one another, they do not superpose. One possibility is that the concentrations used are in error. The difference between the curves for the 5 and 17 atomic % Au alloys corresponds to a 15 % error in the concentrations, which would not be an unusually large difference for dilute alloys. The differences for the other alloys is smaller. In Fig. 36 $\frac{\chi T}{C}$ has been multiplied by a constant (that is the concentrations or

equivalently the impurity spin has been adjusted) to bring the curves into alignment. As would be expected the superposition is much better, but there are still some substantial differences between the curves.

If we now allow both the concentration and T' to vary, we obtain the curve shown in Fig. 37. In this figure, the data points all lie quite closely on a universal curve. Except for AuFe, the concentrations were varied by no more than 8% (a not unreasonable number in view of uncertainties in c), and the values used for T' are not far different from those deduced by Loram, Whall, and Ford [21] from resistivity results. The universal curve thus obtained in Fig. 37 supports our contention that we have effected a separation of the single impurity term, which is in the main correct. Further, we have obtained a universal curve for the susceptibility of CuAu(Fe) in the same manner that Loram, Whall and Ford deduced an equivalent universal curve for the resistivity. The corresponding values obtained for T/T' are in general agreement. This indicates, as it did in the case of the resistivity, that a single parameter, namely T_K, describes the overall behavior of CuAu(Fe) alloys, and that local environment effects are of secondary importance.

Although several of the data points for the AuFe alloy fit the curve, data for several more alloys in the Au-rich region would be needed to definitely establish the behavior of the AuFe alloy as due to the s-d interaction.

We have attempted to fit the susceptibility data for AuFe to the expression (1) $\chi = \frac{C}{T}\left[1 - \left(\ln \frac{T}{T_K}\right)^{-1}\right]$. Loram et al.[76] have fit their AuFe susceptibility data in the temperature range 1.5 to 4.2 K to this expression and found T_K = 0.1 K. Their discussion of the magnetization indicates that they expect this expression to fit their data over the entire range of 1.5 tol20 K. Using the above formula, the inverse susceptibility is plotted as a function of temperature in Fig. 38. We show curves for T_K = 0.1 and 1.0 K over the temperature range 1 to 120 K and only the temperature dependent factors are shown (The Curie constant is set equal to 1). By comparing our AuFe curve in Fig. 34 to the curve shown in Fig. 38 for T_K = 0.1 K, it is obvious that formula (1) will not fit our data over the entire temperature range. We have also done least squares fits to this formula with very poor results. The best fits are with T_K= 0.2 K , but there are 5 and 10% deviations from the measured values for the points above 10 K. (The value of T_K could be found by dividing the value of Θ from the Curie-Weiss law, which fits the 1.4 and 4.2 K points, by 4.5. Our value of Θ in this region is twice the value found by Loram et al.[76] and by Tholence and Tournier.[73] It is quite possible that our value of Θ is in error by 0.5 K.

On the other hand, the high temperature behavior is quite well established and is inconsistent with the behavior predicted by formula 1.)

In Fig. 37 we have also plotted the inverse of the susceptibility derived by Ting [45] and Brenig et al.[46]

$$(2) \quad \chi = \frac{C}{T}\left\{1 - \frac{1}{S+\frac{1}{2}}\left[\frac{1}{2} - \frac{1}{\pi}\operatorname{arc\,tg}\left\{\frac{\ln\left(\frac{T}{T_K}\right)}{\pi\left(S+\frac{1}{2}\right)}\right\}\right]\right\}$$

as a function of temperature for S=1.2 and several values of T_K. Formula 2 is expected to be valid from near T_K to higher temperatures. There is almost no variations of the intercept as T_K is varied and comparison of our data in Fig.34 with the curves in Fig. 38 indicates that our data cannot be described by formula 2.

The theoretical calculations include only the effects of the s-d interaction and it is possible that the neglect of other effects is responsible for the disagreement between theory and experiment. For instance, the temperature dependence of the susceptibility of the LaCe system is similar to the behavior of the AuFe system. DeGennaro and Borchi [90] have found agreement betwen experiment and their calculations, which include the effects of crystal-field splitting. Even though T_K for the two systems is similar, this similarity in behavior does not necessarily indicate that the temperature dependence of AuFe is due to the combination of the s-d interaction and crystal field splitting. There are differences

in the ionic states of Fe and Ce, which will influence the calculation of crystal field effects.

The superposition of χT (for the single impurities) when plotted as a function of T/T' is a strong indication that the susceptibility is due to the s-d interaction and also that local environment effects are not important in the CuAu(Fe) system. In the following section local environment effects will be considered in more detail.

F. Local Environment Effects

As discussed in a previous section, there are several ternary alloy systems in which the impurity behavior is strongly affected by variation of the local environment. For instance, there is evidence that in the MoNb(Co) system, the Co impurity is magnetic only if there are a sufficient number of Mo nearest neighbors, otherwise it is nonmagnetic. Since Fe is magnetic in both Cu and Au, the principal difference to be expected due to local environment effects would be in the interaction of the impurities with the host conduction electrons. Thus in a CuAu(Fe) alloy it might be expected that the temperature dependence would be characterized by several Kondo temperature for impurities in different local environments, rather than a single T_K characteristic of all of the impurities in the alloy. The fact that the

resistivity, specific heat, and single-impurity susceptibility of these alloys can be characterized by a single T_K for each CuAu composition indicates that local environment effects are relatively unimportant. We feel that an even stronger argument against local environemnt effects can be made using our susceptibility data.

The simplest form of the local environment model for CuAu(Fe) would have two terms in the susceptibility: one with temperature dependence characteristic of the CuFe system, the other with a temperature dependence characteristic of the AuFe system (that is, a given Fe atom would behave either as if it were in a Cu or in a Au matrix.) The single impurity susceptibility for the alloys with 5 and 9 atomic % Au are very closely described by a small temperature independent term plus a Curie-Weiss term. An attempt to fit the data to the expression $\chi_0 + \frac{C_1}{T+\Theta_1} + \frac{C_2}{T+\Theta_2}$ (with Θ_1 = 29 K for CuFe and Θ_2 =1K for AuFe), where the temperature dependences of the susceptibility of Fe in Cu or Au have been approximated by Curie-Weiss laws, leads to a much worse fit, than if one uses a single Curie-Weiss law with a single Θ_{CuAu} dependent on the CuAu host composition. Further, attempts to fit to the expression above, letting Θ_1 and Θ_2 vary freely between 1 and 30 K, gave a best fit for Θ_1 near Θ_{CuAu} above, and a small correction in Θ_2 with C_2 negative, which is an unphysical result.

A more complicated form of the local model would ascribe different behavior to an impurity with each of the 12 possible nearest neighbor combinations. In this case the temperature dependence of the susceptibility might be expressed as the sum of 12 different Curie-Weiss terms, with Curie constants proportional to the probability of any combination of nearest neighbors occurring. Our data for the 5 and 9 atomic % Au alloys is well described by $\chi_0 + \frac{C}{T+\Theta}$ with a Θ which decreases rapidly as Au is added to the hosts. This makes it unlikely that such a model would fit the data, and we argue this as follows. In Table 35 we have listed the probabilities of any particular combination of nearest neighbors occurring in our alloys with 5, 9 and 20 atomic % Au, if the alloys random. The probability of any impurity having more than 5 Au nearest neighbors is less than 0.01 and the effects of such a configuration can be neglected. Thus, instead of considering 12 terms, there are only 5 or 6 configurations which will affect the temperature dependence of the susceptibility significantly. When fitting with a single parameter the value of Θ_{CuAu} which fits the data decreases fairly rapidly from 29 K to 15 K as one goes from Cu(Fe) (12 nearest neighbor Cu atoms) to $Cu_{0.95}Au_{0.05}$(Fe) for which the nearest neighbor probabilities are listed. In order to obtain

a value of Θ = 15 K for the alloy with 5 atomic % Au, it must be true that the value of Θ associated with the (11 Cu, 1 Au) configuration is much lower than 29 K; in fact, lower than 15 K. Two Curie-Weiss terms with such dissimilar values of Θ can be recognized as separate terms and cannot be adequately fitted by a single Curie-Weiss term. Further evidence against this model would come from applying similar arguments to the alloy with 9 atomic % Au.

As the occupation of more of the sites surrounding the impurity are considered in this model, it becomes more difficult to argue against the validity of such a model, but such a model also becomes more like a continuous model. The probability of a particular combination of Cu and Au atoms occupying nearby sites for large z (i.e. as we begin to consider further neighbors) will be almost zero except for the Cu to Au ratio typical of the CuAu host concentrations. In this case the rapid variation of Θ with changes in Au concentration would be easily explained, but if a large number of sites is considered there is no sharp difference between the local model and the continuous model.

G. Conclusions

We have measured the magnetization and susceptibility of CuAu(Fe) alloys as a function of magnetic field (1 to 50 kg) and temperature (1.38 to 120 K) for alloys with 5, 9, 17, 20 and 100 atomic % Au and with Fe concentrations between 0 and 600 ppm. In the alloys containing Cu, we have found behavior similar to that observed for Cu(Fe), namely, that there exist terms in the magnetization and susceptibility proportional to c and c^2, which have been attributed, respectively, to single Fe impurities and to pairs of ferromagnetically coupled Fe atoms. A separation of the two terms has been effected using the method applied to Cu(Fe) by Tholence and Tournier.[17]

Our major results concern the single impurity susceptibility. The temperature dependence of the susceptibility is Curie-Weiss like at low temperatures with deviations at higher temperatures. The temperature at which the deviations become apparent decreases as the host Au content is increased. The Θ associated with the Curie-Weiss law decreases as the host Au content is increased in a manner similar to the decrease of T_K observed in resistivity measurements by Loram, Whall and Ford[21] and in specific heat measurements by Delinger, Savage and Schweitzer.[22] More significantly, we can find an appropriate value of a parameter, T', for each alloy, such that plots of $\chi_s T$ as a

function of T/T' superpose. This would indicate that the temperature dependence of the susceptibility is determined by a scaling temperature, T', which is proportional to T_K and in fact, the values of T' found for different host CuAu compositions are in the same ratio as T_K found from resistivity and specific heat measurements. The superposition also indicates that our separation of the single impurity susceptibility is successful, and that local environment effects do not play a strong role in these alloys.

From our results for the susceptibility, it is clear that a simple version of the local environment model, which attributes Cu(Fe)-like behavior to impurities in Cu-rich regions of the host and Au(Fe)-like behavior to Au-rich regions, is not applicable to the CuAu(Fe) alloys studied. Furthermore, we argue on the basis of our results that it is unlikely that a generalization of this model to include the possibility of different impurity behavior for each possible combination of Cu and Au nearest neighbors is also not applicable. Data on more host alloys or more reliable estimates of single impurity behavior would strengthen these arguments and may decide the validity of more complicated local environment models.

The properties of the ferromagnetically coupled Fe atoms are similar to those observed for Fe pairs in pure Cu. The magnetization approaches saturation in a field of 50 kG at 1.38 K.

and the susceptibility is Curie-Weiss like with a Θ less than 5 K. From the saturation magnetization and the Curie constant the spin and concentration of pairs was determined. The spin was near 3 which is consistent with the assumption that this term is really due to pairs of ferromagnetically coupled Fe atoms. For the alloys with 5 and 9 atomic % Au the concentration of pairs is about 1/2 the value for Cu(Fe) alloys found by Tholence and Tournier[17], but is nearly the same as the pair concentration found by Franz and Sellmyer.[63] As the Au composition of our alloys is increased to 17 and 20 atomic % Au, the pair concentration appears to decrease substantially, but this effect could be due to the method used to separate the pair and single impurity terms. Our work indicates that fields sufficient to insure saturation of the pairs, or an independent measure of the single impurity concentration, is necessary for a reliable study of the pair term.

There has been considerable interest in determining how strongly the behavior of Fe in Au is influenced by interaction effects. Our data for the magnetization of more than 60 ppm Fe in Au clearly show the effects of the RKKY interaction, but there is no sharp change in the temperature dependence of the susceptibility as the Fe concentration is varied from near 10 ppm to 400 ppm. The susceptibility for our four lowest temperatures was also fitted on the universal curve of T as a function of T/T'. This result would indicate that the single impurity behavior is dominant. However, there are few data points for large values of T/T', so the actual shape of the curve in this range has not been well determined by our

measurements. Further measurements on alloys with higher Au content or measurements on the Au(Fe) system at lower temperatures would provide more data for large values of T/T', and determine if Au(Fe) does fit the universal curve. More magnetization measurements on Au(Fe) alloys with more accurately known concentrations should also show if the interaction effects noted in the magnetization above 60 ppm are present at lower concentrations.

V. EQUIPMENT

A. Summary

A schematic diagram of the apparatus and a brief explanation is provided in Fig. 39. The susceptibility is measured by the Faraday method. A sample in an inhomogenous magnetic field experiences a force $F_z = m\chi H_o \frac{\partial H}{\partial z}$, which is measured using a sensitive balance. In this apparatus the uniform field, H_0, and the gradient field $\frac{\partial H}{\partial z}$, are provided by separate coils.[91, 92] A Westinghouse superconducting solenoid, A, (Letters and numbers refer to Fig. 39) provides fields H_0, up to 50 Kilogauss, while a gradient of 485 gauss/ cm. is provided by a set of superconducting coils, B. A measurement is made by reversing the current in the Maxwell coils, thus reversing the gradient, and measuring the change in the vertical force, using a Cahn Electrobalance. This method has the advantage that most forces that are not odd powers of the gradient coil current cancel out in the subtraction. Instead of using measured values for the field, the gradient, and the microbalance calibration, the apparatus was standardized by measuring several "pure" Au samples and comparing with the results of Hurd.[74, 93]

Thermometry was provided by a carbon resistor and a platinum resistance thermometer mounted on the copper block, C. These were calibrated by measuring the magnetization of crystals of chrome

potassium alum, which is known to obey a Brillouin function, [94] and by comparison at zero field with a calibrated germanium thermometer. Since the calibration provided by the manufacturer of the platinum resistance thermometer agreed with these measurements, that calibration was used.

The sample was mounted in a gold plated copper bucket, D, which is thermally connected to the copper block, C, by exchange gas. As shown in Figure 39, the sample space, H, is surrounded by an inner helium space, G, which is isolated from the magnet helium space, F, by a vacuum space, E. Temperatures from 1.4 to 4.2 K were obtained by pumping on the inner liquid helium with a Welch Duo Seal Pump and a CVC Booster diffusion pump. To raise the temperature, there is a heater wound on the copper block. The temperature is regulated by feeding the output of the temperature measuring potentiometer to the regulating circuit of the heater current supply.

A more detailed description follows.

B. Uniform Field H_0

The uniform field is provided by a Westinghouse superconducting solenoid. It takes approximately 12 liters of liquid helium to cool the magnet and provide enough liquid for a 10 hour run. The solenoid is powered by a Magnion CFC-100 power supply.

The maximum field is approximately 50 kilogauss, and the current constant is given by Westinghouse as 52.7 $\pm$ 1% amperes per 50 kilogauss. Field uniformity is quoted as 0.1% over a 1cm. axial distance.

During operation, it was assumed that the field was accurately given by the product of the current constant and the magnet current. The 1% uncertainty in the current constant only affects the value of the field. Since the magnetization of any sample is obtained by comparison with the "pure Au" samples, the important point is that the constant must really be a constant. As will be discussed in a later section, several samples were run more than once. The repeatability of the data indicates that the current constant did not vary from day to day, and the linearity of high temperature magnetization curves as a function of field indicates that the current constant is independent of current. The Westinghouse value for the current constant was checked by field measurements with a Grassot fluxmeter. The measurements are no more accurate than 1%, so they only check that nothing in the apparatus effects the value of the field.

Before taking data the field was run from 0 to 50 kilogauss and back at least twice. This was done to train the field. With the power supply turned off, a field of the order of 100

gauss remained in the magnet. It appeared that this residual field was reproducible, but no attempt was made to correct for it.

A 1 milliohm standard resistance was put in series with the solenoid and the voltage across the resistor is a measure of the magnet current. For currents greater than 5 amperes it was possible to maintain the voltage across the shunt to within 0.1%. Below these currents, the leakage current through the transistors in the power supply caused a larger variation in the current.

All data was taken with the solenoid in the persistent current mode. This was necessary since the noise in the power supply output caused a noticeable variation of the force on the sample, when operated in the normal mode. The field was changed at the rate of 10 kilogauss/minute. The current was allowed to remain at the new value for at least one minute before returning to the persistent current mode. This was much longer than the time constant (3 sec.) for the solenoid and the shunt, so all of the current should have been passing through the solenoid. Returning the solenoid to the normal mode and waiting for a longer time before returning to the persistent mode, never had any noticeable effect.

C. Gradient Field

The gradient coils are mounted on the insert. (Refer to Fig. 39) The bottom part of the insert is a stainless steel

tube, 1 7/8" in diameter and 9.1" long. Two brass spacers, J, are soldered to the tube, so that it is centered within the main magnet. An epoxy cylinder was formed upon 1, and machined on a lathe to provide a form for the gradient coils. This allows an accurate form to be made, and since this tube is removable it is possible to change gradient coils. The center of the gradient coils has to be aligned with the center of the large magnet. The procedure is to machine the form so that the center of the gradient coils corresponds to the position of the solenoid center (37 1/8" from top), on purely geometric grounds. Measurements are then performed to see if the centers are aligned , as follows. At the center of the gradient coil with the main solenoid off there is no field, therefore the force is zero. At the center of the main solenoid $\frac{\partial H}{\partial z}$ and there is no force with the gradient coil current off. By moving a sample from one of the zero force positions to the other the distance between the centers of the two fields can be measured. A brass washer, K, is provided at the top of the insert. After removing the insert, the brass washer can be machined to bring the centers into alignment.

Only one set of gradient coils was made. Each coil was circular, with a square cross section 11 turns by 11 turns to provide a total of 121 turns. The wire used was 7.5 mil NbTi

with copper cladding and Formvar insulation. The dimensions of the coils were taken from a chart in Zijlstra.[92]

Dr. Gordon Knapp suggested that performance would be improved if the radius of the gradient coil was small. This proved to be the case, since an earlier effort with the maximum possible coil radius gave results which were not reproducible. Although these earlier difficulties might have had another cause, results were much improved after the system was rebuilt with the smaller coil.

The smallest convenient inner diameter for the coil is 7/8". For a square coil, 11 x 11 turns of 0.0075" wire, the dimensions corresponding to symbols of Fig. 40 are $2d = .0825"$, $\rho_o = \rho_i + d = .442" + .041" = .483"$, $d/\rho_o = \frac{.041}{.483} = .085$. From the chart in Zijlstra $z_o/\rho_o = .863$ or $z_o = .417"$ or $2z_o = .834"$. Thus, the gradient is provided by two coils, of 121 turns each, with an axial separation of 0.834", as shown in Fig. 41. The position of the brass cap relative to the center of the main solenoid can be found by measuring the total length of the insert and subtracting 37 1/8", which is the distance of the center of the solenoid from the top of the insert. Since the center of the gradient should correspond to the center of the solenoid, the distance from the brass cap to the geometric center of the gradient coil is known. It is a matter of simple geometry to locate the position of the cuts in the epoxy form

relative to the brass spacer. The form is mounted in a lathe and a tool .084" wide is used to cut the form. The tool is positioned at the bottom of the brass cap and then moved the requisite distance to the first cut, using the lathe movement. It is quite easy to make a form with dimensions accurate to 0.001".

The brass spacers shown in Fig. 41, fit the inner diameter of the main solenoid to insure that the insert is centered and to prevent motion. The 1/16" cuts shown are for passing leads from the coils.

It was very difficult to wrap 11 turns of wire in the space provided, so the coil was modified to be 10 layers of 10 turns each. Using the equation on page 44 of Zijlstra, [92] the expected gradient is 53.8 I gauss/cm., where the gradient current I, is measured in amperes. This expected value agrees quite well with values obtained from the data on "pure" Au $\Delta F = \Delta m g = 2 \chi H_o \frac{\partial H}{\partial z}$ or $\frac{\partial H}{\partial z} = \frac{\Delta m g}{2 \chi H_o}$, where Δm and χ are for 1 gm of sample. $\chi = -14.28$ emu/gm and $\Delta m = 5.715 \times 10^{-3}$ gm/gm, when H=40 kG. Using g=980 cm/sec^2, $\frac{\partial H}{\partial z} = 481$ gauss/cm. while the theoretical value of $\frac{\partial H}{\partial z}$ when I=9 amps is 484 gauss/cm. This agreement is only an indication that the current constant of the main solenoid is correct. All data is relative to the value of "pure" Au, and no values for the

gradient are used. This will be discussed in greater detail in Section V E.

The gradient coils were wound turn-by-turn, with each turn alongside the previous one. Tension was maintained by hand, and each layer was painted with GE 7031 varnish. The two coils were wound separately, and then wired in series opposition and soldered to copper wires at a height such that the solder joints and superconductor would be below the helium level. The leads consisted of several copper wires in parallel to maximize thermal contact with the helium vapor, and are capable of carrying at least 20 amperes. The leads are brought out of the dewar through an octal feed-thru, L, as shown in Fig. 39.

The current used to energize the gradient coils is provided by a Hewlett-Packard 6264 B power supply. The circuit used to switch the polarity of the current is shown in Fig. 42.

The power supply operates as a constant voltage source until a preset current is reached, and the supply then switches to the constant current mode. The current limit is set with a 10 turn precision potentiometer, while the voltage is set with an ordinary single turn 13 KΩ pot. The 13 KΩ pot is mechanically coupled to an on-off switch by a cam, so that whenever the pot is turned to zero ohms the state of the switch is changed, which

switches the poles of the relay, thus switching the polarity of the current to the gradient coil. The zero ohm position on the voltage limiter corresponds to zero current. A high wattage resistor is used in series with the load so that the voltage output of the supply is approximately 9 volts. This is necessary, since the gradient coil and the leads to it have almost zero resistance. The current can be measured using a standard shunt with resistance $\frac{50 \text{ mv}}{30 \text{ amps}} = 1.667 \times 10^{-3} \Omega$ in series with the gradient coil.

This curcuit operated remarkably well. From day to day there were very slight changes required in the setting of the current limiter, rarely exceeding 0.3%, while changes during any single day were usually not necessary. No ripple or other power supply noise was ever a factor.

D. Microbalance

The force on the sample is measured with a Cahn RH Electrobalance with a resolution of 2 micrograms. Details of the mounting are shown in Fig. 43. A vertical aluminum plate, A, is supported by an aluminum frame built on a table. Two thick rods, B, are mounted on the aluminum plate, A. They are set parallel with each other and form a vertical track. A movable plate, C, is fixed to this track. A threaded rod with

20 threads per inch is fixed to the plate C and is also passed through a threaded piece, D, which is fixed to the plate, A. The result is that the position of the movable plate, B, is controlled by turning the rod. A lathe movement, E, is fixed to the movable plate, C, in such a way that its two degrees of freedom are in the horizontal plane. The microbalance is attached to the lathe movement. Vertical motion of the plate, C, and horizontal motion of the lathe movement allow accurately controlled positioning of the microbalance in three dimensions. There is a copper bellows between the microbalance and insert, which allows several inches of motion. The vertical motion is sufficient so that there is clearance to remove the insert from the magnet and then remove the magnet itself, without demounting the microbalance.

Before discussing the importance of adequate mounting of the balance and various sources of noise, a brief explanation of the microbalance operation will be supplied. The arms of the balance are connected to a DC motor, which in operation provides the proper torque to maintain the balance arms in a fixed position. The output of the balance is the voltage, which is caused by the motor current flowing through a fixed resistor, after it has been reduced by various voltage dividers and an offset voltage has been added or subtracted. The proportionality constant between the forces applied to the balance arms and the voltage output will be called K_B.

Since the various controls, which condition the output voltage so it can be conveniently measured, also change the value of K_B all data was taken with the same control settings. A more important source of change in K_B, results from a tilt of the balance mounting. This tilt causes a change in the angle between the balance arms and the forces exerted on it, causing a corresponding change in the torques produced by these forces. An angular change of a little more two degrees is needed to change the calibration constant by 0.1%, but since there was usually an unbalance of about 35 milligrams between the masses of the balance loads, the change in the calibration constant produces significant change in the signal due to this unbalance. Since data is taken by measuring the difference between the force with positive and negative gradient, the latter effect is important only if a tilt occurs during the one minute interval between the two readings. The mounting of the balance is sufficiently rigid so that the only sources of tilt are long term motions of the building or direct blows to the apparatus. Unfortunately, such motions effect the balance calibration constant, and subtle shifts from day to day would be difficult to detect. Two degrees is a large angle and it is unlikely that the constant would vary by the corresponding 0.1%, but there is no simple way to verify the angular shifts directly.

Besides mounting the balance as rigidly as possible, the balance was disturbed as little as possible when the data to be reported was taken. Samples were changed through a port in the side of the insert as shown in Fig. 39. Since the same suspension was usually used, it was only necessary to make small changes in the vertical position of the balance. Fortunately, while this series of measurements was in progress, it was never necessary to remove the insert.

There is another type of noise that depends upon how well the microbalance is mounted. Any vibrations transmitted to the balance through the mounting appear as noise. The most important such noise is due to coupling of pump vibrations into the system. The electronics of the balance is equipped with filters, which ideally remove the sinusoidal noise without effecting the DC signal. If the meters used to measure the balance output have finite input resistance, there will be a loading effect depending upon the filter used. A Medistor microvoltmeter was used in all measurements reported and a Hewlette-Packard 7001 X-Y recorder was used to check noise levels when setting up for a run. The balance was used with Filter No. 2, which has a time constant of 0.35 sec. In this mode a sinusoidal noise of approximately 4 micrograms peak-to-peak was evident on the recorder, but

the frequency (8cps.) was too high for the microvoltmeter to follow.

There are also noises caused by different combinations of temperature and pressure in the sample space. The most troublesome of these is a sinusoidal oscillation of period 30 - 60 seconds. This period is very nearly the interval between the force measurements with positive and negative gradient, and resultant error will be nearly equal to the amplitude of the oscillation (about 10 micrograms). Under some conditions there would be spikes in the balance output. These were all eliminated by setting the exchange gas pressure to 2 mm. when the temperature was 4.2 K.

A minor irritation was the appearance of occasional spikes at all temperatures and pressures. No explanation was ever found for this noise, which only appeared occasionally.

It is very difficult to verify that the microbalance has full sensitivity, but some attempts were made. Repeated measurements were made on a 50 mg. calibration mass. This is a good way to check the calibration constant of the balance, but it is not good enough to check that the balance will respond to small changes in mass. The values obtained for the calibration constant in measurements a year apart agree to better than 0.1%. This was at a time when no precautions were taken about moving or positioning the balance. Recordings of the balance output were made as a liquid on the balance pan was evaporating. The

recorder trace was always continuous with no sign of a dead zone, but the liquids used always evaporated too fast to provide a real good test of sensitivity. The best test of balance operation is to measure the magnetization of a sample, since very small forces can occur. All data appears to be consistent and reproducible. The good comparison possible between a series of samples run on different days, indicates that no important change in the balance calibration occured. Small changes in the forces to be measured could be provided by a small change in the gradient current. Such tests indicate that the balance did indeed have the sensitivity to measure small differences in force.

E. Standardization

Instead of calibrating the balance output to be in dynes or grams, andusing measured values of the fields to calculate M from the force, a single constant which relates the balance output, V, in volts to M, in emu was found. Essentially a sample with known magnetization is run and all other measurements are comparisons with the known sample. If a sample with known magnetization, M in emu/ gm, and mass m, produces a balance output, V, the force on the sample is $F = K_B V = m M \frac{2H}{2Z}$, where K_B converts the balance output to dynes. The current constants of the main solenoid and of the gradient are represented by K_H and K_G, while the currents are I_H and I_G . The force can now be rewritten as $F = K_B V = m M K_G I_G$. If K_I is identified with $K_B / K_G I_G$ the relationship between the magnetization and the balance output is $m M = K_I Y_I$ where K_I does depend on the

gradient current, which was 9 amperes when this series of measurements was made. If a sample with known magnetization independent of field was measured, K_I could be determined independently of K_H, and measured values of K_B would be sufficient to accurately determine K_G. There is no great advantage in this extra knowledge.

Two samples of nominally pure Au were measured as the known samples. Comparison of the data obtained with measurements by Hurd [74] on AuFe alloys and comparison with other AuFe measurements reported in this thesis, indicate the Fe concentration in these "pure" samples to be approximately 10 and 20 ppm. There is a less than 1% variation of the susceptibility of these samples from about 60 K to room temperature, in agreement with data obtained by Hurd for a sample with 15 ppm Fe. K_I can be found to an accuracy better than 2% by equating the values for the "pure" Au samples found by extrapolating the data to higher temperature, where the value for pure Au is approached, with the value of $-(14.31 \pm .05) \times 10^{-8}$ emu/gm found by Hurd for pure Au. The result is $K_I = .9924 \times 10^{-3}$ emu/mv. Magnetization was found by using $M = \chi H = \chi K_H I_H$, where the value of K_H quoted by Westinghouse was assumed correct. The uncertainty in the value of K_H accounted for the main part of the 2% error quoted for K_I. The value of K_I is confirmed by measurements on Rh, Pd, and W.

F. Sample Positioning and Reproducibility

Since the field and gradient are functions of position, the reproducibility of the data depends on how well the sample position can be repeated and how strongly the force varies with position. All data was taken with the sample in the center of the gradient. This point is easily found, since the field due to the gradient coil vanishes at this point. If the main field is not turned on, there is no field and the force at this point vanishes. As the sample is moved from this point, the field due to the gradient coils increases and there will be a change in the force on the sample when the gradient is changed from zero to some value. Most samples can be positioned within $\mp$ 0.006". For those samples with vanishing susceptibility at 4.2 K., the field must be turned on and the point where the force is a maximum used.

Several runs were made to study the reproducibility of data and the effects of varying the position of the sample. A sample of nominally pure gold was measured on three different occasions. The largest deviation in the magnetization at 4.2 K. was 0.11%. Similar results were found at 1.4 K. and higher temperatures, although the amount of data is not as extensive. On a fourth occasion an attempt was made to change the sample, while the sample space was at 4.2 K. The sample gained a great deal of weight indicating that air had gotten into the sample

space. At low tempratures the magnetization of this sample is much larger than the other runs, but above 77 K. there is agreement.

The conclusion to be drawn from this, is that with proper care, samples can be remounted and repositioned without introducing any significant errors due to location of the sample in the field or due to dirt on the sample. When running several samples in a day, it is difficult to change samples without introducing oxygen unless the dewar is warmed up. The data to be reported was taken by running a sample every other day and allowing the dewar to warm up to room temperature before changing samples.

To check the variation of force with position a AuFe alloy with a nominal Fe concentration of 400 ppm. was run. This was a poor choice, since the magnetization of this alloy is strongly temperature dependent, and it is difficult to separate effects due to changing temperature with those due to changing position. At 4.2 K. and 30 kG the force on the sample was measured as a function of horizontal position as the sample was moved over the entire range available to it. To check on the temperature effects, the sample was returned to the center position to check on possible variation of the force. The measurements indicate a 0.3% change when the sample is moved over the entire available range, while the force at the center

changes by 0.1%. Over the region where the sample would normally be located (a circle of 0.040" diameter) there was a 0.1% variation. The sample was usually centered with much greater accuracy, by moving the sample from one end of the sample space to the other. It is obvious from the microbalance output when the sample is touching the walls of the sample space. By taking the total distance traveled in moving from wall to the other and moving back $\frac{1}{2}$ this distance, the center is located quite accurately.

In a similar fashion a profile of the force as a function of vertical position was taken. At 20 and 40 kG there is less than 20.1% variation of the force with a $\pm$ .006" axial movement about the center of the gradient coil. Since we can easily reproduce the position of the sample within this accuracy, this source of error will be less than 0.1% of the magnetization.

G. Thermometry and Temperature Control

A removable tube, M, is mounted in the sample space. The upper part is thin walled stainless steel, while the bottom 6 inches are of OFHC copper. The bottom section is capped with a 1/2" thick plug of OFHC copper, in which a carbon and a platinum resistance thermometer are mounted. One side of each is connected to the copper to provide electrical and thermal contact.

The thermal contact is further improved by mounting the thermometers in holes in the copper block.

The resistance of the thermometers is measured using a 4-terminal method. Since one side of the thermometers is common, only 6 leads are needed. The voltage and current leads are number 40 copper wire. There is a demountable connector, N, at the top of the insert, so the tube may be easily removed. The leads are brought out of the dewar through a hermetically sealed connector, P, and a cable connects them to a thermometer panel.

The thermometer panel performs several functions. A 9.45 volt battery plus a set of resistors which may be placed in series, provide 7 current ranges. A 1000 ohm standard is also in series so that the current can be measured. A switch allows the selection of thermometer or a decade resistance. Other switches permit reversing the thermometer voltage and current. The thermometer voltage is measured with a Leeds and Northrup K3 potentiometer and a Leeds and Northrup null detector. A measurement is made by adjusting the potentiometer until the null detector reads null. The decade resistor is then substituted for the thermometer and adjusted until the decade matches the thermometer.

Temperature is controlled by using the output of the null detector as an error signal to control the output of a H-P 6200 B power supply, which provides current to a heater wound on the copper block.

Cooling below 4.2 K is accomplished by pumping on the liquid helium in the helium space. From 4.2 to 10 K, a small amount of helium gas provides a thermal link with the liquid helium in the magnet space. Above 10 K, the exchange gas is pumped out of the helium space and only a weak thermal link to the liquid helium in the magnet space is provided through the spacers used to ceter tube 3 in 2.

Since there is no access to the inner helium space for a transfer tube, helium gas must be condensed in this space. By connecting the inner space to a helium gas supply with several pounds overpressure for five minutes, enough liquid helium can be condensed for several hours pumping.

The thermometers used were a platinum resistance supplied by Rosemont Engineering and an Allen-Bradley carbon resistor. The platinum resistance, which was supplied with a calibration, was used for temperatures above 40 K, while the carbon, which was used for the range 1.4 K to 10 K had to be calibrated. The thermometers also cover the intermediate range and were calibrated in this region, but very little of the data to be reported was taken in this temperature range. The calibration was performed bu substituting a calibrated Germanium thermometer for the sample. Actually two different calibrated thermometers had to be used to cover the entire range effectively.

In the 2 - 7 K range which both thermometers covered the results are in agreement. It was found that the calibration of the platinum resistance was in agreement with the calibration supplied by Rosemont, so that the latter calibration was used. Several samples of chrome potassium alum were measured. Since the susceptibility is known to follow a Curie law to very low temperatures, this provided a check on the thermometer calibrations. Since the thermometers were calibrated in terms of the temperature at the sample, there is no reason to worry about the possible temperature difference between the copper block and the sample. Measurements of the vapor pressure of the liquid helium coolant indicate that the liquid helium is consistently cooler than the sample at the lowest temperatures. The agreement between the platinum thermometer and sample temperature indicate that at higher temperatures there is no significant difference between the block and sample temperatures.

Data was taken with the resistance of the thermometer held fixed without trying to compensate for the magneto-resistance, except at 4.2 K where temperature was maintained by the liquid helium bath boiling at atmospheric pressure. Above 40 K this causes no error, but there is a significant magneto-resistance effect for the carbon thermometer. The magneto-resistance of the carbon thermometer was estimated from values

given by Neuringer and Shapiro.[95] At 1.4 K there will be about a 3% difference in the temperatures corresponding to a fixed resistance at 0 field and at 50 kilogauss. At 10 K the magnitude of the effect is reduced to about 1%. In these field ranges the magneto-resistance varies as the square of the field, so the error is much less in lower fields. In studies of the susceptibility, only low field data is used (at the lower temperatures) and the magneto-resistance error will not be important. Comparisons of the magnetization of various samples were made at fixed resistance or temperature, so there will be no effect on these comparisons. The only effect will be on studies of the magnetization as a function of both temperature and field.

VI. SAMPLE PREPARATION

A. General

A series of $Cu_{1-x}Au_x$(Fe) samples was prepared with Fe concentrations in the range 0-600 ppm. Five values of x, the atomic fraction of Au, were used, namely x = 0.05, 0.09, 0.17, 0.20 and 1.00.

The alloys were prepared from pure (99.999%) starting materials by melting in an argon atmosphere arc furnace with a water cooled hearth. All materials were cleaned before melting or annealing, the Cu in nitric acid, Au in aqua regia, and Fe in hydrocloric acid. Alloys of $Cu_{1-x}Au_x$ were electropolished in a solution of ammonium hydroxide and potassium cyanide in water. Drawings of the arc furnace and annealing apparatus, along with further details of sample preparation are contained in the thesis of R. Caton.[88]

An original AuFe alloy with about atomic 1% Fe was made, and then for each value of x a $(Cu_{1-x}Au_x)$Fe master was made by melting slices of the above AuFe alloy with appropriate amounts of Cu and Au. For each value of x, a $Cu_{1-x}Au_x$ master without Fe was made at the same time. For a given value of x, a series of samples was then made by melting together slices of the two masters in the correct proportion to give a particular Fe concentration. The materials for the 6 samples were loaded

into separate cups in the arc furnace hearth and melted in turn, starting with the most dilute Fe concentration. Similar settings of the furnace power supply and similar melting times were used. Usually, only 2 or 3 mg. difference in mass was observed before and after melting.

The data will be used in three types of comparison, which will be effected by the values of the concentrations. Neglecting the mass lost during melting and impurities introduced in the melting, the nominal concentrations can be calculated from the measured masses of the constituents. There is an uncertainty of $\pm 1\%$ in the mass of Fe in the original AuFe alloy, which will lead to an absolute error of 1.2% in the Fe concentrations of the CuAu samples, when compounded with a 0.2% error in the masses of the slices of CuAu masters. The absolute error effects comparisons with other published results. When comparing the results of measurements on alloys with the same value of x, only relative values of the concentrations are necessary. Since these alloys are made from the same $Cu_{1-x}Au_x$ masters, only uncertainties in the measurement of the masses of the slices of master contribute to the relative error. The largest uncertainty is 0.2%. If one concentration is taken to be correct the ratio of the other concentrations with that one is accurate to 0.2%. A similar argument is true for comparison

between Fe concentrations for alloys with different values of x. The error will be due to the 0.2% error discussed above and an error in the measurement of the mass of original AuFe alloy used to make the CuAu masters. Since this mass was large enough to make the latter error negligible, there is a 0.2% error in comparing Fe concentrations for alloys with different values of x. Of course, the mass lost in melting is of the same order as the total mass of Fe in the alloy, so that if Fe is lost preferentially, the above arguments are meaningless. However, magnetization measurements indicate that this is not the case.

Magnetization measurements of the nominally "pure" samples show the presence of Fe. The assumption that this Fe is in the starting material or that it is present in the "pure" master would lead to the addition of a constant background term for each concentration.

Several samples were run without annealing or with annealing times of several days. To varying degrees, these samples all exhibited a magnetic moment before the field was turned on, indicating the presence of undissolved Fe. Various annealing procedures were tried until the following procedure produced samples without a zero field moment.

The samples to be reported on were annealed for 8 days at 830° C in vacuum and then quenched in an iced brine solution.

The annealing apparatus consisted of a tube containing the samples, which was pumped on with a diffusion pump; surrounded by another space which was pumped on with a mechanical pump. After annealing, all samples were stored in liquid nitrogen except when being measured.

The first set of $CuAu_{17}$ alloys was cold worked before annealing and given only a 1 day anneal. One of these samples was then reannealed for 8 days with no significant change in the measured magnetization. As was shown earlier (See pg 57), there is a slight difference in the magnetic behavior of these samples and others which were not cold worked, but had the longer anneal. Since this slight difference was not noticed at the time, the inconvenient cold-working was replaced with the longer annealing time.

A more detailed description of procedures in making each set of samples will be given and any deviation from the above mentioned procedures pointed out.

B. $Cu_{.9497}Au_{.0503}$ alloy preparation

Only one set of six samples were prepared from the two $CuAu_{5.03}$ masters and were annealed together. These had nominal Fe concentrations in atomic parts per million of Fe of 0, 54.9, 89.8, 206, 324.6 and 436.3.

C. $Cu_{.91}Au_{0.09}$ Alloy Preparation

Two sets of samples were made from the same pair of $CuAu_9$ masters. The first set had six samples with nominal concentrations 0, 55, 90, 151, and 252 ppm of iron. They were melted and annealed as described above. A second set of three samples was later made and annealed with a set of $CuAu_{20}$ samples. These were to have concentrations of 291, 358, and 398 ppm of Fe. Magnetic measurements, which were discussed earlier, show that the concentrations were closer to 257, 352 and 467 ppm of Fe. No satisfactory explanation has been found for this descrepancy between planned and apparent Fe concentration. Since chemical analysis indicated that the composition of the CuAu host was the same as the rest of the series, the data for these samples was presented with the rest of the $Cu_{.91}Au_{.09}$ series. There is a difference in the magnetic behavior of the two sets of samples, which could be due to differences in preparation, differences in composition, or both.

D. $Cu_{.825}Au_{.175}$ Alloy Preparation

Two sets of $CuAu_{17.5}$ samples were made. The first set was made by diluting the original AuFe master with appropriate amounts of Cu and Au. Iron concentrations were 88, 185, 288, and 400.2 ppm. As previously discussed, this set of four samples was cold worked and annealed for only one day.

A second set of six samples was made from a pair of $Cu_{.825}Au_{.175}$ masters and heat treated in the usual manner. This set, which was melted and annealed in the usual fashion, had concentrations

of 0, 61.5, 127.1, 234, and 232 ppm.

E. $Cu_{.793}Au_{.207}$ Alloy Preparation

Three sets of alloys were made. Each of these sets was heat treated in the usual way. The first set was made from a pair of $Cu_{.793}Au_{.207}$ masters and had iron concentrations of 0, 18.5, 43, 93, 157 and 207 ppm. The second set was made from the same pair of masters. They were melted and annealed at the same time as the second set of $CuAu_9$ samples. Only the alloy with Fe concentration of 509 ppm was measured, since the other two stuck in the annealing tube and were therefore not rapidly quenched.

A third set of samples was made from the master of $Cu_{.793}Au_{.207}$(Fe) and a new $Cu_{.793}Au_{.207}$ master. Two samples with concentrations 289 and 246 ppm of Fe were measured.

F. Au Alloy Preparation

The original AuFe master was used to make a more dilute master. By diluting this master with more Au, samples with 61, 120, 185, 288, and 395 ppm of Fe were made. These were annealed, along with a "pure" gold sample, at 1000° C for 24 hours. Another "pure" sample was also made but not annealed.

VII. ANALYSIS OF DATA

A. Summary

Magnetization of each sample was measured at 1.4, 4.2, 9.5, 44, 77, and 100 K at fields of 0, 1, 2, 5, 10, 20, 30, 40, 45, and 50 kilogauss. For some samples measurements were made at several other temperatures and fields. After subtracting the magnetization of the copper bucket, fits of the magnetization at temperatures of 44 K and above to the form, $M = M_c + \chi H$, where H was 5 kilogauss or greater, yielded for each sample a value of M_c nearly independent of temperature. M_c was attributed to large clusters of Fe and subtracted from M. Two different methods were then used to analyze the data. For each Au concentration the magnetization and intial susceptibility were fit to a form $M(H,T) = M_0 + M_1 n_s + M_2 n_s^2$, where n_s is the concentration of single impurities, which was obtained from the high field susceptibility. The data was also analyzed by fitting data for each sample to the form of a constant plus Curie-Weiss terms. These analyses allowed for the presence of pairs (or larger groupings) of interacting Fe atoms as found in CuFe. A more detailed discussion follows.

B. Bucket Correction

The sample was held in a gold plated copper bucket while measurements were being made. The magnetization of the bucket was measured at most of the fields and temperatures used.

These values are listed in Table 36. The first step in any analysis of thedata was the subtraction of the bucket magnetization, M_B , from M' the measured magnetization. Data was then normalized by dividing by the sample mass.

C. Large Clusters

For all alloys containing Cu, at temperatures above 40 K and in fields of 5 kG or more, the sample magnetization was well described as a linear function of field with a non-zero intercept, i.e. (1) $M(H,T) = M_c + \chi(T)\, H$. Table 37 shows the values of M_c obtained for the various samples at different temperatures, by fitting data to the above expression, using the method of least squares. Although data at lower fields is not sufficient to find the dependence of M_c on H at fields below 5 kilogauss, it does indicate that there is a continuous decrease of M_c to zero as the field is reduced to zero. Any remanent moment is too small to be measured.

At lower temperatures the magnetization is no longer a linear function of field. Fits of the magnetization to polynomial functions of the field with more powers of H than above yield values of M_c of the same order of magnitude as those obtained from high temperature data. Combined with the lack of systematic temperature dependence above 40 K, this indicates that M_c is at most very weakly temperature dependent.

Further evidence that there is no large increase of M_C at lower temperatures is to be found in the low field data, which is inconsistent with any such increase.

The magnetization M_c is ascribed to superparamagnetic clusters. Such clusters are known to occur in CuFe [1, 14, 64, 82].

At temperatures above 40 K, these clusters are saturated by a field of 5 kG, while at lower temperatures even smaller fields will lead to saturation. Assuming that each Fe impurity in such a cluster contributes 2.2 μ_B, a calculation for the $CuAu_5$ alloy with 430 ppm of Fe shows that a total of 2 ppm of the Fe are involved in the clusters. This is about 0.5% of the Fe in the sample, and is obtained for one of the largest values of M_C.

Figure 44 is a plot of M_C as a function of nominal Fe concentration. There does not appear to be any systematic variation, except for a general increase as the concentration of Fe is increased. It would seem, therefore, that the amount of Fe involved in the clusters is a small part of the Fe in the sample and is an indication of how well the samples were prepared. Ideally, M_c would be zero, as it was for the AuFe alloys.

For each sample an appropriate value of M_C was selected and subtracted from the magnetization. Tables 3 through 6 give the values of magnetization after correction for M_C. Since M_C was zero for the AuFe alloys, this correction was not necessary for thedata in Table 7.

The main effect of M_C is that a great deal of additional data must be taken to determine it accurately. Instead of taking a measurement at a single field for each of the high temperatures, enough data must be taken to accurately find the zero field intercept of the linear magnetization curve.

D. Initial Susceptibility

At high temperatures where the magnetization is a linear function of field, the high field data can be used to find χ, but at low temperatures there is significant curvature of the magnetization curves and it is more difficult to obtain the low field slope. An attempt was made to make use of the high field data in such a determination by fitting the magnetization at a given temperature and at fields of 5 kilogauss or more to an expression of the following form

$$(2)\quad M(H) = \chi_1 H + C_3 H^3 + \cdots + C_9 H^9$$

At 9.46 and 4.2 K there is little difference in the coefficient χ_1 as the seventh and ninth powers of H are added. At the lowest temperatures, however, this is not a good representation of the actual curve, since χ_1 is usually less than the 5 kilogauss magnetization divided by the field, even though $\chi(H) \equiv M/H$ is expected to decrease as the field is increased. The value used for χ was $\chi(H)$ with H=2 or 5 kilogauss when that value was consistent with $\chi(10)$ and values of χ_1 from fits of the magnetization to formula 2. At4.2 and 9.46 K the

values of $\chi(5)$ and χ_1 are nearly the same (within 1%). Tables 3 through 7 also list the values of χ .

E. Separation of Pair and Single Impurity Magnetization

1. Determination of n_s

Using the same method Tholence and Tournier[17] applied to CuFe, the magnetization has been separated into terms due to single impurities and interacting pairs. Larger clusters of Fe atoms would be unobservable, unless there were some distinctive temperature or field dependence, since the concentration of these larger clusters is expected to be very small. If the pairs and single impurities are the dominant contributors to the magnetization, the impurity magnetization can be expressed as, (3) $M_{Fe} = M_s n_s + M_p n_p$ where M_s and M_p are respectively the single impurity and pair magnetization, while n_s and n_p are the single impurity and pair concentrations. Assuming that M_p saturates at fields near 50 kG, when the temperature is 1.4 K, the change in impurity magnetization from 45 to 50 kilogauss , ΔM_{Fe} would be due only to single impurities. The actual change in magnetization, ΔM , also includes a term due to the host magnetization, which is found from the ΔM of the "pure" alloy.

The temperature dependence of the initial susceptibility for the nominally "pure" samples indicates the presence of

some Fe impurity, as evidenced by a clear upturn at low temperature. Comparison with the data for the higher concentration samples gives an estimate for the concentration of Fe K , in the "pure" sample. The estimates of K varied from 4 to 5 ppm. for the various samples. The quantity, ΔM_{Fe} therefore depends not on the concentration of single impurities in the sample but on the difference in the concentration of single impurities in the sample and the concentration in the "pure" sample, i.e. (4) $\Delta M_{Fe} \equiv \Delta M_{Sample} - \Delta M_{"pure"} = \Delta M_S (n_s - K)$. This defines a linear relationship between ΔM_{Fe} and n_s. By using the nominal concentration for one value of $n_s - K$, all other values of the concentration can be determined.

This method of determining n_s introduces three types of error. There are uncertainties in the measurement of ΔM_{Fe}, an error due to assuming that one value of $n_s - K$ is the same as the nominal concentration, and a systematic error if the pair magnetization is not saturated. In the following paragraph only the uncertainty due to the measurement will be considered, leaving the others until more details of the analysis are presented.

Equation 4 can be rewritten in terms of the measured magnetization of a sample with Fe, M', the magnetization of the nominally pure sample, M'_o, the masses of these samples m and

m_o respectively, and the bucket magnetization, M_B. Thus, using subscripts to indicate the value of the magnetic field, equation 4 becomes (5)

$$\Delta M_{Fe} = \frac{(M'_{50} - M'_{45})}{m} - \frac{(M'_{o_{50}} - M'_{o_{45}})}{m_o} - (M_{B_{50}} - M_{B_{45}})\left(\frac{1}{m} - \frac{1}{m_o}\right).$$

Since m and m_o are very nearly equal, the term involving M_B cancels. The errors in the measured terms have three sources.

(i) Setting of fields and the measurement of the force introduce an uncertainty of 0.1% of the measured magnetization. This leads to a possible error of $.002M_{50}$.

(ii) There is an uncertainty of $\pm$ 0.2% $(M_{50}-M_{45})$ due to possible sample positioning errors.

(iii) Error due to non-reproducibility of tempratures for different runs. The temperature variation is probably less than 0.2%. Since the temperature dependence is only reflected in $M-M_o$, this leads to an uncertainty of $0.002(M-M_0)$. This is an overestimate based on the assumption that $(M'-M'_o)$ varies as $1/T$ instead of $1/(T+\theta)$ and neglects the decrease in temperature dependence at high fields. Thus the total uncertainty in ΔM_{Fe}, $e_{\Delta M_{Fe}}$ is then (6) $e_{\Delta M_{Fe}} = .002\, M'_{50} + .002[M'_{50} - M'_{45}] + .002\, \Delta M_{Fe}$.

Values of η_s calculated using equation 4 are listed in Tables 8 through 11. Table 8 also includes the various uncertainties calculated from formula 6 for the alloy with 5 atomic % Au. The uncertainties in η_s are on the order of 4 ppm for

the 100 ppm samples and increase to about 15 ppm for 400 ppm samples.

The concentrations found in this way are in substantial agreement with the nominal concentrations, except in the alloys with 5 and 9 atomic % Au, where there is a clear trend for n_s to be less than the nominal concentration as the nominal concentration is increased. This is the expected result if some part of the nominal concentration is in pairs of ferromagnetically coupled Fe atoms, causing a decrease in the concentration of single impurities.

2. Relation of n_p to n_s

One possible model to explain the formation of pairs, assumes that a pair is formed if any of "z" sites surrounding an impurity atom is occupied by another Fe impurity. If the further assumption that the alloys are random is made, the concentrations of single impurities, pairs and larger groupings can be calculated. The probability of the central site being occupied by an Fe impurity is c. The probability of the central site being occupied by an Fe impurity and all of the z nearby sites being occupied by host atoms is $c(1-c)^z$. The probability that the central site is occupied by an Fe atom is $c(1-(1-c)^z)$. For small c this is approximately zc^2. This is the probability of a larger grouping than single Fe atoms, but the probability of

groupings larger than pairs involves terms of at least the third power in c, so that in this approximation zc^2 is the probability of pairs. Since this expression counts each pair twice, the concentration of pairs is $\frac{1}{2} z c^2$.

Assuming that there are two types of magnetic entities, namely single impurities and pairs, depending on the occupation of the z nearby sites, the magnetization can then be separated in two contributions, (7) $M_{Fe} = M_s n_s + M_p n_p$. In formula 7, M_s is the magnetization of single impurities, M_p the magnetization per pair, $n_s = c(1-c)^z \approx c - zc^2$ the concentration of single impurities, and $n_p \simeq \frac{1}{2} zc^2$ the concentration of pairs. (If the possibility that half of the pairs are coupled antiferromagnetically and are not magnetic, is considered, z would be replaced by $\frac{1}{2}$ z in the above formulas.) Rewriting formula 7 with n_s and n_p replaced with the appropriate functions of c, gives (8) $M_{Fe} = M_s(c-zc^2) + M_p \frac{1}{2} zc^2 = M_s c + zc^2 (\frac{1}{2} M_p - M_s)$. Thus, if the magnetization is expanded as a function of concentration c, the coefficient of the c^2 term involves a combination of the magnetization of single impurities and pairs.

If the expression $n_s = c(1-zc)$ is solved for c, n_p can be expressed in terms of n_s . The results are $c \approx n_s + z n_s^2$ and $n_p \approx \frac{z}{2} n_s^2 + z^2 n_s^3$. For the values of z and n_s expected, the second terms is at most a 5% correction. The magnetization

can now be written as (9) $M_{Fe} = M_S n_s + M_p \frac{1}{2} z n_s^2$. If terms including n_s^3 wereincluded, the coefficient of that term would involve the difference of the magnetization per pair and the magnetization per triplet. It is possible that such terms do exist, but the difference in magnetization vanishes. In any case formula 9 was used to analyze the data, and no systematic deviations, which would indicate higher order terms, were observed.

The data were actually analyzed in terms of the expression $M = M_0 + M_1 n_s + M_2 n_s^2$. Since M is in emu/gm, M_1 is $\frac{M_s N_o}{m}$, and $M_2 = \frac{M_p N_o}{m} \frac{z}{2}$, where M_s and M_p have been previously defined as the magnetization per single impurity and the magnetization per pair, N_o is Avagadro's number, z is the number of sites defined above, and m is the molar mass of the alloy. Even if the previously discussed model of the pair formation is incorrect, the fact remains that the formula does describe the data with the concentration of pairs proportional to n_s^2 .

3. Determination of pair spin and concentration

If M_2 can be saturated, the saturation magnetization and the Curie constant, C, found from fitting $\chi_2 = \frac{C}{T+\theta}$, can be used to find the concentration and spin of the pairs. The

formulas to be used are as follows:

$$(10) \quad \left[M_2 n_s^2\right]_{Sat.} = \frac{M_{P_{sat}} N_0}{m} n_p = \frac{g \mu_B S_{P_{pair}} N_0}{m} n_p$$

$$(11) \quad C n_s^2 = \frac{g^2 \mu_B^2 S(S+1)}{3k} \frac{N_0}{m} n_p .$$

The values listed in Table 23 were found in this fashion. There are uncertainties in the Curie constant, but the major source of uncertainty is in the determination of the saturation magnetization, since our analysis assumes that the pair magnetization is saturated to find the concentration of single impurities. The uncertainties listed in Table 23 are due to uncertainties in the measured magnetization, which are reflected as uncertainties in C and the saturation magnetization. Before discussing these uncertainties we would like to consider the effect of changing n_s by a single multiplicative factor. This is the type of error mentioned in E 1 which is caused by setting one value of ($n_s - K$) equal to $c_{nom.}$ in the determination of n_s . From equations 10 and 11 it can be seen that this type of error does not affect the value of the spin, but as would be expected causes an error twice as large in values of z if $n_p = \frac{1}{2} z n_s^2$.

4. Effect of measurement errors on separation

In this section we will show how we traced the uncertainties in the measured magnetization of the sample with Fe and the magnetization of the pure sample into the uncertainties in the coefficients M_1 and M_2. Let M' be the measured magnetization of the sample, this includes the bucket magnetization and any magnetization due to clusters. There are three major sources of error in the measurement of M'.

(i) The resolution of the microbalance is .002 μ gm and there is an additional .002 μgm of noise.

(ii) The uncertainty in reproducing the fields introduces an uncertainty of 0.1% M'.

(iii) The force on the sample depends upon the position in the fields. Thus when comparing data for two different runs there is an uncertainty of 0.2% M'.

The impurity magnetization, M_{imp}, is obtained by subtracting the bucket magnetization, the cluster magnetization, and the host magnetization. Since the bucket magnetization was also subtracted from the data for a nominally pure sample to obtain the host magnetization, the errors in the bucket magnetization tend to cancel. The uncertainty in the impurity magnetization is then the sum of the errors in M' discussed previously and the estimated uncertainties in M_c, the cluster

magnetization, and M_H, the host magnetization. There is also an uncertainty caused by possible variations in the temperature for different runs. Assuming the impurity magnetization varies as 1/T, this error would be 0.2% M_{imp}.

Putting these terms together and including the uncertainty in η_s, the uncertainty in the impurity magnetization per ppm single impurity, e_{M_{imp}/η_s} can be found from formula 12.

$$(12) \quad e_{\frac{M_i}{\eta_s}} = \frac{.0015\ M'}{\eta_s} + \frac{.002}{\eta_s} + \frac{e_{M_c}}{\eta_s} + \frac{e_{M_H}}{\eta_s} + \frac{M_i}{\eta_s}\left(.001 + \frac{e_{\eta_s}}{\eta_s}\right).$$

At low temperatures e_{M_c} and e_{M_H} are much smaller than the other terms.

To find the effect of these uncertainties on the coefficients M_1 and M_2, plots similar to those of Fig. 4 were made at various temperatures and fields. Because of the large uncertainty caused by the concentrations, it is possible that there is curvature in the plots, which would indicate the presence of higher order terms in the expansion of the magnetization as a function of concentration. If this possibility is disregarded, errors in

the concentration will then change the slope of all the plots for various fields and temperatures in the same manner, so that the important variation in the slope is due only to the uncertainty in the magnetization measurements. The uncertainties in M_1 and M_2 are thus found from the values of the slope and intercept of the straight lines with the largest and smallest slopes consistent with the magnetic error bars.

5. Effect of systematic error in n_s if pairs are not saturated

As discussed previously, there is a systematic error in the values of n_s if the pair magnetization is not saturated. To derive formula 4, it was assumed that the magnetization per pair is saturated so the high field susceptibility is due only to single impurities. Labeling quantities obtained by assuming M_p saturates with primes, while the actual values are left unprimed, the following equations can be written for ΔM_{Fe}, the change in high field magnetization used to find n_s,

$$(13)\quad \Delta M_{Fe} = \Delta M_s' n_s' \quad \text{and} \quad (14)\quad \Delta M_{Fe} = \Delta M_s n_s + \Delta M_p \tfrac{z}{2} n_s^2.$$

Since the measured quantity ΔM_{Fe} is the same in both cases and $\Delta M_S \approx \Delta M_S'$, $n_s' \simeq n_s + \frac{z}{2}\frac{\Delta M_p}{\Delta M_s} n_s^2$. This formula can be inverted to find

$$n_s \approx n_s' - \frac{z}{2}\frac{\Delta M_p}{\Delta M_s} n_s'^2.$$

Since $M_{Fe} = M_s n_s + \frac{z}{2} M_p n_s^2$, $(15)\quad M_{Fe} \approx n_s' M_s + n_s'^2 \frac{z}{2}\left(M_p - \frac{\Delta M_p}{\Delta M_s} M_s\right)$.

This formula shows that the main effect of the systematic error in the concentration of single impurities is to couple the magnetization per pair and the magnetization per single impurity in the coefficient of the second term. Estimates using the data of Tholence and Tournier[17] to find ΔM_P and the data reported in this thesis to find ΔM_S, indicate that these two quantities are nearly equal for all concentrations of Au in the host (for this range of field and temperature). There is a large uncertainty in these estimates, since most data on the pair magnetization come from such a separation.

Fortunately in the copper rich alloys, the temperature dependence of M_P is quite different from that of M_S. In the temperature range of interest M_P is much bigger than M_S, so the separation procedure used is valid. As Au is added to the host the Kondo temperature of the single impurity term decreases and the temperature dependence of M_p and M_S become similar. Since M_P is caused by a moment with higher spin than the single impurity, M_P starts to saturate before M_S. This could cause the coefficient of the n_s^2 term to decrease as the field is increased. Since this type of behavior was observed in $Cu_{0.83}Au_{0.17}$ alloys, it is possible that the decrease in magnitude of this coefficient is not due to the decrease in the number of pairs, but is instead due to the systematic error

discussed here. To check the results of this separation, an alternate method of analysis was also used.

F. Analysis as a Function of Temperature

The single impurity susceptibility in most alloys is usually fit to a temperature independent term plus a Curie-Weiss term, while the pair susceptibility usually fits a single Curie-Weiss term. If there are no pairs or other interactions the initial susceptibility should be a linear function of Fe concentration, but if there are pairs the additional Curie-Weiss term should have a Curie constant which varies as the square of the concentration. By fitting the initial susceptibility to the form (16) $\chi = \chi_0 + \frac{C_1}{T+\Theta_1} + \frac{C_2}{T+\Theta_2}$, the results of the previous analysis can be checked.

REFERENCES

1. A. J. Heeger, in "Solid State Physics" (F. Seitz, D. Turnbull, and H. Ehrenriech, eds.) Vol. 23, Academic Press, New York, 1969.

2. A.M. Clogston, B.T. Matthias, M. Peter, H.J. Williams, E. Corenzwit, and R.G. Sheofwood, Physical Review 125, 541 (1962).

3. J. Friedel, Can. J. Phys. 34, 1190 (1956); Nuovo Cimento (Suppl.) 7, 287 (1958), in "Metallic Solid Solutions" (J. Friedel and A. Guinier, eds.). Benjamin, New York, 1963.

4. P.W. Anderson, Physical Review 124, 41 (1961).

5. J. Kondo, Progr. Theoret. Physics (Kyoto) 32, 37 (1964).

6. M.D. Daybell and W.A. Steyert, Rev. Mod. Physics 40, 380 (1968).

7. See for instance ref. 38.

8. For example see: L.B. Welsh and J.E. Potts, Phys. Rev. Letters 26,1320 (1971), J.B. Boyce and C.P. Slichter, Phys. Rev. Letter 32, 61 (1974); or P.Steiner, W.V. Zdrojewski, D. Gumprecht, and S. Hufner, Phys. REv. Letter, 31, 355 (1973).

9. M.D. Daybell and W.A. Steyert, Phys. Rev. Letters 18, 398 (1967).

10. M.D. Daybell and W.A. Steyert, Phys. Rev. 167, 536 (1968).

11. R.B. Frenkel, N.A. Blum, B.B. Schwartz, and D.J. Kim, Phys. Rev. Letters. 18, 1051 (1967).

12. M.A. Jensen, A.J. Heeger, L.B. Welsh, and G. Gladstone, Phys. Rev. Letters 18, 997 (1967).

13. A.J. Heeger, L.B. Welsh, M.A. Jensen, and G. Gladstone, Phys. Rev. 172, 302 (1968).

14. D. Golibersuch and A.J. Heeger, Phys. Rev. 182, 584 (1969).

15. B. Dreyfus, J. Souletie, J.L. Tholence, and R. Tournier, J. Appl. Phys. 39, 846 (1968).

16. P. Monod, Phys. Rev. Letters 19, 113 (1967).

17. J.L. Tholence and R. Tournier, Phys. Rev. Letters 25, 867 (1970).

18. V. Jaccarino and L.R. Walker, Phys. Rev. Letters 15, 258 (1965).

19. K.C. Brog and Wm. H. Jones, Jr., Phys. Rev. Letter 24, 58(1970).

20. M.P. Sarachik and G.S. Kanpp, J. Appl. Phys. 40, 1105 (1969).

21. J.W. Loram, T.E. Whall, and P.J. Ford, Phys. Rev. B 2, 857 (1970).

22. W.C. Delinger, W.R. Savage and J.W. Schweitzer, Phys. Rev. B 7, 1066 (1973).

23. E.W. Fenton, Phys. Rev. B 7, 3144 (1973).

24. A.A. Abrikosov, Soviet Physics Uspekhi 12, 168 (1969).

25. J. Kondo in "Solid State Physics" (F. Seitz, D. Turnbull, H. Ehrenreich, Eds.) Vol. 23, p. 183, Academic Press, New York, 1969.

26. The Entire Contents of "Magnetism" (G. T. Rado and H. Suhl, Eds.) Vol. 5, Academic Press, New York, 1973, is devoted to this problem.

27. G.J. van den Berg, in "progress in Low Temperature Physics" (G.J. Gorter, Ed.) Vol. IV, p. 194, North Holland Publishing Co., Amsterdam, 1964.

28. E.C. Stoner, Rep. Progr. Phys. 11, 43 (1948).

29. J.R. Schrieffer, J. Appl. Phys. 38, 1143 (1967).

30. J. Kondo, Prog. Theor. Phys. 28, 846 (1962).

31. J.R. Schrieffer and P.A. Wolff, Phys. Rev. 149, 491 (1966).

32. K.D. Schotte, Z. Physik 235, 155 (1970).

33. M.P. Sarachik, E. Corenzwit, and L.D. Longinotti, Phys. Rev. A 135, 1041 (1964).

34. A.A. Abrikosov, Physics 2, 5 (1965).

35. Y. Nagaoka, Phys. Rev. A 138, 1112 (1965).

36. H. Suhl and D. Wong, Physics 3, 17 (1967).

37. H. Suhl, Phys. Rev. A 138, 515 (1965); Physics 2, 39 (1965); Phys. Rev. 141, 483 (1966).

38. K.D. Schotte, Z. Physik 230, 99 (1970).

39. G. Yuval and P.W. Anderson, Phys. Rev. B 1, 1522 (1970).

40. D.R. Hamann, Phys. Rev. Letters 23, 95 (1969).

41. P.W. Anderson, G. Yuval, and D.R. Hamann, Phys. Rev. B 1, 4464 (1970).

42. K.D. Schotte and U. Schotte, Phys. Rev. B 4, 2228 (1971).

43. D.J. Scalapino, Phys. Rev. Letters 16, 937 (1966).

44. K. Yosida and A. Okiji, Progr. Theor. Phys. (Kyoto) 34, 505 (1964).

45. C.S. Ting, Physics Letters 32 A, 21 (1970); J. Phys. Chem. Solids 32, 395 (1971); Phys. Rev. B 4, 904 (1971).

46. W. Brenig, J.A. Gonzalez, W. Götze, and P. Wolfle, Z. Physik 235, 52 (1970).

47. W. Brenig and W. Götze, Z. Physik 217, 188 (1968).

48. W.Götze and P. Schlottmann, Solid State Comm. 13, 17 (1973).

49. P.W. Anderson and G. Yuval in "Magnetism" (G.T. RAdo and H. Suhl, Eds.) Vol. 5, Academic Press, New York, 1973.

50. S. Alexander and P.W. Anderson, Phys. Rev. 133, A. 1594 (1964).

51. D.J. Kim, Phys. Rev. B 1, 3725 (1970)

52. B. Caroli, J. Phys. Chem. Solids 28, 1427 (1967).

53. T. Moriya, Progr. Theoret. Physics (Kyoto) 33, 157 (1965).

54. M.A. Ruderman and C. Kittel, Phys. Rev. 96, 99 (1954).

55. K. Yosida, Phys. Rev. 106, 893 (1957).
T.Kasuya, Prog. Theoret. Phys. (Kyoto) 16, 45 (1956).

56. W. Marshall, Phys. Rev. 118, 1519 (1960).

57. M. W. Klein and R. Brout, Phys. Rev. 132, 2412 (1963).

58. W. Klein and L. Shen, Phys. Rev. B 5, 1174 (1972).

59. J. Souletie and R. Tournier, J. of Low Temp. Physics 1, 95 (1969).

60. J.A. Blackman and R.J. Elliott, J. Phys. C 2, 167 (1969).
Y. Karata, Progr. Theor. Phys. (Kyoto) 45, 50 (1971).
See Reference 61 for further references and discussion.

61. Y.C. Tsay and M.W. Klein, Theory of the Many-impurity Kondo Effect of Weakly Interacting Impurities. (to be published).

62. J.E. van Dam and G.J. van den Berg, Phys. Stat. Sol. (a) 3, 11 (1970).

63. J.M. Franz and D.J. Sellmyer, Phys. Rev. B 8, 2083 (1973).

64. H.E. Ekström and H.P. Myers, Phys. Kondens, Materie 14, 265 (1972).

65. J. C. F. Brock, J.C. Ho, G.P. Schwartz, and N.E. Phillips, Solid State Comm. 8, 1139 (1970).

66. W.M. Star, B.M. Boerstoel, and C. von Baarle, J. Appl. Phys. 1152 (1970).
W.M. Star and G.J. Nieuwenhuys, Phys. Letters 30A, 22 (1969).

67. B. Window, J. Phys. C: Metal Physics Suppl. 3, S 323 (1970).

68. S.J. Campbell, P.E. Clark, and P.R. Liddell, J. Phys. F: Metal Physics 2, L 114 (1972).

69. E.C. Hirschkoff, M.R. Shanaberger, O.G. Symko, and J.C. Wheatley, Phys. Letters 34 A, 341 (1971).

70. R.J. Borg and T.A. Kitchens, J. Phys. Chem. Solids 34, 1323 (1973).

71. J.W. Loram, T. E. Whall, and P.J. Ford, Phys. Rev. B 2, 857 (1970).

72. V. Canella, J.A. Mydosh, and J.J. Budnick, J. Appl. Phys. 42, 1689 (1971).

73. J.L. Tholence and R.J. Tournier, J. Phys. Paris 32, 211 (1971).

74. C.M. Hurd, J. Phys. Chem. Solids 28, 1345 (1967).

75. C.M. Hurd, J. Phys. Chem. Solids, 30, 539 (1969).

76. J.W. Loram, A.D.C. Grassie, and G.A. Swallow, Phys. Rev. B 2, 2760 (1970).

77. H.G. Hoeve and D.O. van Ostenburg, Solid State Comm. 9, 941 (1971).

78. H. Claus, Phys. Rev. B 5, 1134 (1972).

79. P. Steiner, G.N. Beloserskij, D. Gumprecht, W.V. Zdrojewski and S. Hufner, Solid State Comm. 13, 1507 (1973).

80. R. Caton and M. P. Sarachik, Proceedings of the 18th Annual Conf. on Magnetism and Magnetic Materials, AIP Conference Proceedings (C. D. Graham, Jr. and J. J. Rhyne, eds.) No. 10, Part 1, pg. 791, 1972.

81. C. M. Hurd, Phys. Rev. Letters 18 , 1127 (1967).

82. P. M. Chaikin and M. A. Jensen, Solid State Comm. 8, 977 (1970).

83. S. Mishra and P. A. Beck, Phys. Stat. Solidi A 19, 267 (1973).

84. F. W. Smith, Magnetization of a Dilute Magnetic Alloy With Magnetic Interactions: ZnMn, (to be published).

85. A. I. Larkin and D. E. Kheml'nitskii, Soviet Physics JETP 31, 958(1970).

86. P. A. Beck, Metallurgical Transactions 2, 2015 (1971).

87. C. Kittel, "Introduction To Solid State Physics, 3rd ed.", pg. 217, John Wiley and Sons, Inc., New York, 1966.

88. R. Caton, Thesis, City University of New York, 1972.

89. W. M. Star, F. B. Basters, and C. van Baarle, in "Proceedings of the Eleventh International Conference on Low Temperature Physics", (J. F. Allen, D. M. Finlayson, and D. M. McCall, eds.), pg. 1250, University of St. Andrews Printing Department, St. Andrews, Scotland, 1969.

90. S. DeGennaro and E. Borchi, Phys. Rev. Letters 30, 377 (1973).

91. We would like to thank Dr. Gordon Knapp for making available to us the design details of a similar apparatus which he constructed. The basic operation of our equipment is based on his design.

92. H. Zijlstra, in "Selected Topics In Solid State Physics" (E. P. Wohlfarth, ed.) Vol. IX, John Wiley and Sons, Inc., New York, 1967.

93. C. M. Hurd, J. Phys. Chem. Solids 27, 1371 (1966).

94. L. J. Neuringer and Y. Shapiro, Rev. Sci. Insruments 40, 1314(1969).

FIGURE CAPTIONS

Fig. 1. Impurity magnetization plotted as a function of field for 325 ppm Fe in a $Cu_{0.95}Au_{0.05}$ host at 77 K. Curvature below 5 kG is attributed to the presence of superparamagnetic clusters.

Fig. 2. Impurity magnetization per mole of Fe impurity at 40 kG and 1.38 K for Fe in each of the CuAu hosts plotted as a function of nominal Fe concentration.

Fig. 3. $(M-M_H)/n_s$ plotted as a function of n_s for Fe in $Cu_{0.95}Au_{0.05}$. The temperature is 1.38 K while the field is varied. The error bars shown are mainly due to the uncertainty in n_s.

Fig. 4. $(M-M_H)/n_s$ plotted as a function of n_s for Fe in $Cu_{0.95}Au_{0.05}$. The field is 40 kG while the temperature is varied. Error bars shown are mainly due to the uncertainty in n_s.

Fig. 5. $(M-M_H)/n_s$ plotted as a function of n_s for Fe in $Cu_{0.91}Au_{0.09}$. Data are shown for various fields at 1.38 K. Different behavior of two batches of samples is shown. Error bars shown are mainly due to uncertainty in n_s.

Fig. 6. $(M-M_H)/n_s$ plotted as a function of n_s for Fe in $Cu_{0.91}Au_{0.09}$. Data are shown for several temperatures at a field of 40 kG. Samples were made in two batches and the data points for each batch lie on a separate straight line. Error bars shown are due mainly to the uncertainty in n_s.

Fig. 7. M_1 from fits of $M=M_o+M_1n_s+M_2n_s^2$ shown as a function of field for Fe in $Cu_{0.95}Au_{0.05}$. Error bars only include the effects of uncertainty in the magnetization measurement.

Fig. 8. M_2 for Fe in $Cu_{0.95}Au_{0.05}$ is shown as a function of field. Error bars only include effects of uncertainty in the magnetization measurements.

Fig. 9. M_1 for Fe in $Cu_{0.91}Au_{0.09}$ is shown as a function of field. Error bars only indicate effects due to the uncertainty in the magnetization measurements.

Fig. 10. M_2 for Fe in $Cu_{0.91}Au_{0.09}$ is shown as a function of field. Error bars only indicate effects of the uncertainty in the magnetization measurements.

Fig.11. χ_1 for Fe in $Cu_{0.95}Au_{0.05}$ is plotted as a function of $1/(T+15.8)$. Error bars are estimated from the uncertainty in M_1.

Fig. 12. χ_1 for Fe in $Cu_{0.91}Au_{0.09}$ plotted as a function of $1/(T+8.4)$. Error bars are estimated from the uncertainty in M_1.

Fig. 13. χ_2^{-1} for Fe in $Cu_{0.95}Au_{0.05}$ plotted as a function of T. Error bars are estimated from the uncertainty in M_2.

Fig. 14. χ_2^{-1} for Fe in $Cu_{0.91}Au_{0.09}$ plotted as a function of T. Error bars are estimated from the uncertainty in M_2.

Fig. 15. $(M-M_H)/n_s$ plotted as a function of n_s for Fe in $Cu_{0.83}Au_{0.17}$. The temperature is 1.39 K, while data for fields from 5 to 50 kG are shown. Error bars shown are mainly due to the uncertainty in n_s.

Fig. 16. $(M-M_H)/n_s$ plotted as a function of n_s for Fe in $Cu_{0.83}Au_{0.17}$. The field is 40 kG, while data for temperatures from 1.4 to 122 K are shown. Error bars shown are mainly due to the unceratinty in n_s.

Fig. 17. M_1 is shown as a function of field for Fe in $Cu_{0.83}Au_{0.17}$. Error bars include only effects due to the uncertainty in the measurement of the magnetization.

Fig. 18. M_2 for Fe in $Cu_{0.83}Au_{0.17}$ shown as a function of field. Error bars include only the effects due to the uncertainty in the measurement of the magnetization. The maximum in M_2 as a function of field at 1.38 K is a possible indication that there is a systematic error in n_s (See pg. 64).

Fig. 19. χ_2^{-1} for Fe in $Cu_{0.83}Au_{0.17}$ plotted as a function of temperature. The error bars are estimated from the uncertainty in M_2.

Fig. 20. χ_1 shown as a function of $1/(T+3.3)$ for Fe in $Cu_{0.83}Au_{0.17}$. The straight line indicates the best computer fit of χ_1 to $\chi_o+C_s/(T+\theta_s)$. The error bars are estimated from the uncertainty in M_1.

Fig. 21. χ_o, C_s, and C_p from fits of susceptibility data for Fe in $Cu_{0.83}Au_{0.17}$ to $\chi_o+C_s/(T+\theta_s)+C_p/(T+\theta_p)$ shown as a function of n_s. The behavior of the same coefficients found from expanding M as a function of n_s are also shown. There are substantial disagreements in the behavior of the two sets of coefficients which prevent definite attribution of the term quadratic in n_s to pairs of ferromagnetically coupled Fe atoms.

Fig. 22. $(M-M_H)/n_s$ plotted as a function of n_s for Fe in $Cu_{0.8}Au_{0.2}$. Data for a temperature of 1.38 K and several different fields are shown. The straight lines indicate the behavior of the samples with concentration below 250 ppm which were made in one batch, while the higher concentration samples were made in several other batches.

Fig.23. $(M-M_H)/n_s$ plotted as a function of n_s for Fe in $Cu_{0.8}Au_{0.2}$. The field is 40 kG while data taken at several temperatures are shown. See the caption of Fig. 22 for an explanation of the straight lines.

Fig. 24. χ_o, C_1, and C_2 from fits of $Cu_{0.8}Au_{0.2}$ susceptibility data to $\chi=\chi_o+C_1/(T+\theta_1)+C_2/(T+\theta_2)$ shown as a function of n_s. It is apparent from the figure that all of coefficients are nearly linear functions of concentration. It is thus not possible to attribute one of the terms to pairs of ferromagnetically coupled Fe atoms.

Fig. 25. $(M-M_H)/c_{nominal}$ as a function of $c_{nominal}$ for Fe in Au. Data for several values of field at 1.38 K are shown. The curves through the data points appear to rise sharply near 50 ppm indicating that the impurity magnetization increases less rapidly than linearly in concentration. Other analyses indicate that there is a maximum in the impurity magnetization per impurity near 100 ppm in conflict with this indication. The uncertainties in the concentrations are too large to permit any conclusion about the shape of the curve below 100 ppm. See pg. 69 for an explanation of the absence of error bars.

Fig. 26. $(M-M_H)/c_{nominal}$ as a function of $c_{nominal}$ for Fe in Au. Data for several temperatures at a field of 5 kG are shown. Other details simililar to Fig. 25.

Fig. 27. $(M-M_H)/c_{nominal}$ as a function of $c_{nominal}$ for Fe in Au. Data for several temperatures at a field of 40 kG are shown. Other details are similar to Fig. 25.

Fig. 28. $c_{nominal}/\Delta\chi$ for Fe in Au shown as a function of temperature for T in the range 1.4 to 133 K. At most temperatures the difference in the values of $c_{nominal}/\Delta\chi$ for different concentrations is too small to be shown in the figure. At points where the values for the 61 ppm sample differ significantly from the values for other concentrations, they are indicated by a separate symbol. Error bars due to the uncertainty in $\Delta\chi$ are shown for the 61 ppm sample. From 44 to 133 K the susceptibility fits a Curie-Weiss law.

Fig. 29. An expanded view of the portion of Fig. 28 below 10 K. The extension of the Curie-Weiss law fitting the data above 44 K is also shown. See pg. 72 for more details.

Fig. 34. The single impurity susceptibility per mole of Fe impurity, χ/n_s, for Fe in each of the CuAu hosts is shown as a function of temperature. For more details of the definition of the single impurity susceptibility see pg. 77.

Fig. 35. $(\chi/n_s)T$ is shown as a function of T/T', where a different value of T' has been chosen for each host and (χ/n_s) is the single impurity susceptibility per mole of impurity plotted in Fig. 34. Values of T' were found by multiplying the values of T_K found from resistivity measurements[21, 90] so that the value of T' for the alloy with 5 atomic % Au is the same as .

Fig. 36. The values of $(\chi/n_s)T$ for each alloy have been multiplied by a different constant factor before plotting as a function of T/T'. The factor has been chosen to bring the curves into superposition and corresponds to adjusting the values of the concentrations or the impurity spins.

Fig. 37. To improve the superposition of the curves the values of both T' and the concentration have been adjusted before plotting $(\chi/n_s)T$ as a function of T/T'.

Fig. 38. χ^{-1} from the theoretical expressions

$$1)\ \chi = \frac{C}{T}\left[1 - \left[\ln\left(\frac{T}{T_K}\right)\right]^{-1}\right]^{43,44} \quad \text{and}$$

$$2)\ \chi = \frac{C}{T}\left\{1 - \frac{1}{S+\frac{1}{2}}\left[\frac{1}{2} - \frac{1}{\pi}\arctan\left(\frac{\ln[T/T_K]}{\pi(S+\frac{1}{2})}\right)\right]\right\}^{45,46}$$

is plotted as a function of T for several values of T_K. C is set equal to 1 and S= 1.2.

Fig. 39. A schematic diagram of the magnet and the insert. To show all of the details the diagram has been expanded to cover 2 pages.

Fig. 40. A schematic diagram of the gradient coils illustrating the relevant dimensions.

Fig. 41. A drawing showing the form for the gradient coils.

Fig. 42. This is the circuit used to switch the polarity of the current to the gradient coils. See text on page 98 for an explanation of the operation.

Fig. 43. Details of the mounting of the microbalance. See text on page 99 and 100 for an explanation.

Fig. 44. A plot of M_c, the cluster saturation magnetization discussed on page 120, as a function of concentration for each of the hosts containing Cu.

Figure 1

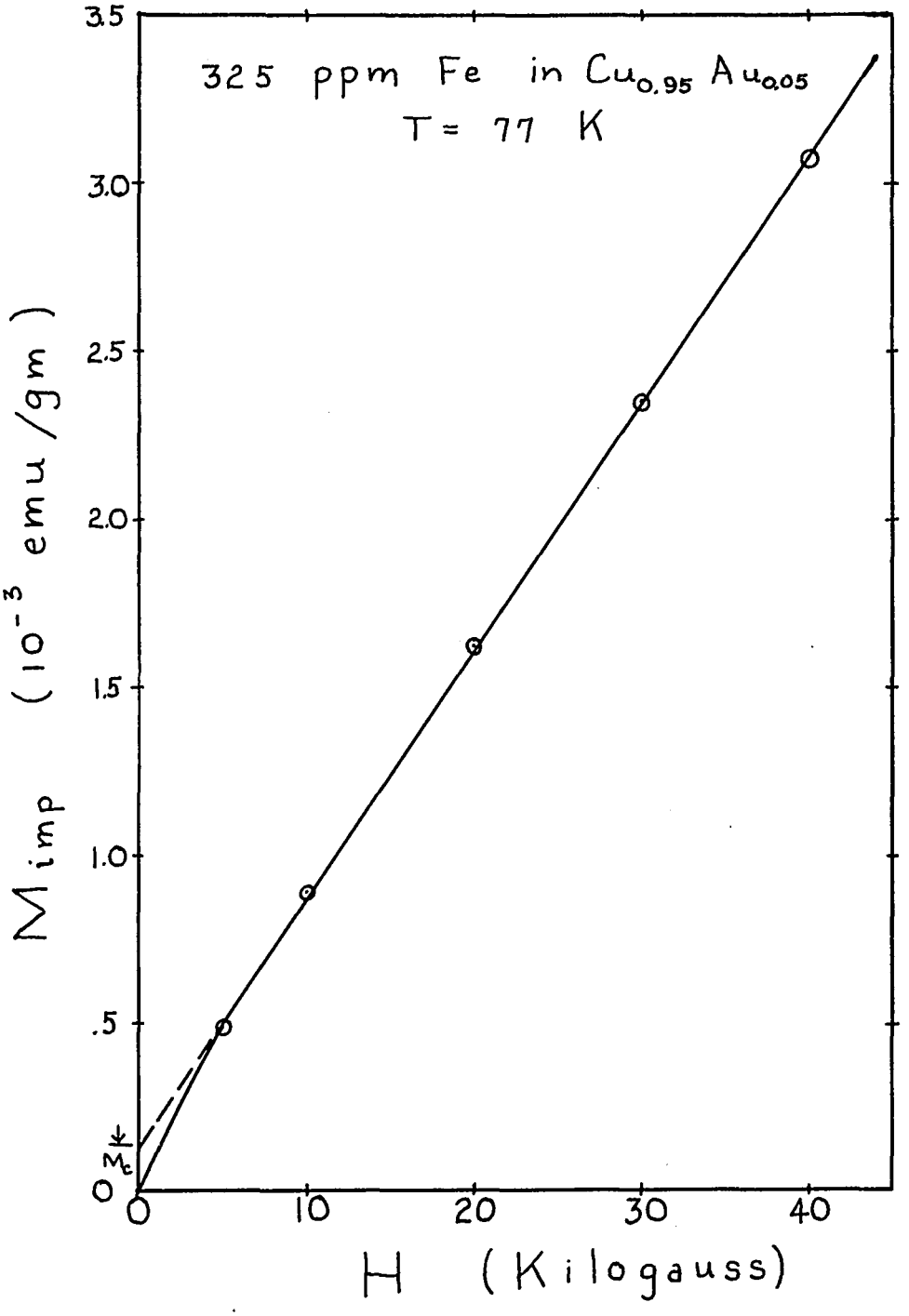
325 ppm Fe in $Cu_{0.95}Au_{0.05}$
T = 77 K
M_{imp} (10^{-3} emu/gm)
3.5
3.0
2.5
2.0
1.5
1.0
.5
0
M_c
0
10
20
30
40
H (Kilogauss)

Figure 2

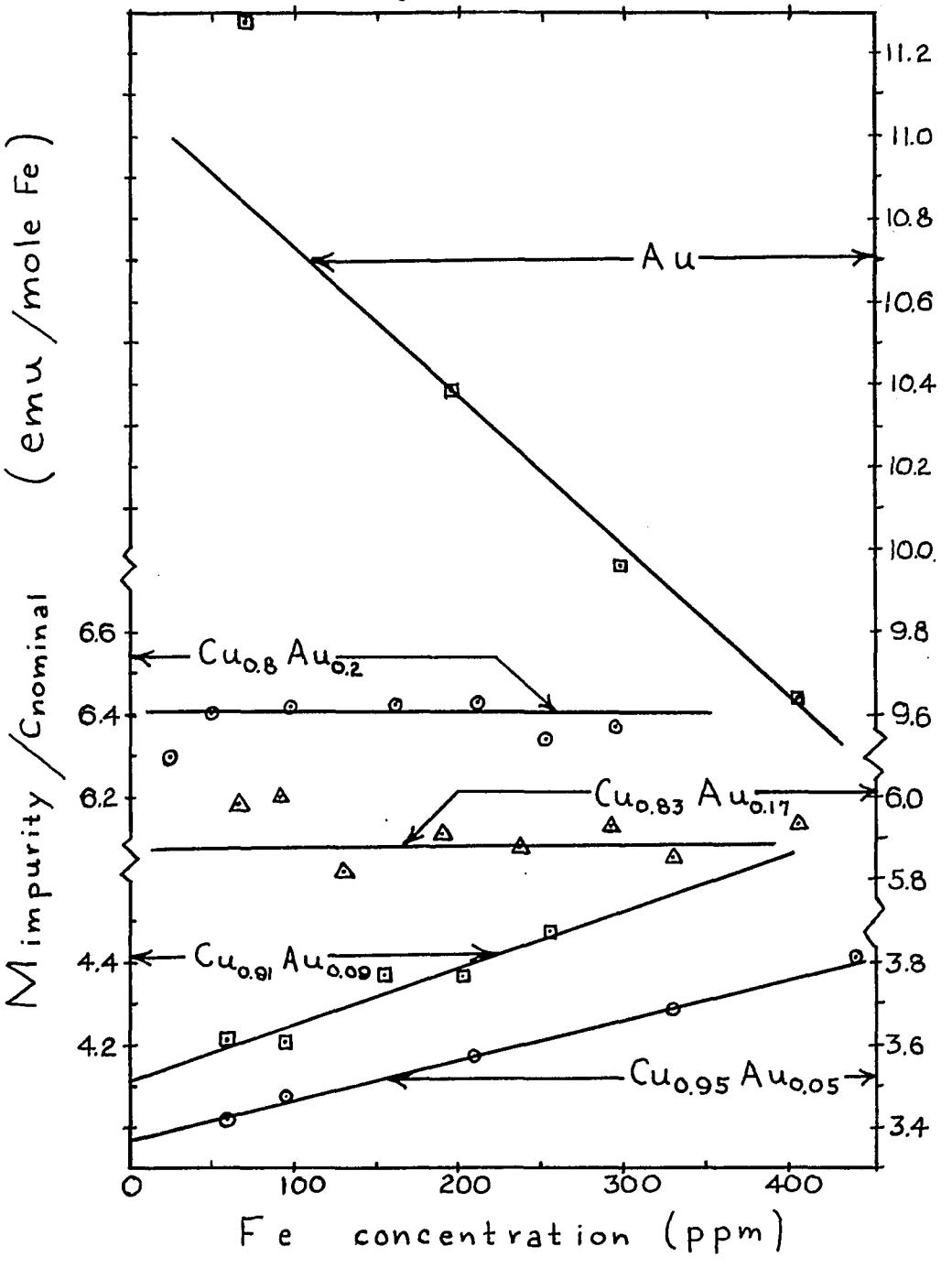
M impurity / Cnominal (emu / mole Fe)
11.2
11.0
10.8
10.6
10.4
10.2
10.0
9.8
9.6
6.6
6.4
6.2
6.0
5.8
4.4
4.2
3.8
3.6
3.4
Au
Cu0.8 Au0.2
Cu0.83 Au0.17
Cu0.91 Au0.09
Cu0.95 Au0.05
0
100
200
300
400
Fe concentration (ppm)

Figure 3

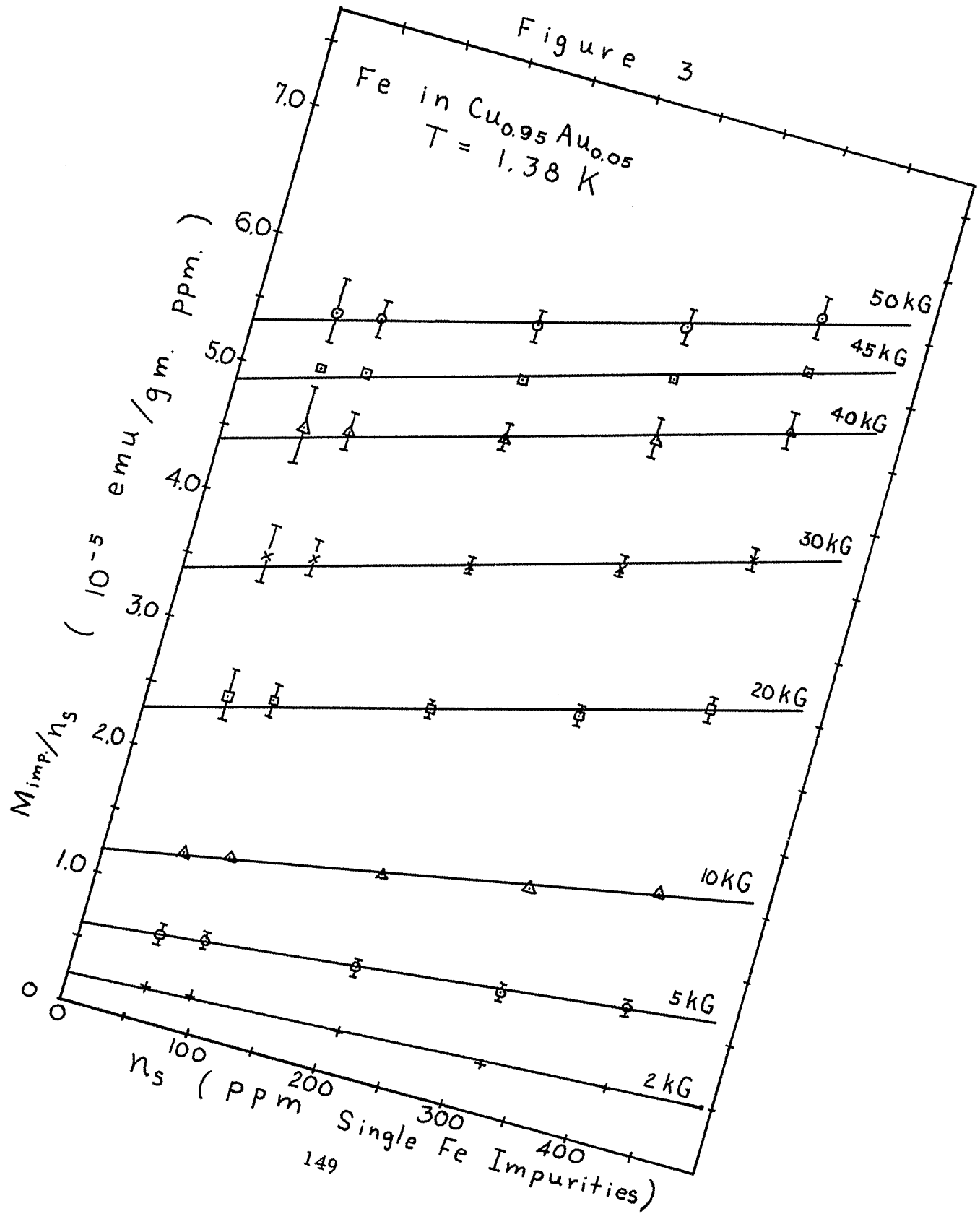
Fe in $Cu_{0.95}Au_{0.05}$
T = 1.38 K
M_{imp}/n_s (10^{-5} emu/gm. Ppm.)
n_s (Ppm Single Fe Impurities)
0
1.0
2.0
3.0
4.0
5.0
6.0
7.0
100
200
300
400
50kG
45kG
40kG
30kG
20kG
10kG
5kG
2kG

Figure 4

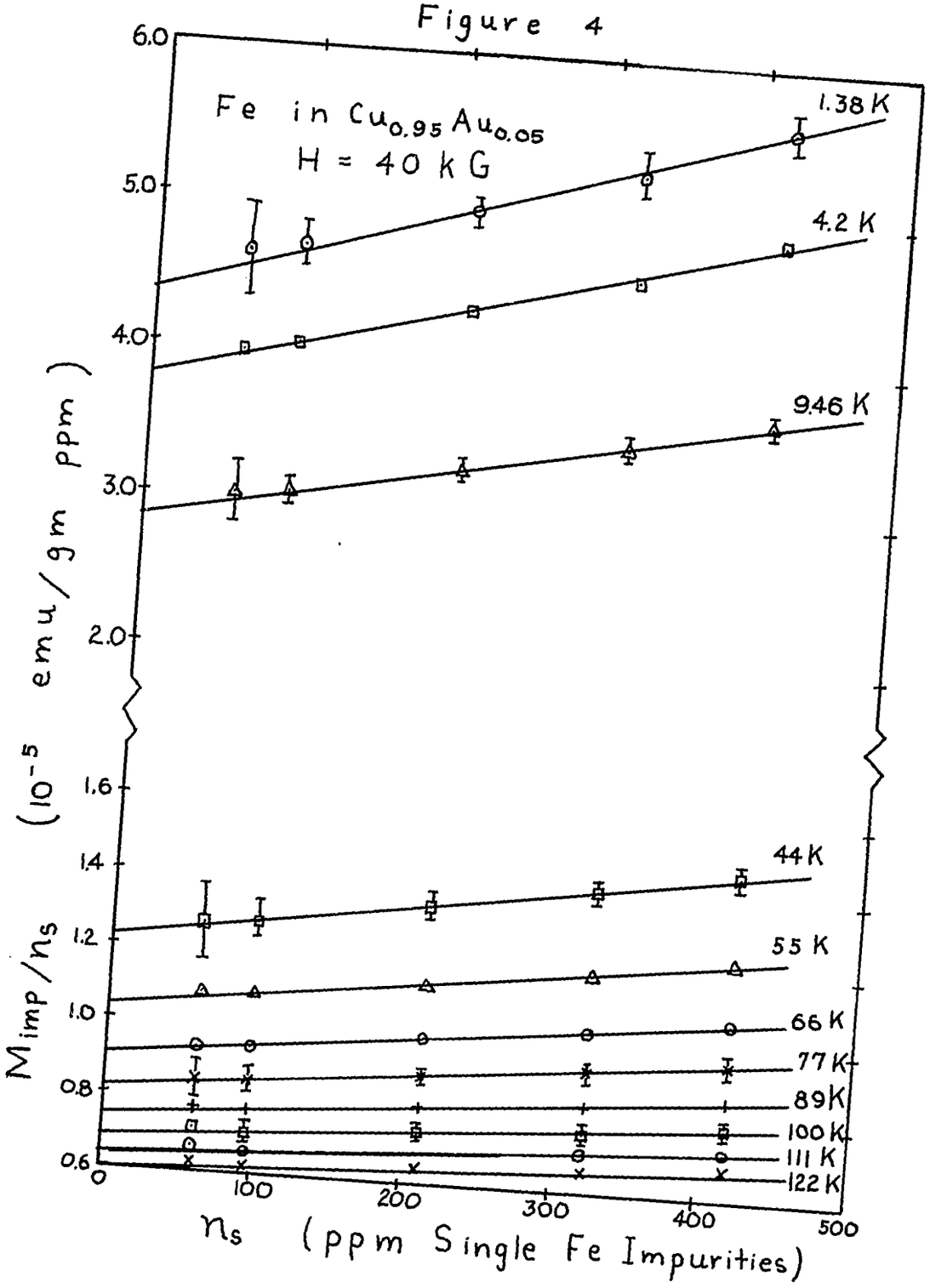
Fe in $Cu_{0.95}Au_{0.05}$
H = 40 kG
1.38 K
4.2 K
9.46 K
44 K
55 K
66 K
77 K
89K
100 K
111 K
122 K
M_{imp}/n_s (10^{-5} emu/gm ppm)
n_s (ppm Single Fe Impurities)
6.0
5.0
4.0
3.0
2.0
1.6
1.4
1.2
1.0
0.8
0.6
0
100
200
300
400
500

Figure 5

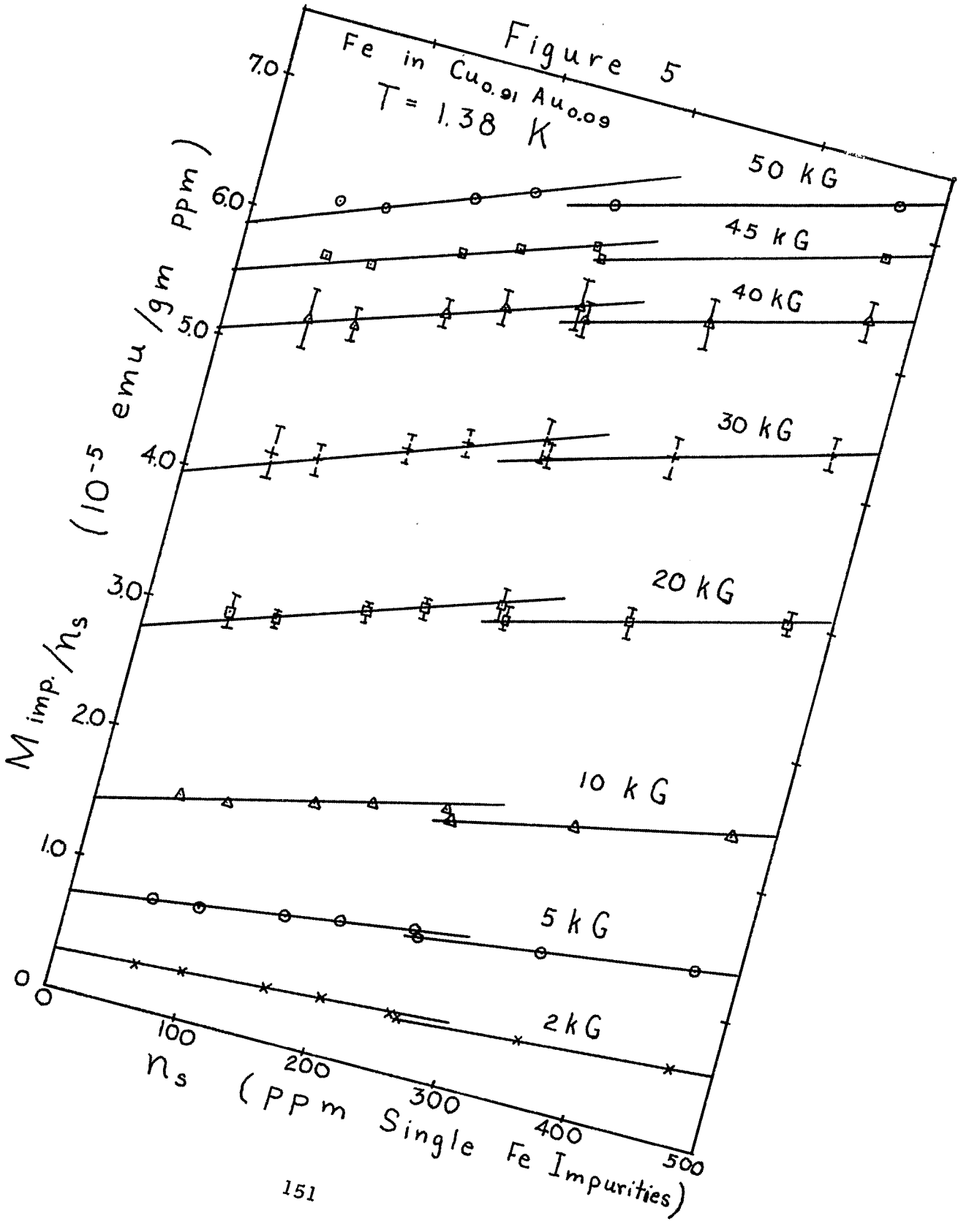
Fe in Cu0.91 Au0.09
T = 1.38 K
50 kG
45 kG
40 kG
30 kG
20 kG
10 kG
5 kG
2 kG
7.0
6.0
5.0
4.0
3.0
2.0
1.0
0
0
100
200
300
400
500
(10-5 emu/gm ppm)
M imp./ns
ns (PPm Single Fe Impurities)

Figure 6

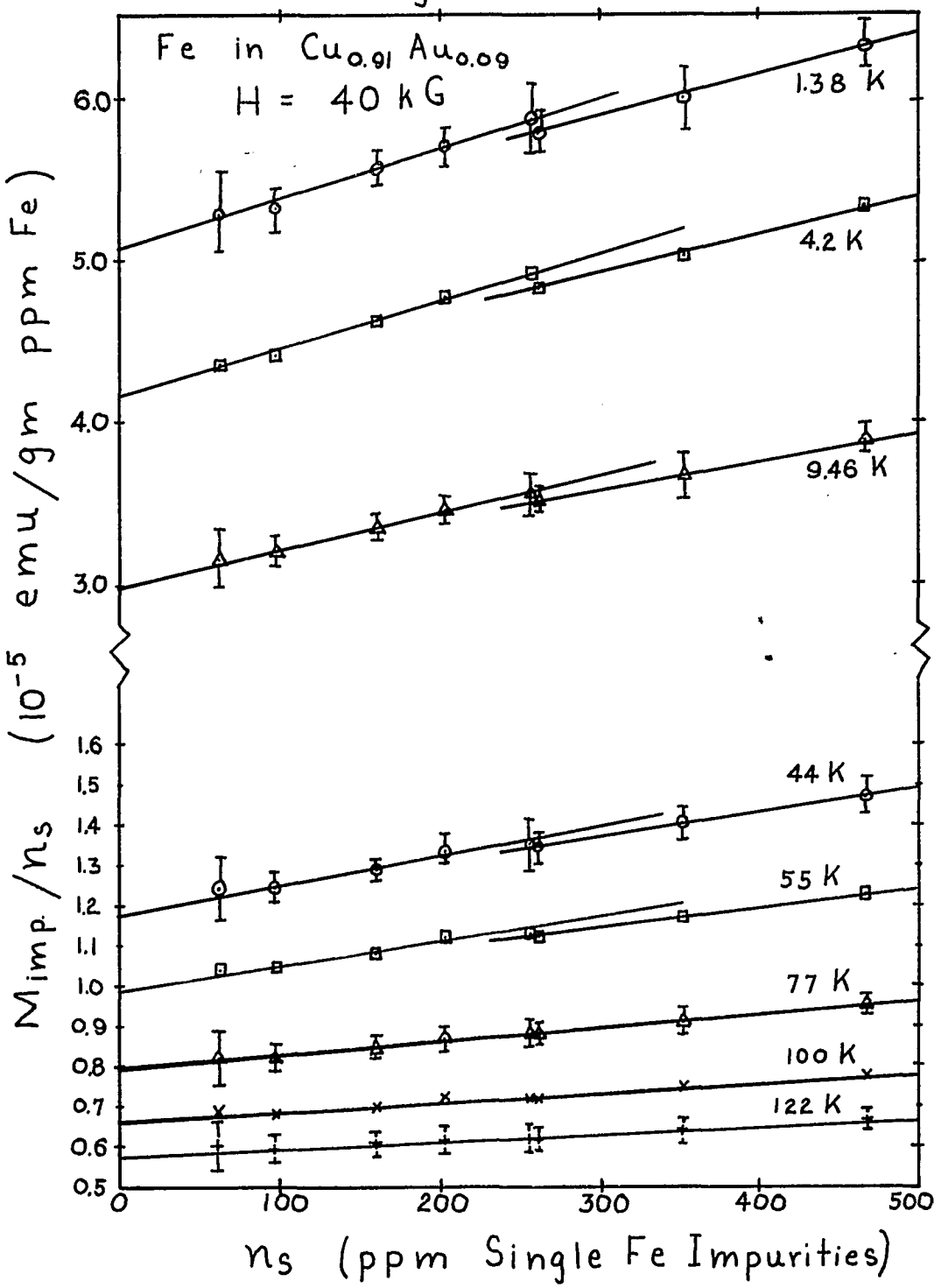
Fe in $Cu_{0.91}Au_{0.09}$
H = 40 kG
1.38 K
4.2 K
9.46 K
44 K
55 K
77 K
100 K
122 K
$M_{imp.}/n_s$ (10^{-5} emu/gm ppm Fe)
n_s (ppm Single Fe Impurities)
6.0
5.0
4.0
3.0
1.6
1.5
1.4
1.3
1.2
1.1
1.0
0.9
0.8
0.7
0.6
0.5
0
100
200
300
400
500

Figure 7

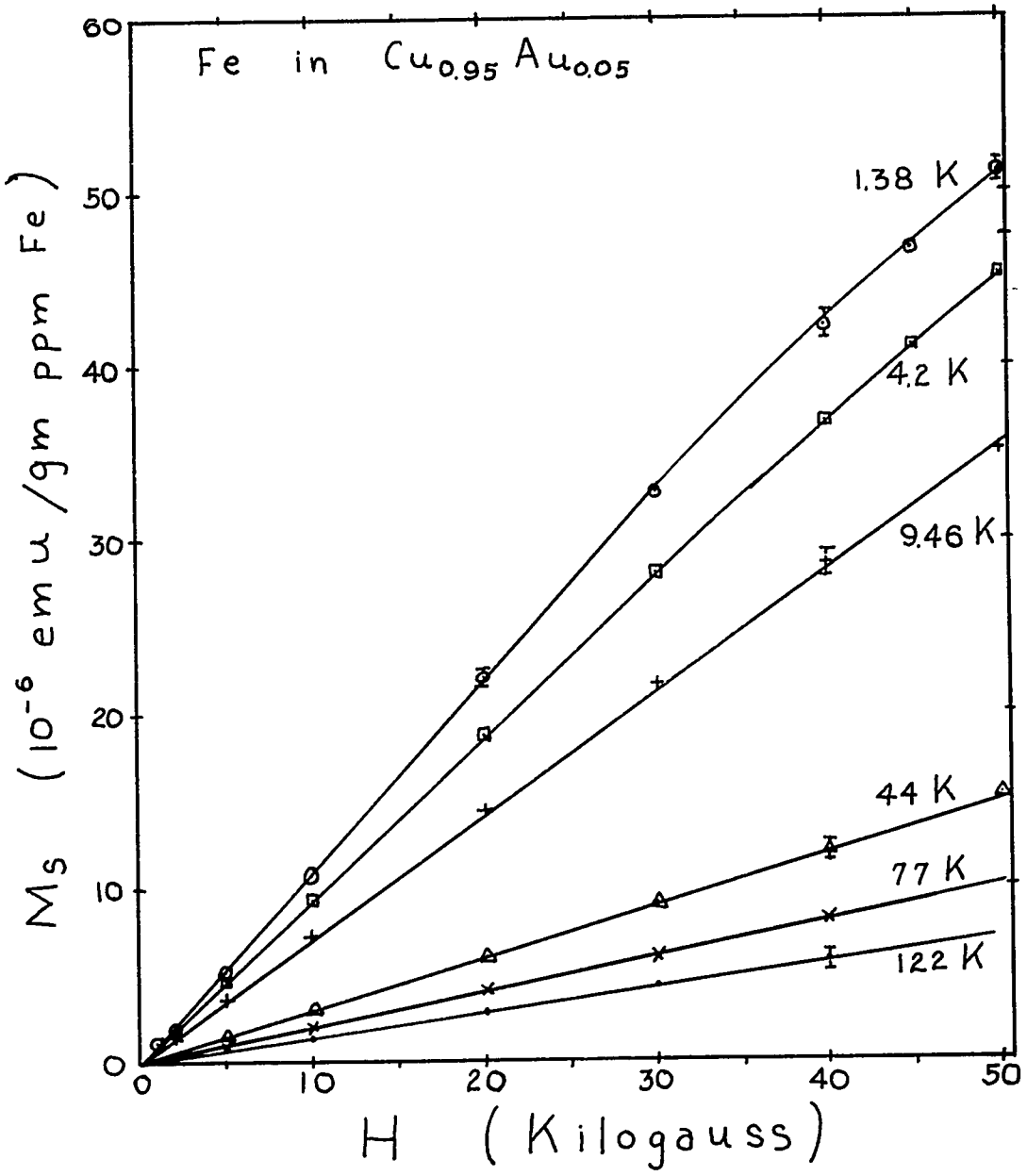
Fe in $Cu_{0.95}Au_{0.05}$
1.38 K
4.2 K
9.46 K
44 K
77 K
122 K
M_S (10^{-6} emu/gm ppm Fe)
H (Kilogauss)
0
10
20
30
40
50
60

Figure 8

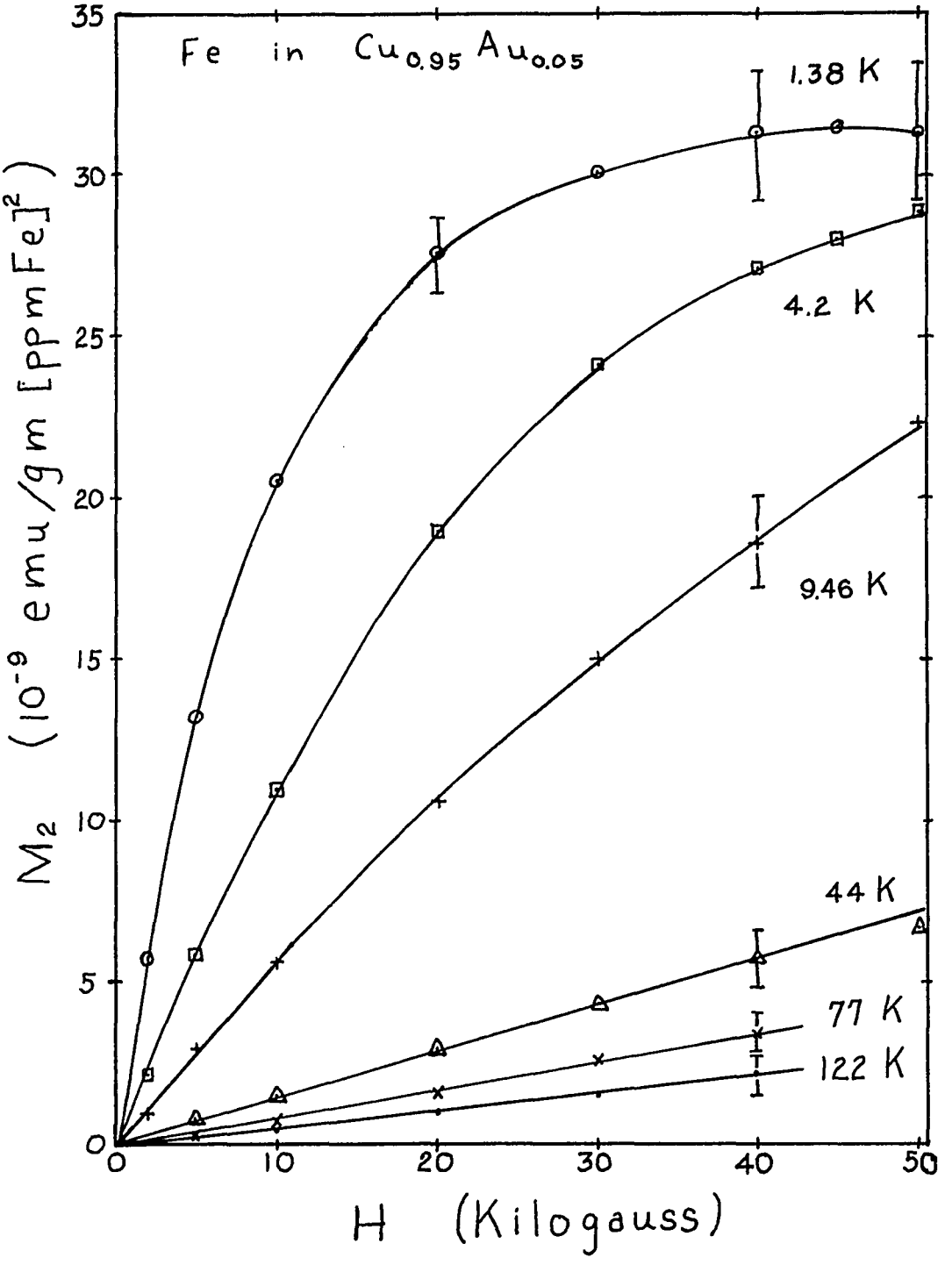
Fe in $Cu_{0.95}Au_{0.05}$
1.38 K
4.2 K
9.46 K
44 K
77 K
122 K
M_2 (10^{-9} emu/gm [PPm Fe]^2)
H (Kilogauss)
0
5
10
15
20
25
30
35
0
10
20
30
40
50

Figure 9

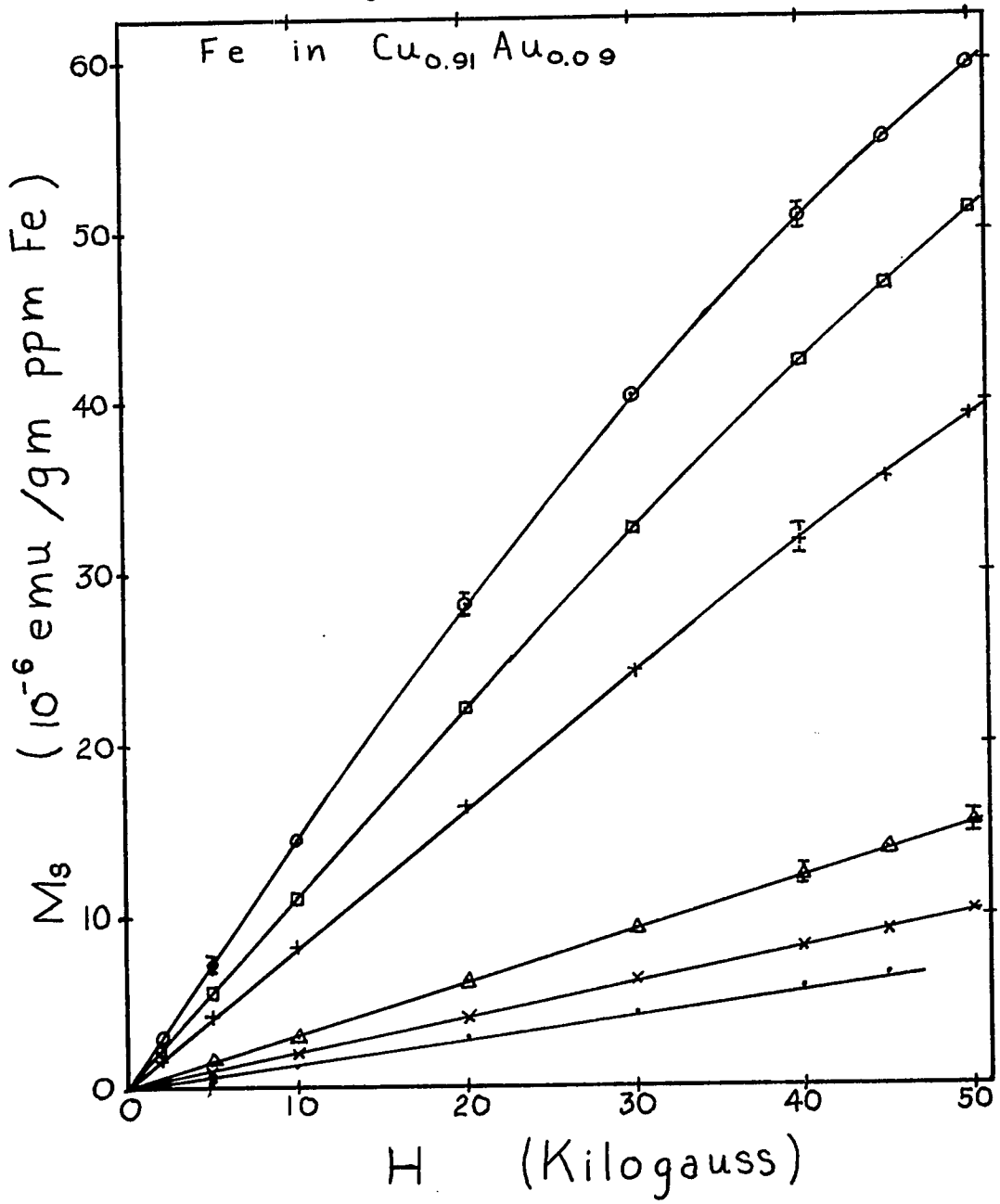
Fe in $Cu_{0.91}Au_{0.09}$
M_s (10^{-6} emu /gm ppm Fe)
0
10
20
30
40
50
60
0
10
20
30
40
50
H (Kilogauss)

Figure 10

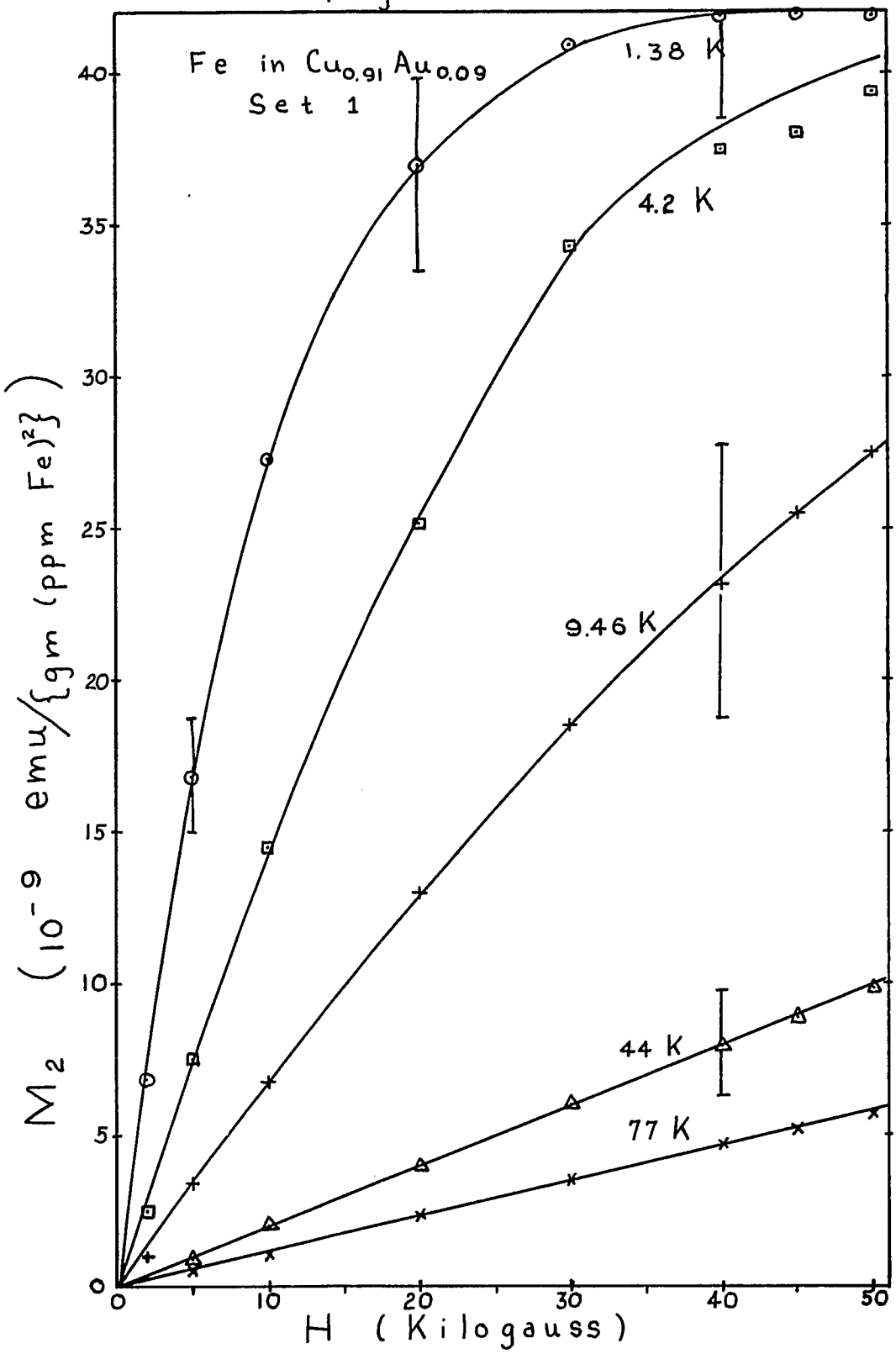
Fe in Cu0.91 Au0.09
Set 1
1.38 K
4.2 K
9.46 K
44 K
77 K
M2 (10-9 emu/{gm (ppm Fe)2})
H (Kilogauss)
0
5
10
15
20
25
30
35
40
0
10
20
30
40
50

Figure 11

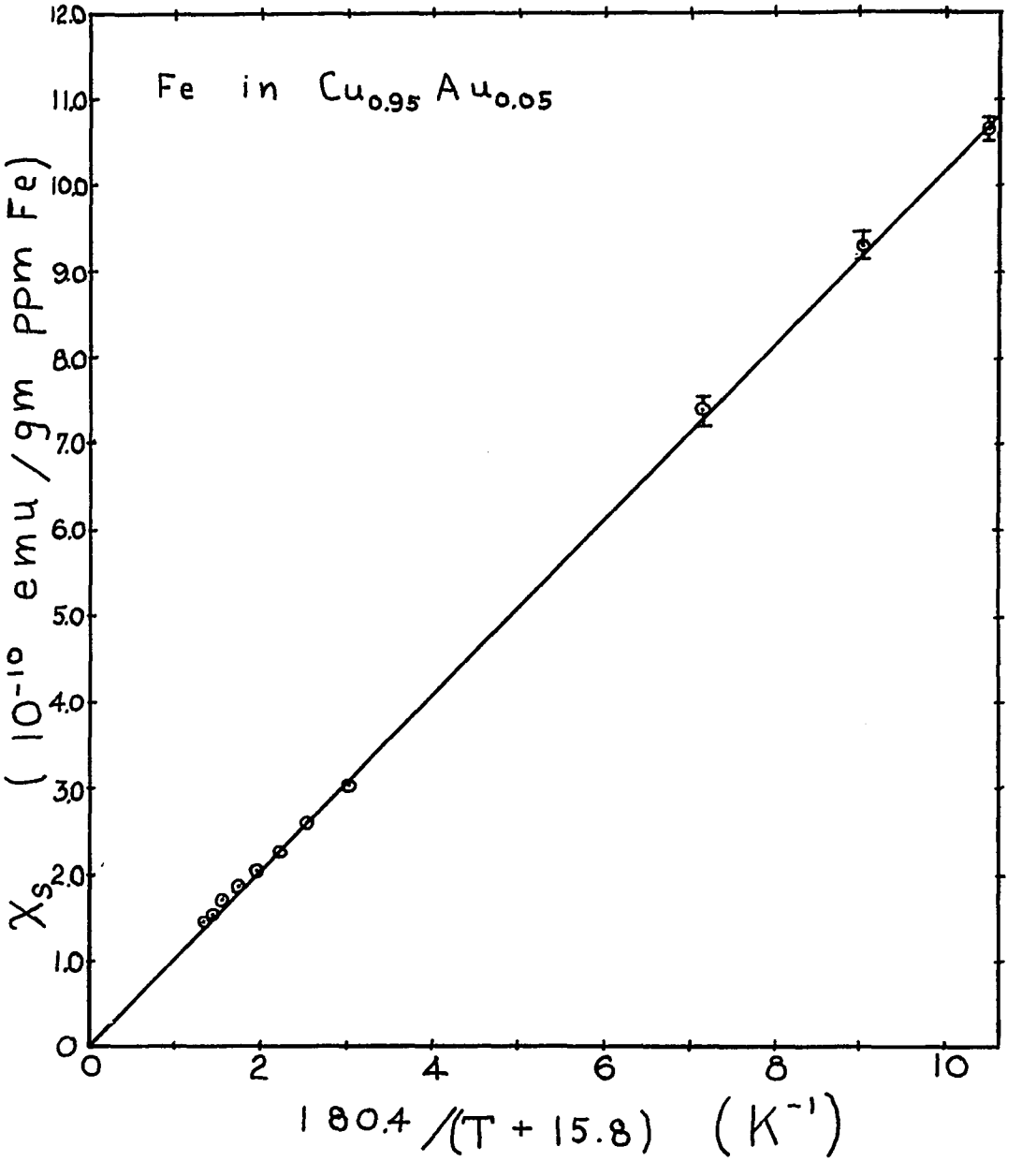
Fe in $Cu_{0.95}Au_{0.05}$
χ_s (10^{-10} emu / gm ppm Fe)
12.0
11.0
10.0
9.0
8.0
7.0
6.0
5.0
4.0
3.0
2.0
1.0
0
0
2
4
6
8
10
180.4 /(T + 15.8) (K^{-1})

Figure 12

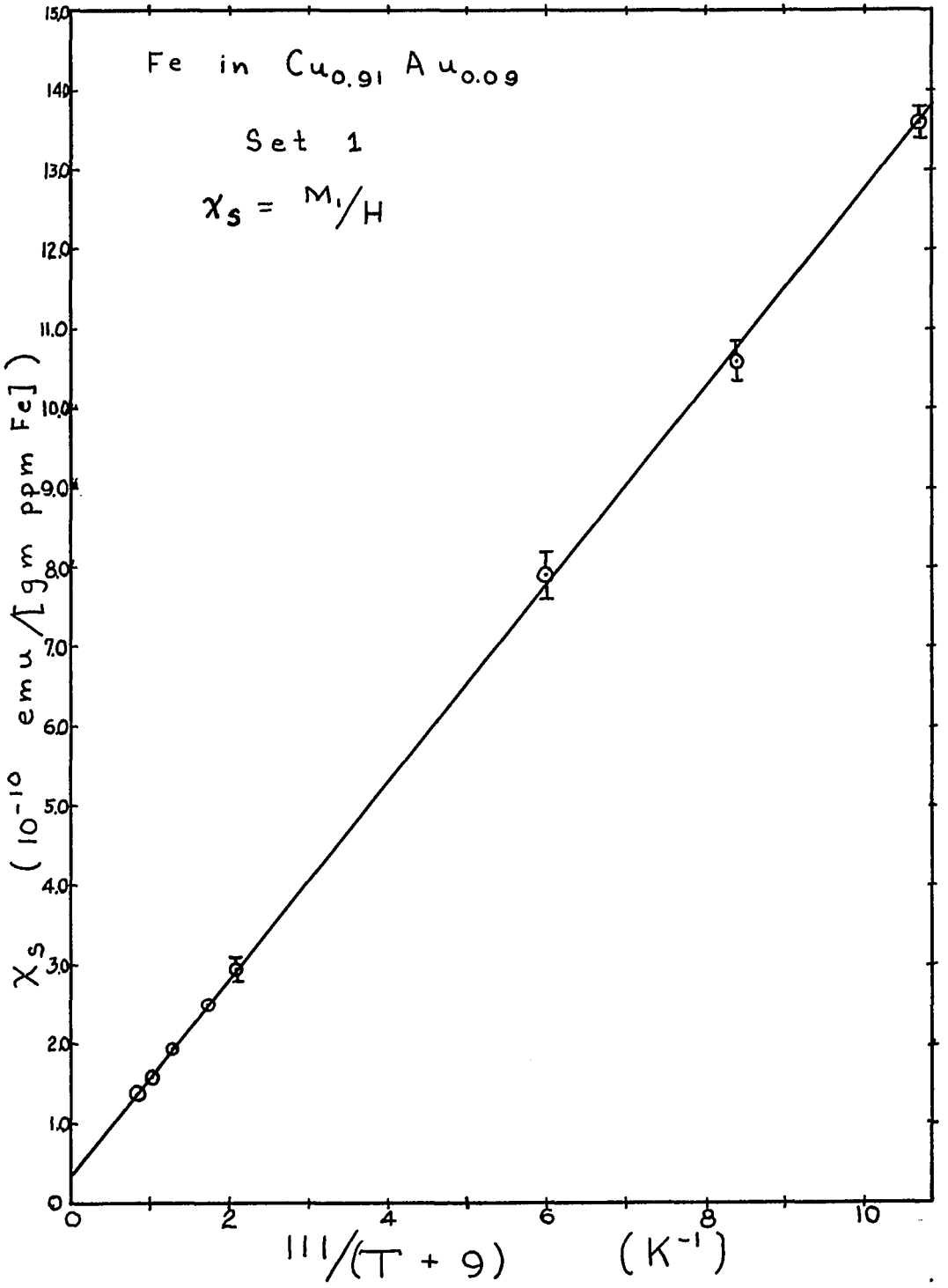
Fe in $Cu_{0.91}Au_{0.09}$
Set 1
$\chi_s = M_1/H$
χ_s (10^{-10} emu/[gm ppm Fe])
0
1.0
2.0
3.0
4.0
5.0
6.0
7.0
8.0
9.0
10.0
11.0
12.0
13.0
14.0
15.0
0
2
4
6
8
10
$1/(T + 9)$ (K^{-1})

Figure 13

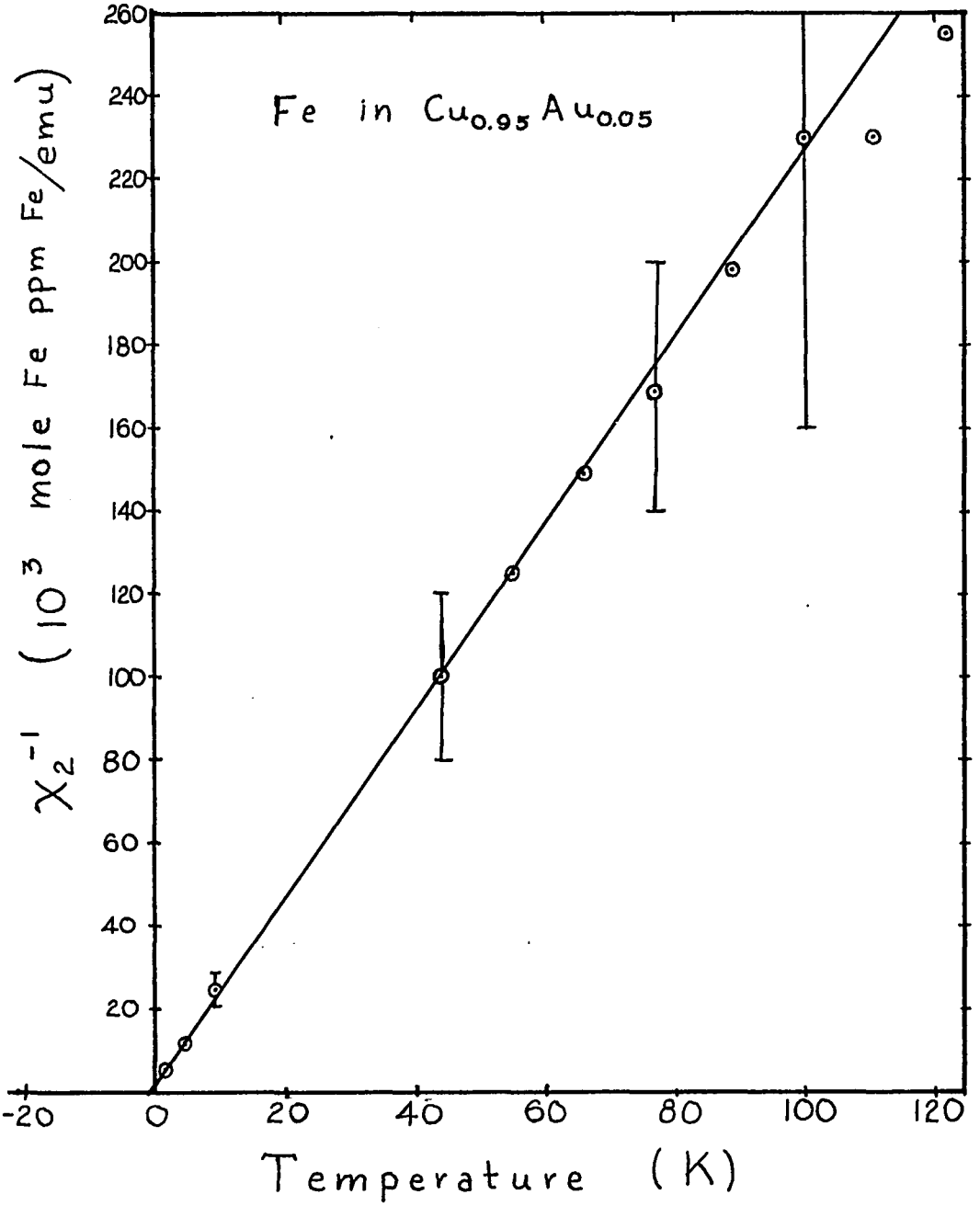
Fe in $Cu_{0.95}Au_{0.05}$
χ_2^{-1} (10^3 mole Fe ppm Fe/emu)
260
240
220
200
180
160
140
120
100
80
60
40
20
-20
0
20
40
60
80
100
120
Temperature (K)

Figure 14

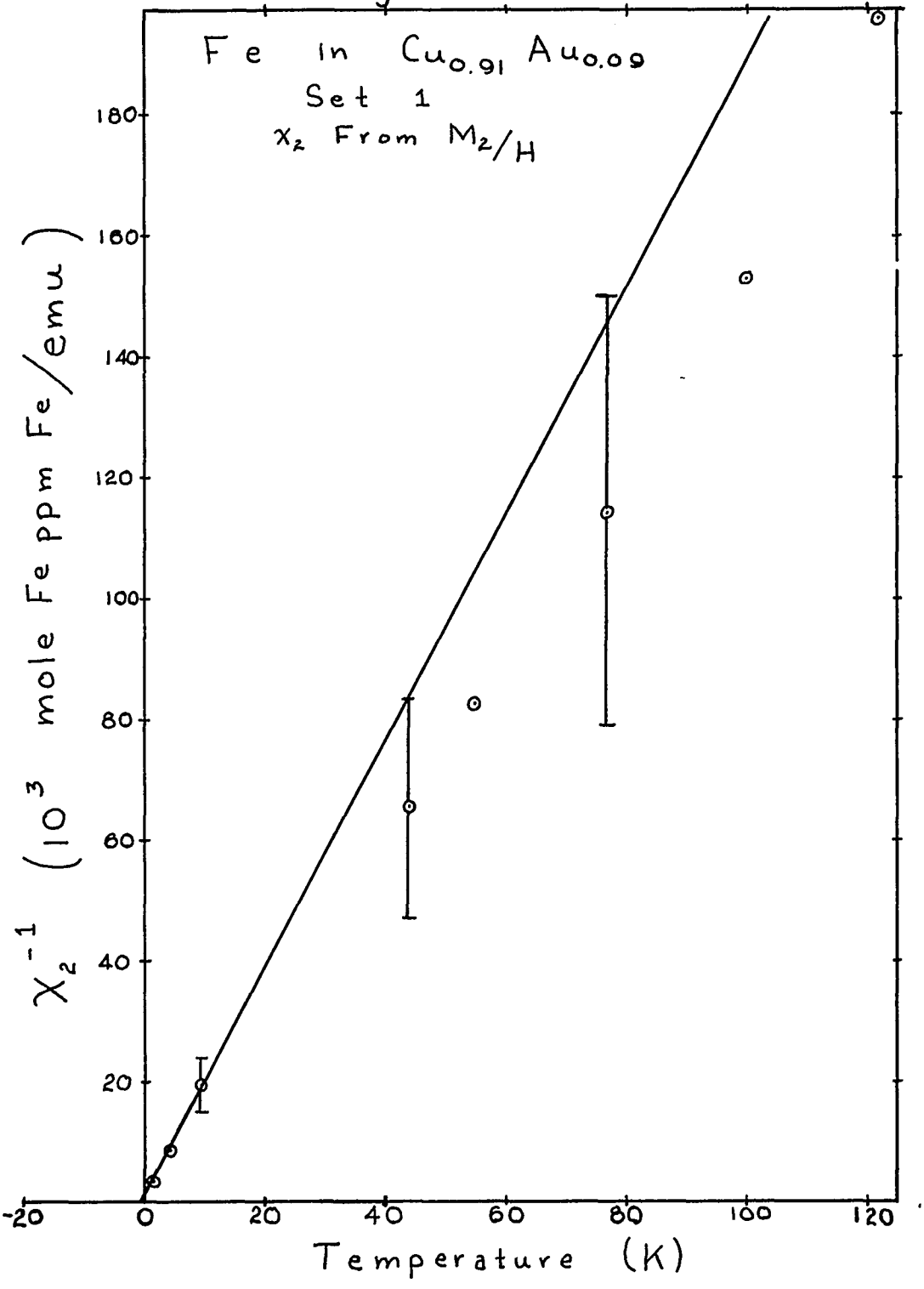
Fe in $Cu_{0.91}Au_{0.09}$
Set 1
χ_2 From M_2/H
χ_2^{-1} (10^3 mole Fe ppm Fe/emu)
180
160
140
120
100
80
60
40
20
-20
0
20
40
60
80
100
120
Temperature (K)

Figure 15

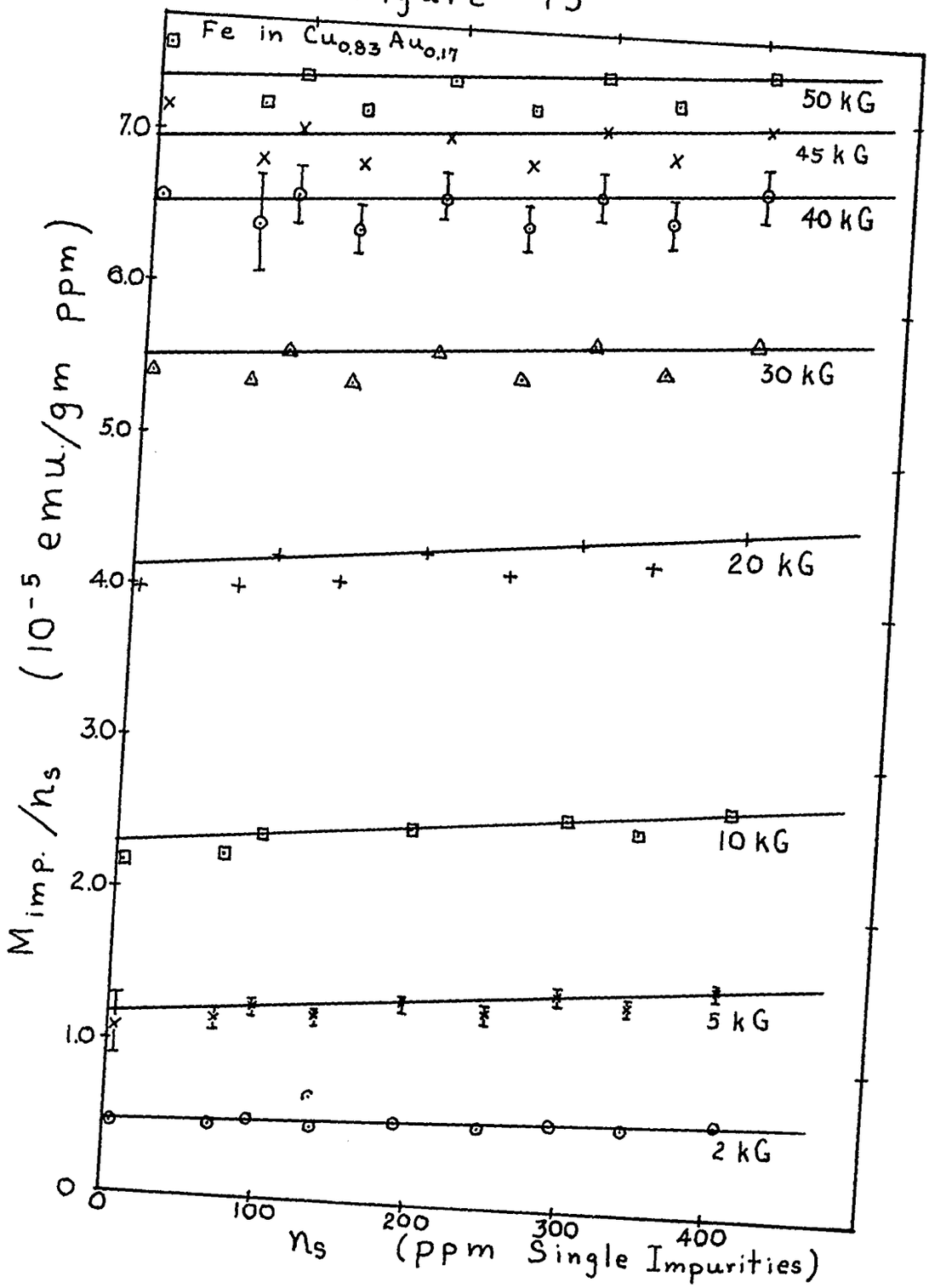
Fe in $Cu_{0.83}Au_{0.17}$
50 kG
45 kG
40 kG
30 kG
20 kG
10 kG
5 kG
2 kG
7.0
6.0
5.0
4.0
3.0
2.0
1.0
0
0
100
200
300
400
$M_{imp.}/n_s$ (10^{-5} emu./gm ppm)
n_s (ppm Single Impurities)

Figure 16

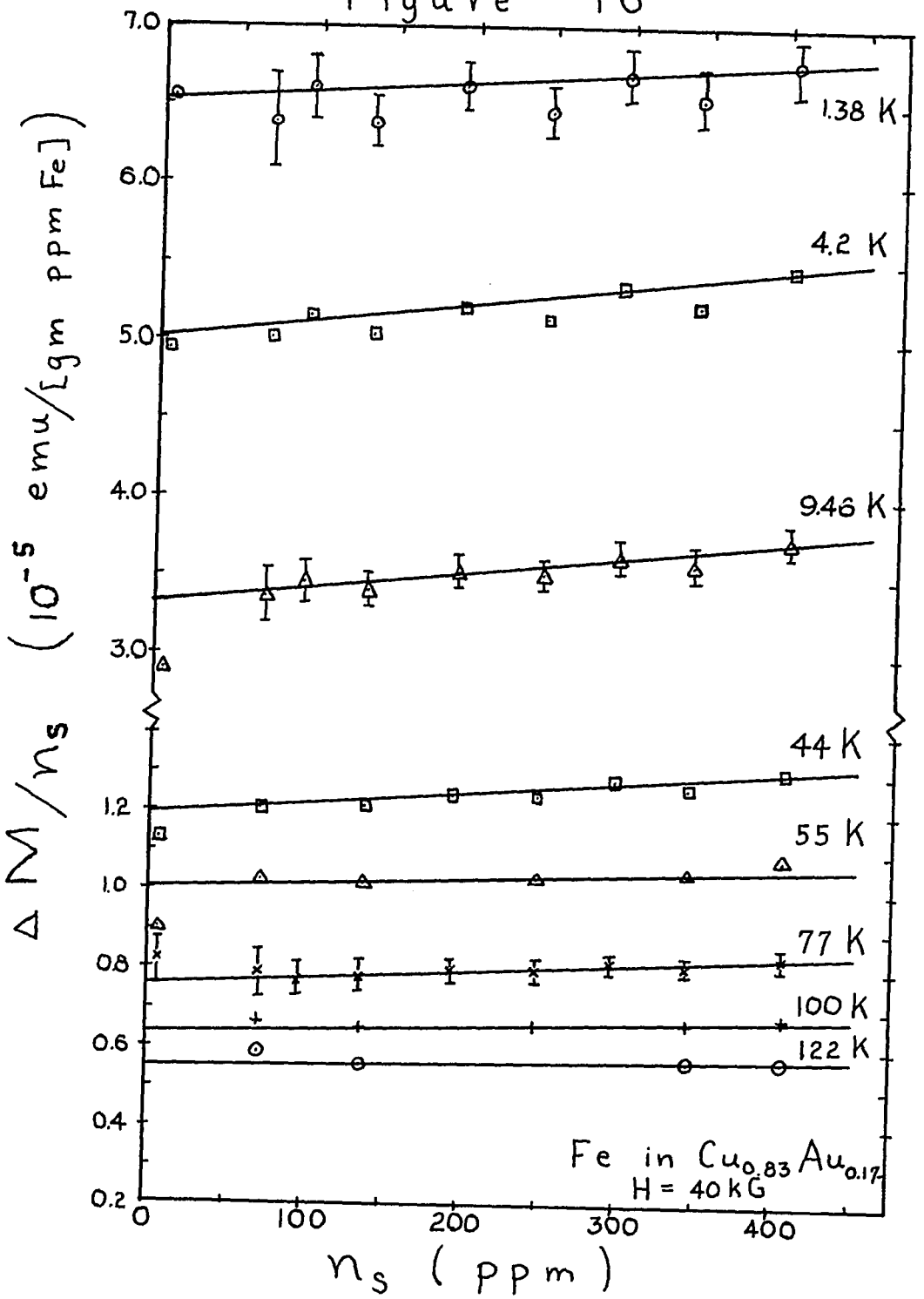
7.0
6.0
5.0
4.0
3.0
1.2
1.0
0.8
0.6
0.4
0.2
0
100
200
300
400
1.38 K
4.2 K
9.46 K
44 K
55 K
77 K
100 K
122 K
Fe in Cu0.83 Au0.17
H = 40 kG
ΔM/ns (10^-5 emu/[gm ppm Fe])
ns (ppm)

Figure 17

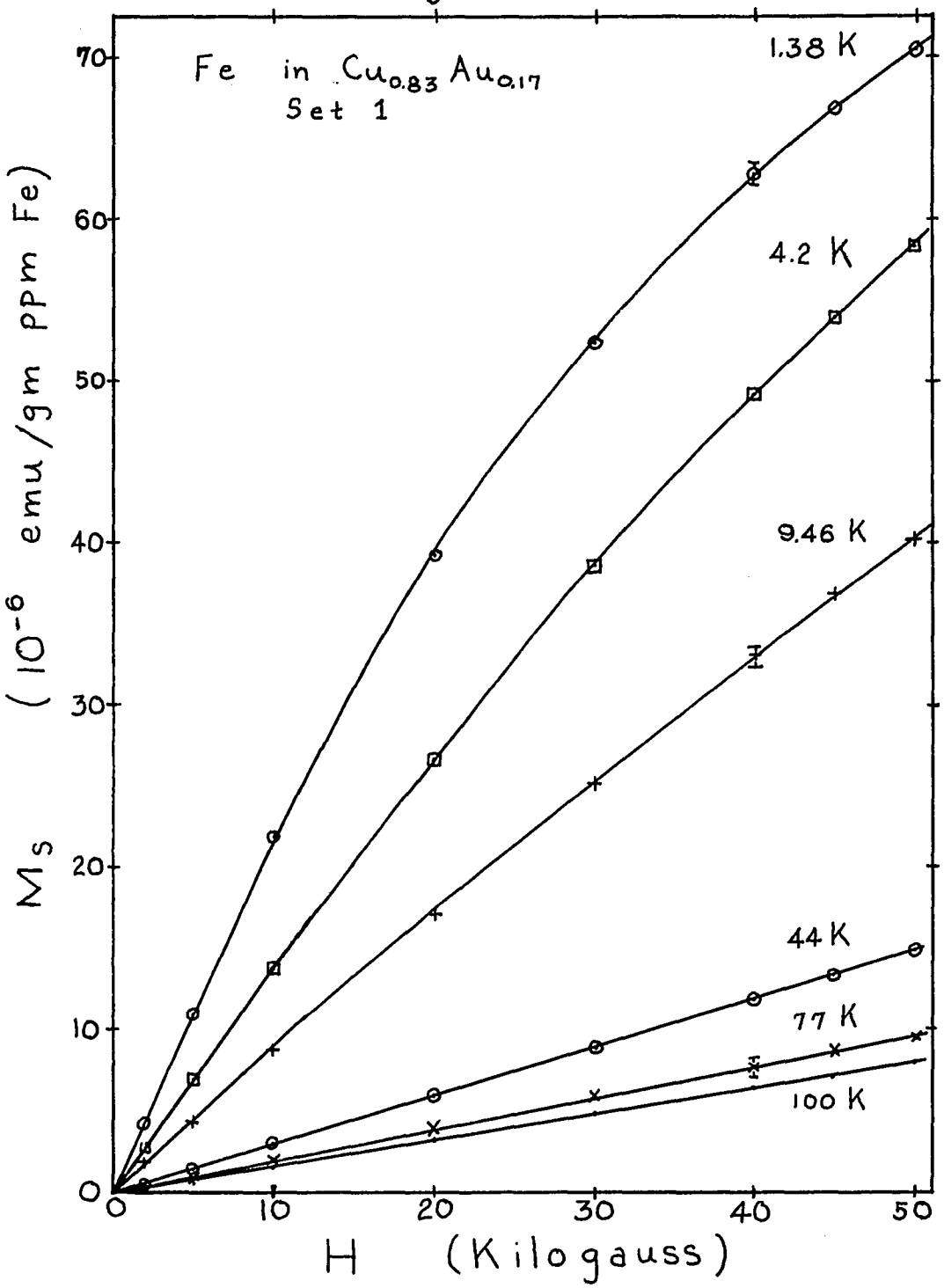
Fe in $Cu_{0.83}Au_{0.17}$
Set 1
1.38 K
4.2 K
9.46 K
44 K
77 K
100 K
M_S (10^{-6} emu/gm ppm Fe)
H (Kilogauss)
0
10
20
30
40
50
60
70

Figure 18

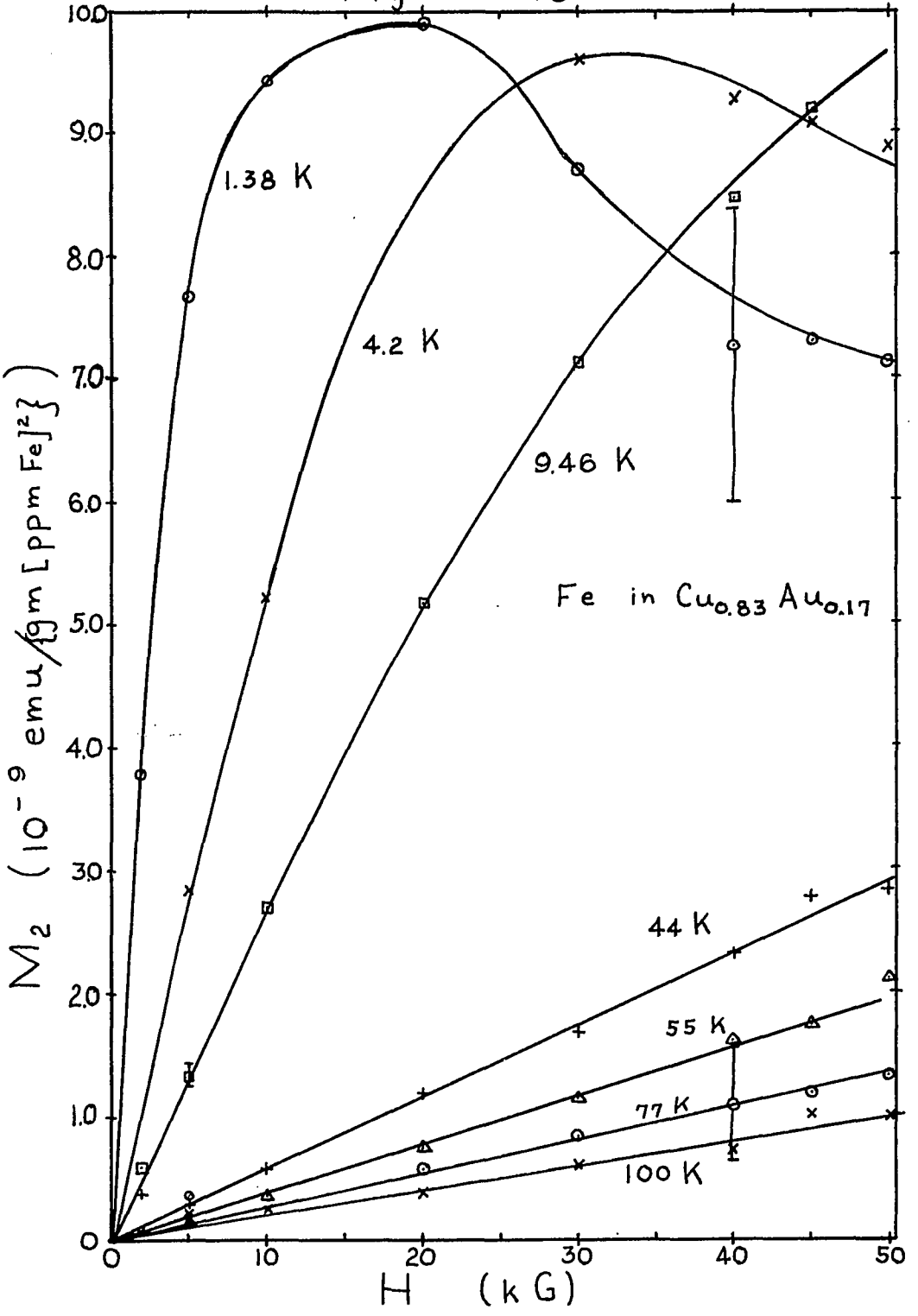
1.38 K
4.2 K
9.46 K
44 K
55 K
77 K
100 K
Fe in Cu0.83 Au0.17
M2 (10-9 emu/gm [ppm Fe]2)
H (kG)
0
1.0
2.0
3.0
4.0
5.0
6.0
7.0
8.0
9.0
10.0
0
10
20
30
40
50

Figure 19

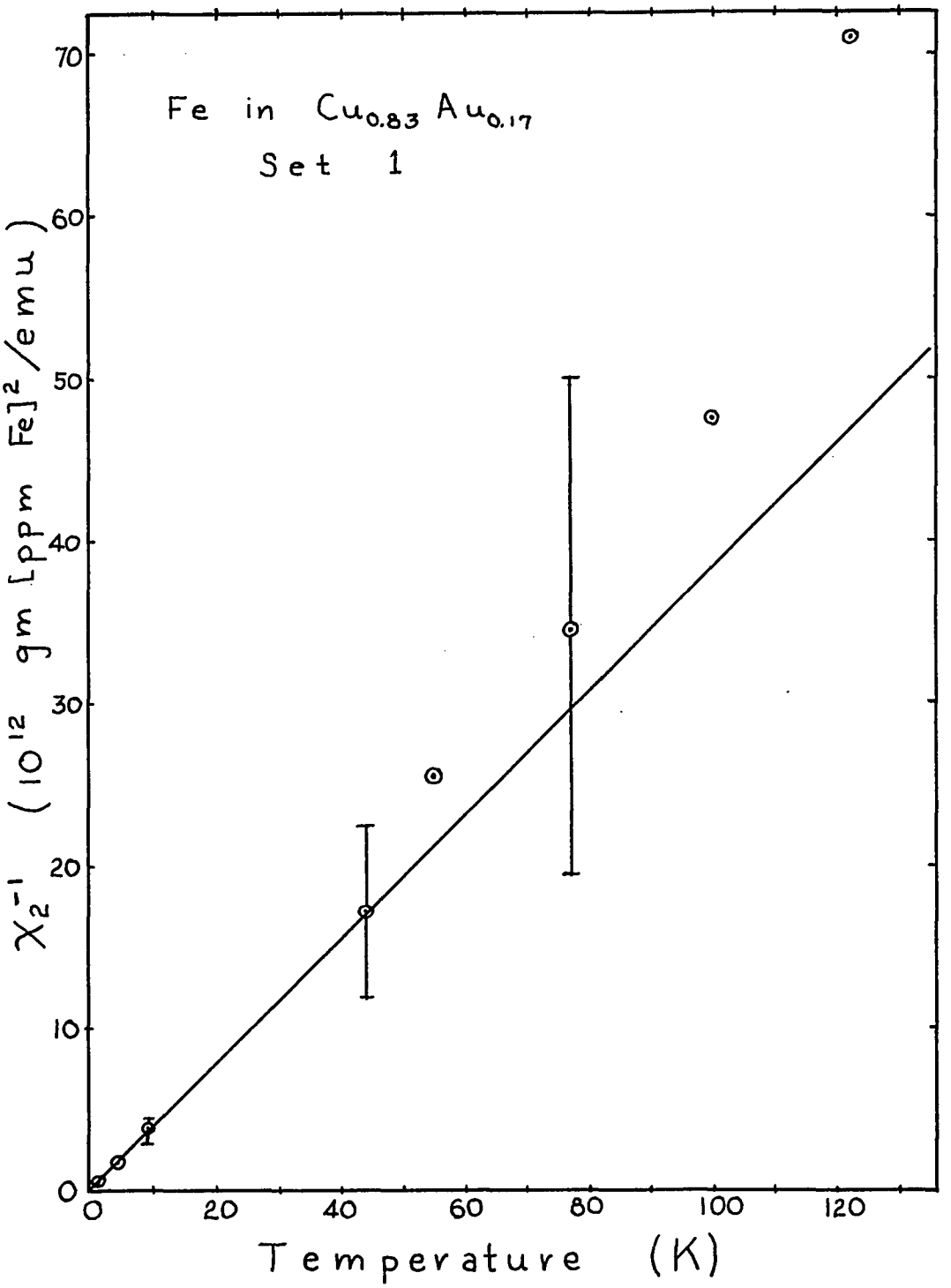
Fe in $Cu_{0.83}Au_{0.17}$
Set 1
χ_2^{-1} (10^{12} gm [ppm Fe]^2/emu)
Temperature (K)
0
10
20
30
40
50
60
70
0
20
40
60
80
100
120

Figure 20

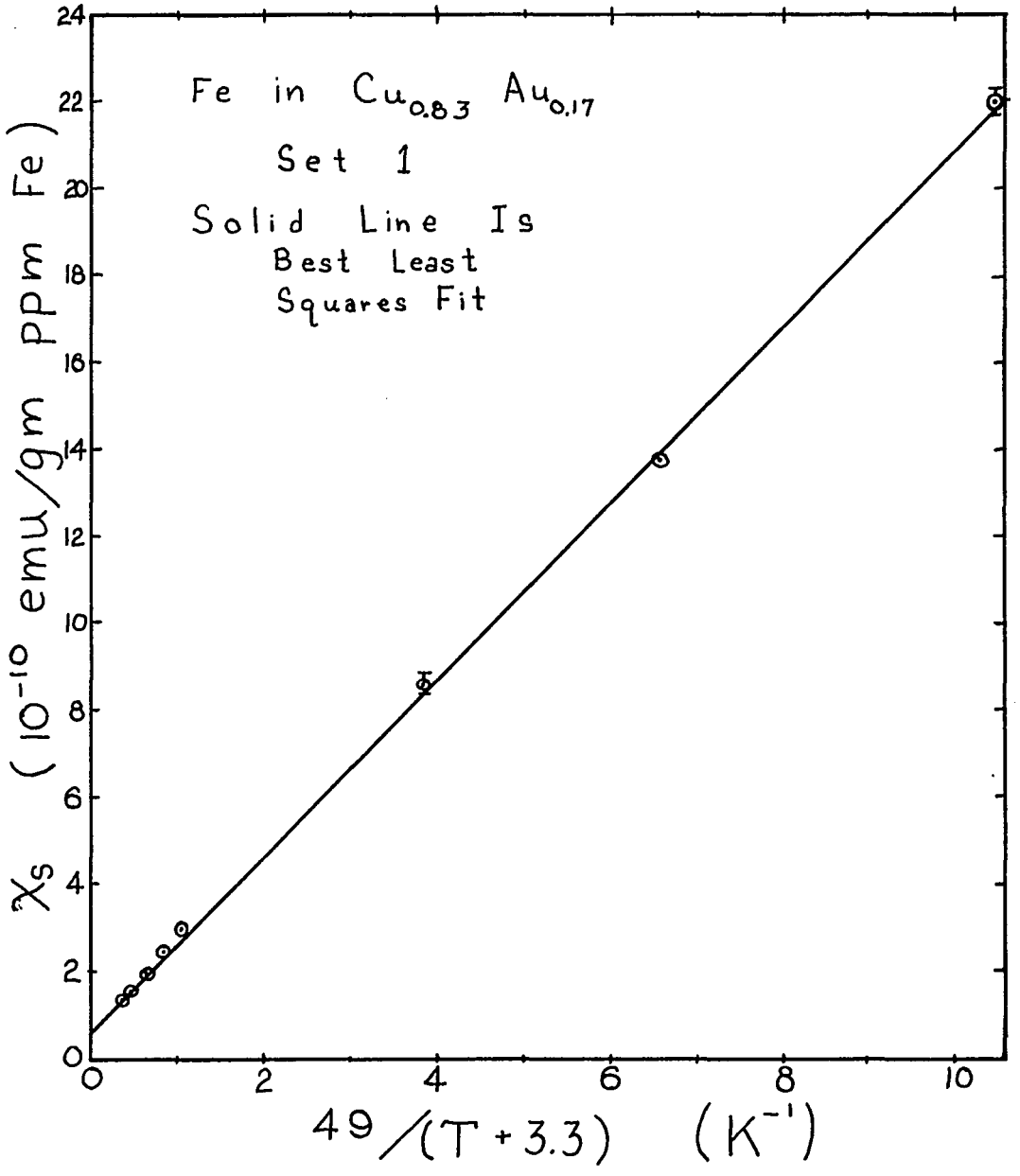
Fe in $Cu_{0.83}$ $Au_{0.17}$
Set 1
Solid Line Is
Best Least
Squares Fit
χ_s (10^{-10} emu/gm ppm Fe)
$49/(T+3.3)$ (K^{-1})
0
2
4
6
8
10
12
14
16
18
20
22
24

Figure 21

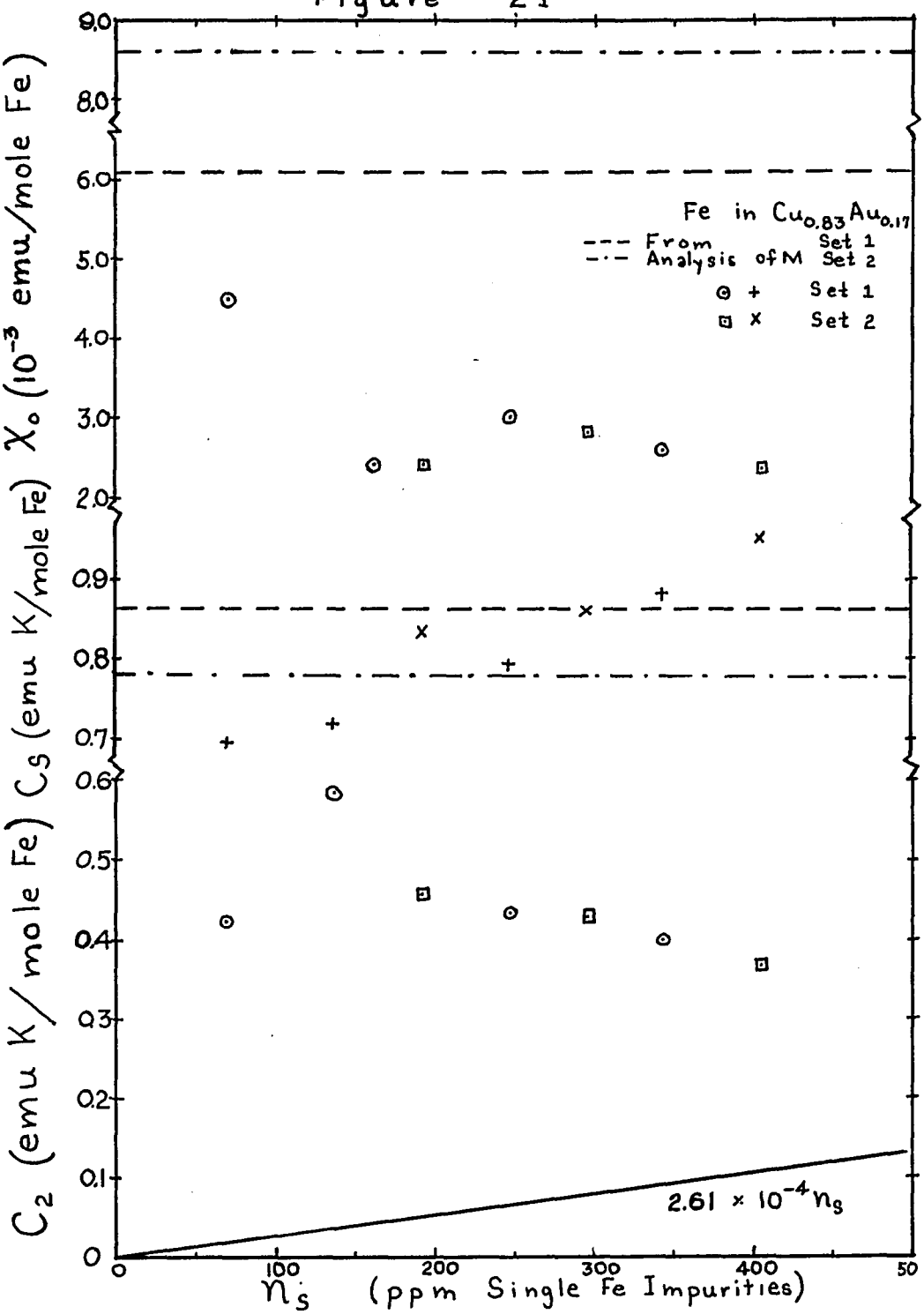
Fe in $Cu_{0.83}Au_{0.17}$
From Analysis of M
Set 1
Set 2
Set 1
Set 2
$2.61 \times 10^{-4} n_s$
C_2 (emu K/mole Fe) C_s (emu K/mole Fe) χ_o (10^{-3} emu/mole Fe)
n_s (ppm Single Fe Impurities)
9.0
8.0
6.0
5.0
4.0
3.0
2.0
0.9
0.8
0.7
0.6
0.5
0.4
0.3
0.2
0.1
0
100
200
300
400
50

Figure 22

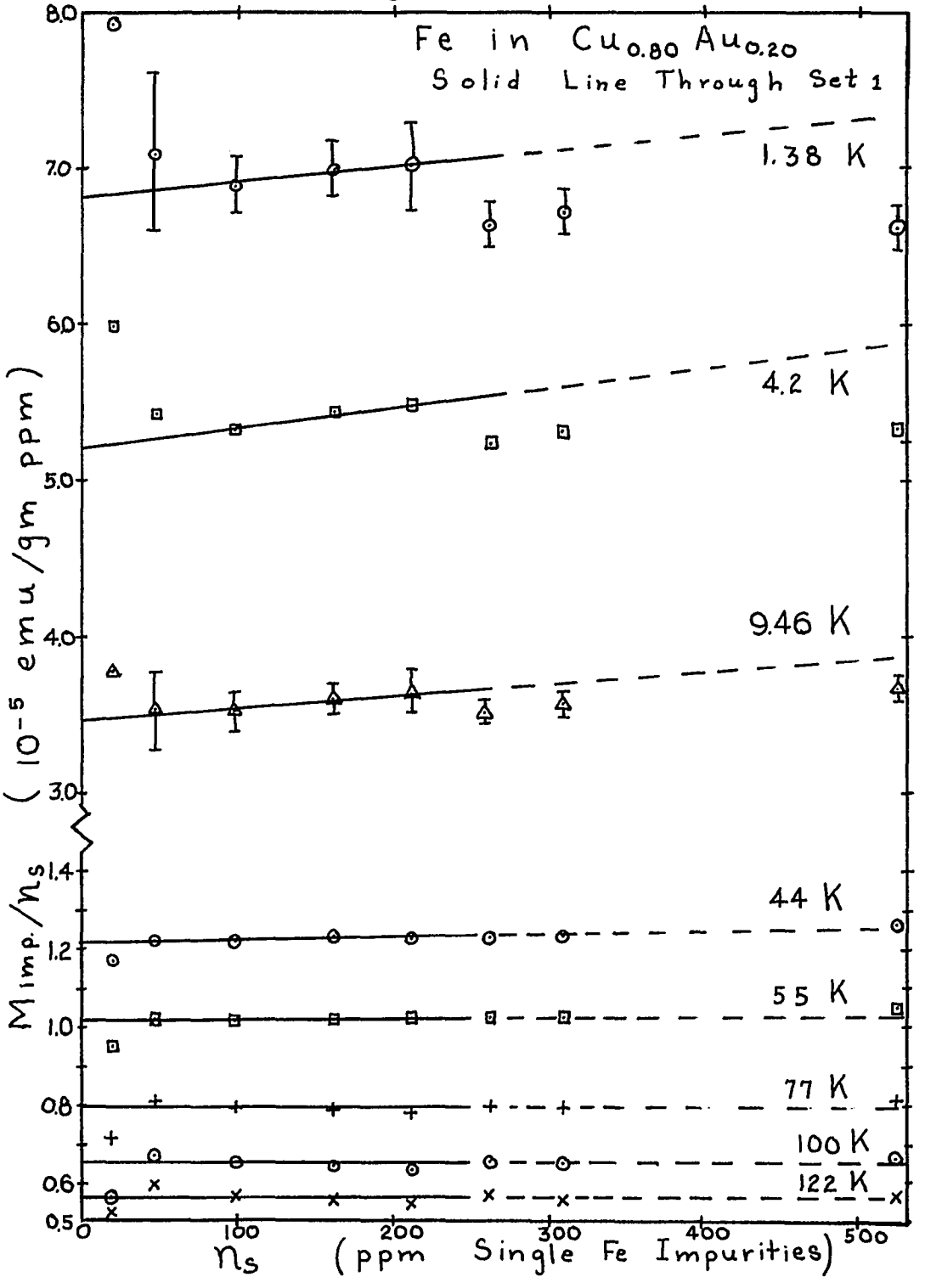
Fe in Cu0.80 Au0.20
Solid Line Through Set 1
1.38 K
4.2 K
9.46 K
44 K
55 K
77 K
100 K
122 K
8.0
7.0
6.0
5.0
4.0
3.0
1.4
1.2
1.0
0.8
0.6
0.5
0
100
200
300
400
500
Mimp./ns (10-5 emu/gm ppm)
ns (ppm Single Fe Impurities)

Figure 23

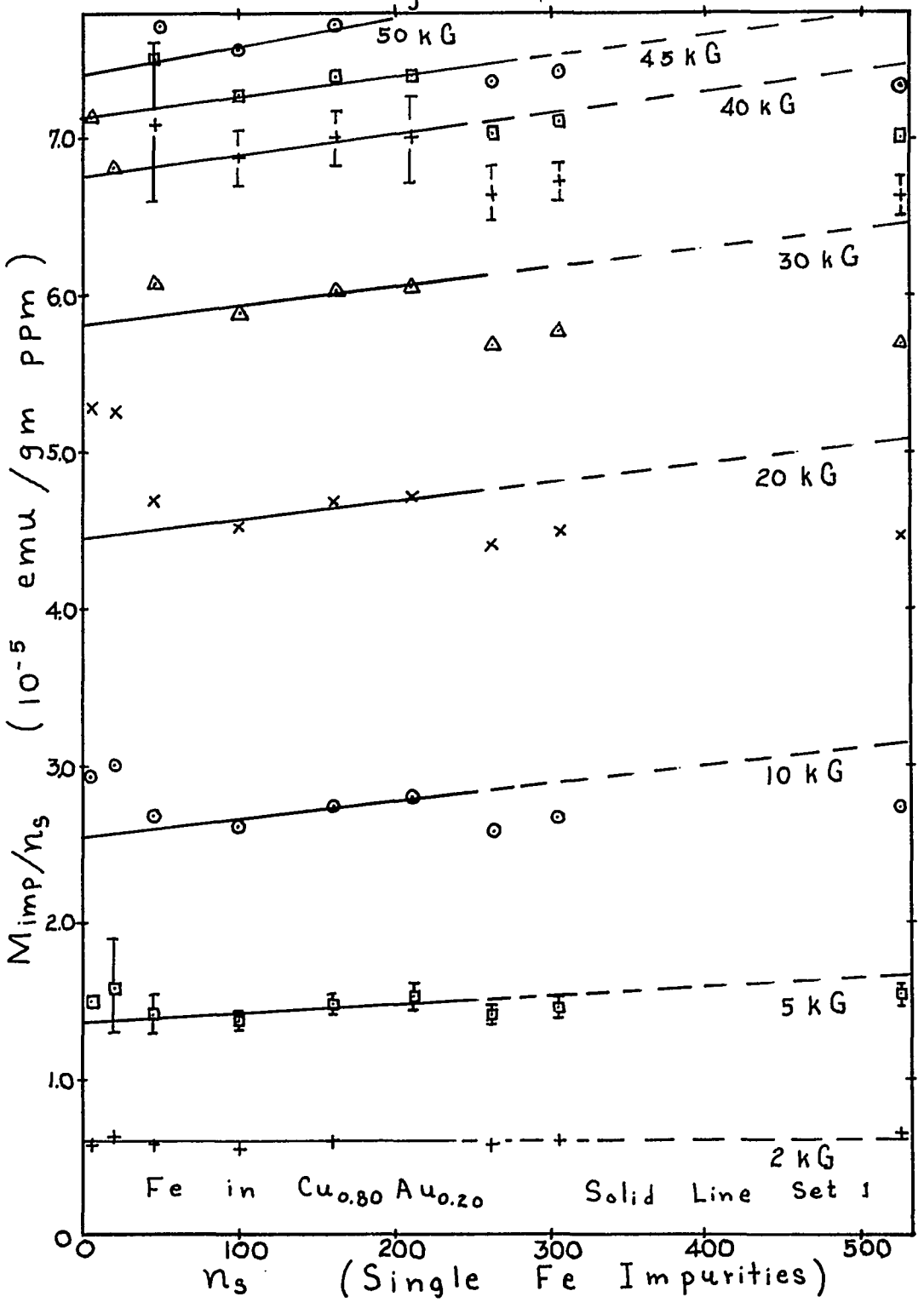
50 kG
45 kG
40 kG
30 kG
20 kG
10 kG
5 kG
2 kG
Fe in Cu0.80 Au0.20 Solid Line Set 1
Mimp/ns (10-5 emu/gm ppm)
ns (Single Fe Impurities)
0
1.0
2.0
3.0
4.0
5.0
6.0
7.0
100
200
300
400
500

Figure 24

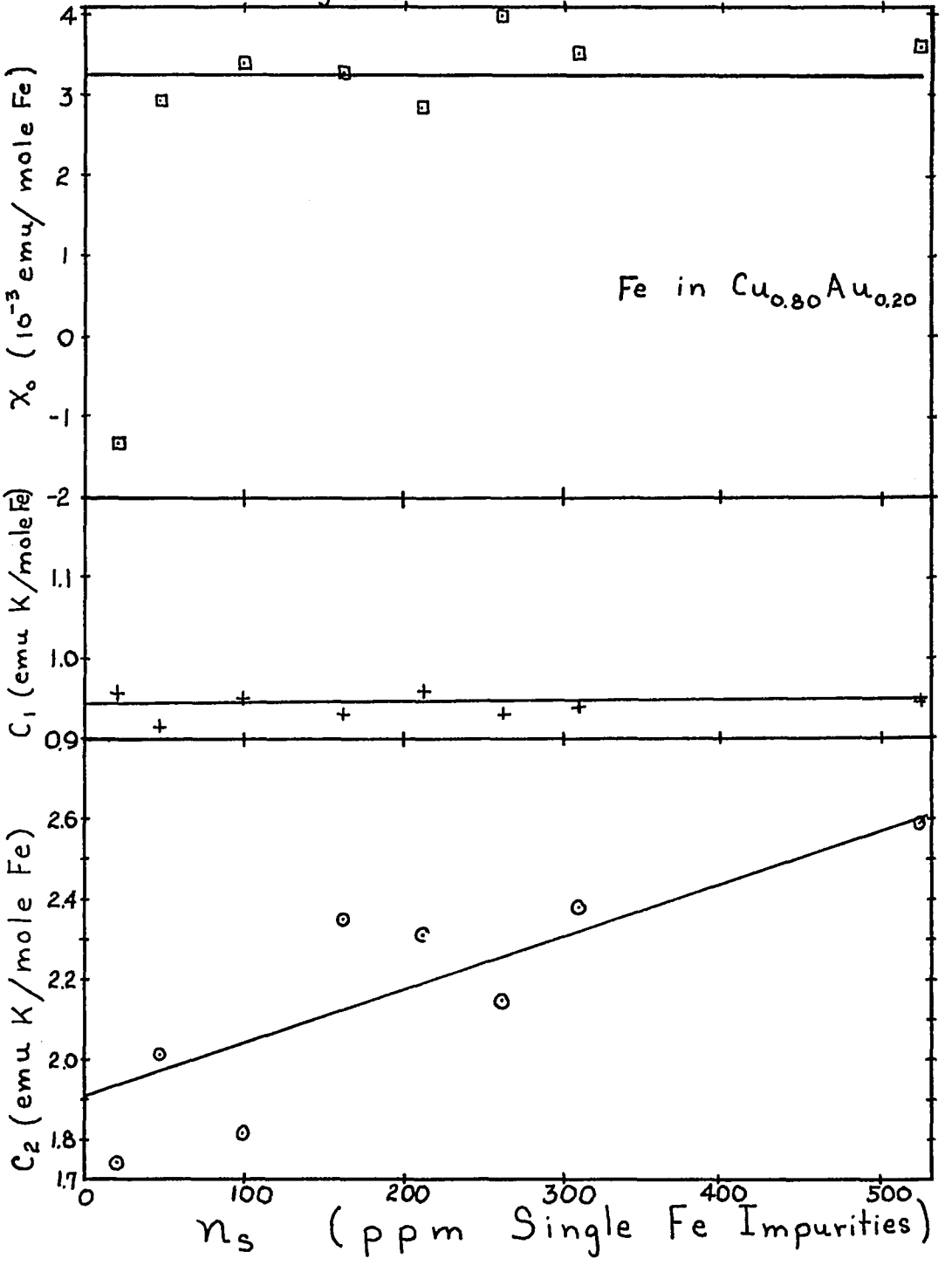
Fe in $Cu_{0.80}Au_{0.20}$
χ_o (10^{-3} emu/ mole Fe)
C_1 (emu K/mole Fe)
C_2 (emu K/mole Fe)
n_s (ppm Single Fe Impurities)
4
3
2
1
0
-1
-2
1.1
1.0
0.9
2.6
2.4
2.2
2.0
1.8
1.7
0
100
200
300
400
500

Figure 25

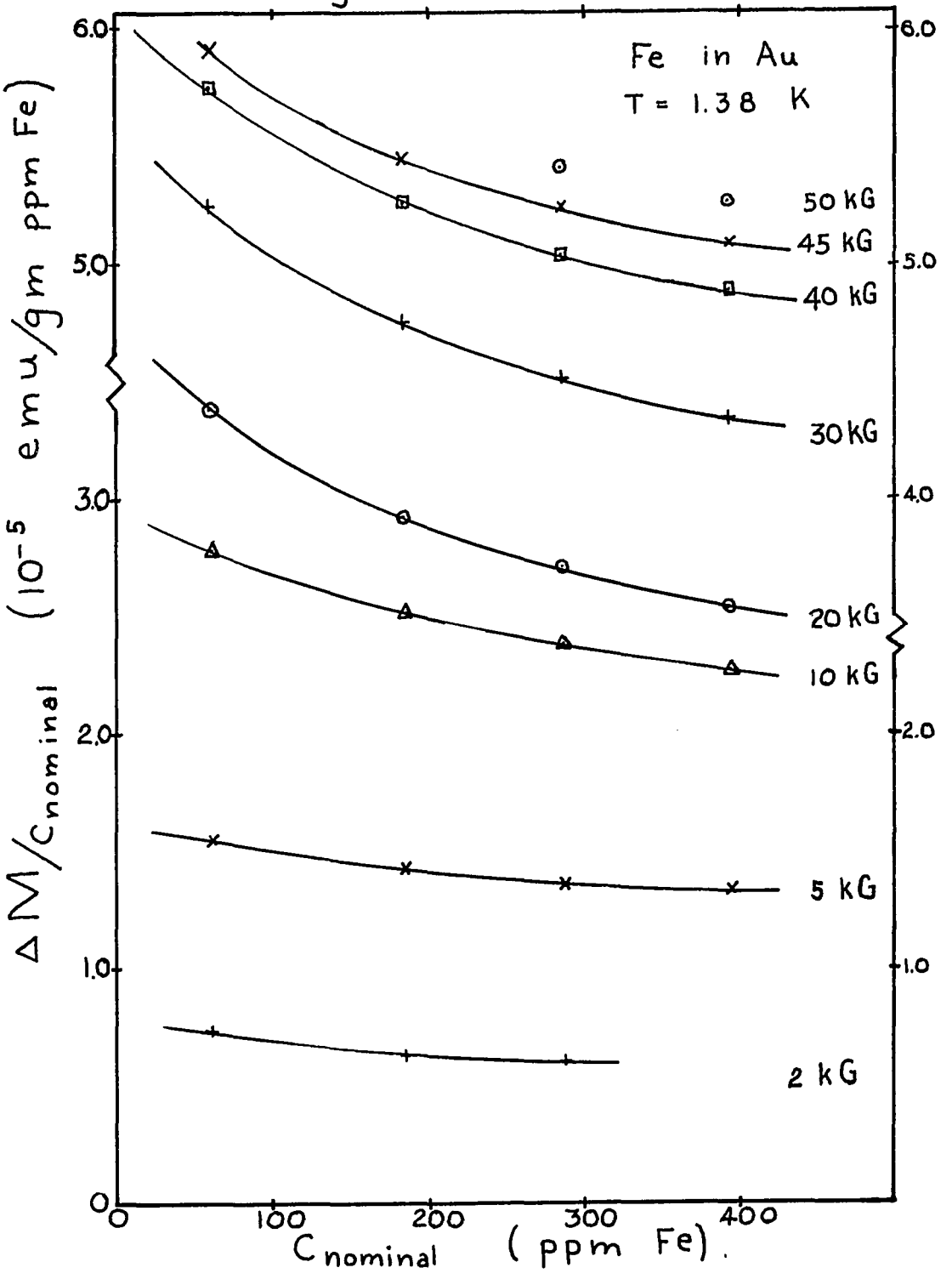
Fe in Au
T = 1.38 K
50 kG
45 kG
40 kG
30 kG
20 kG
10 kG
5 kG
2 kG
6.0
5.0
4.0
3.0
2.0
1.0
0
100
200
300
400
$\Delta M/C_{nominal}$ (10^{-5} emu/gm ppm Fe)
$C_{nominal}$ (ppm Fe).

Figure 26

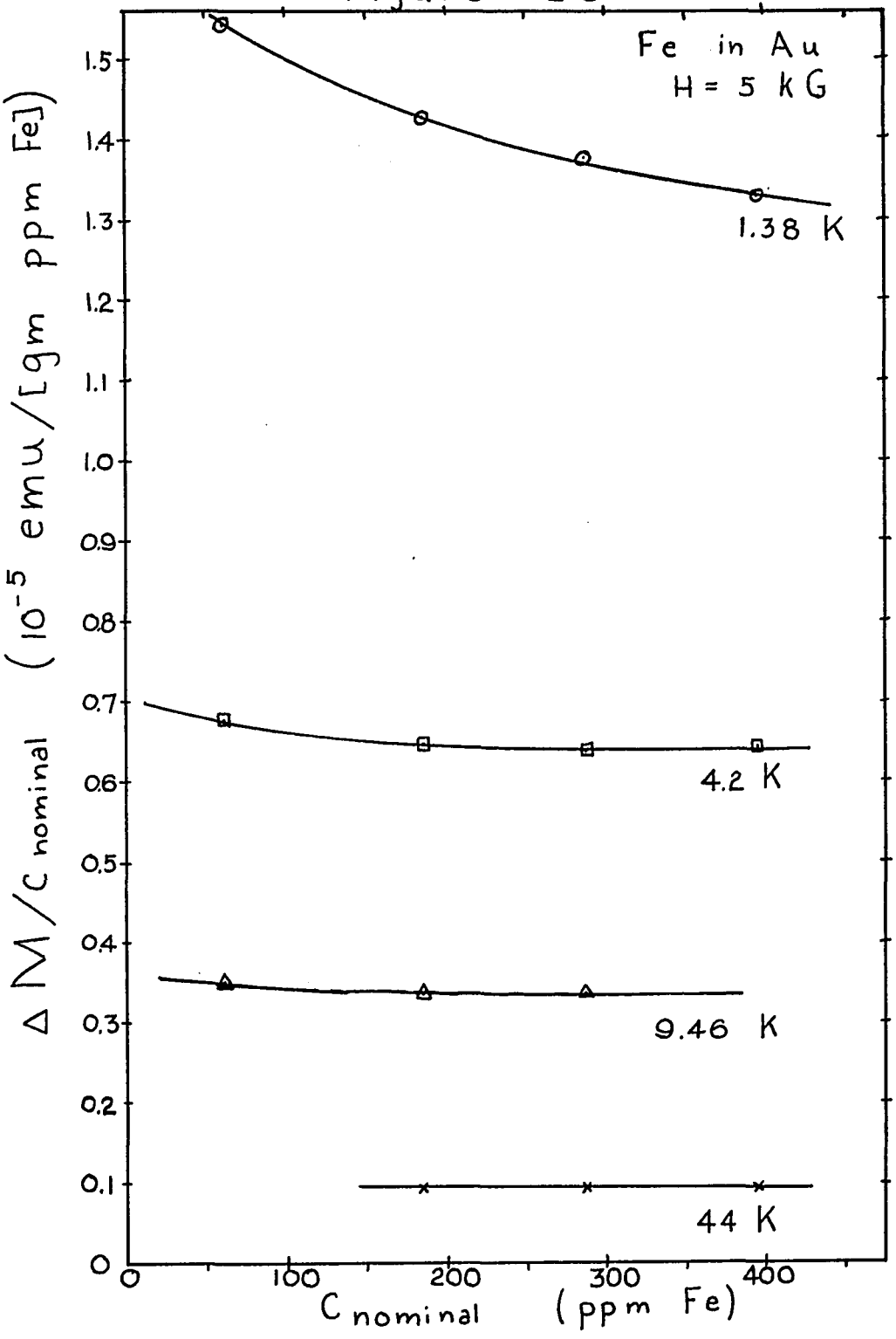
Fe in Au
H = 5 kG
1.38 K
4.2 K
9.46 K
44 K
Δ M/C nominal (10⁻⁵ emu/[gm ppm Fe])
C nominal (ppm Fe)
0
0.1
0.2
0.3
0.4
0.5
0.6
0.7
0.8
0.9
1.0
1.1
1.2
1.3
1.4
1.5
0
100
200
300
400

Figure 27

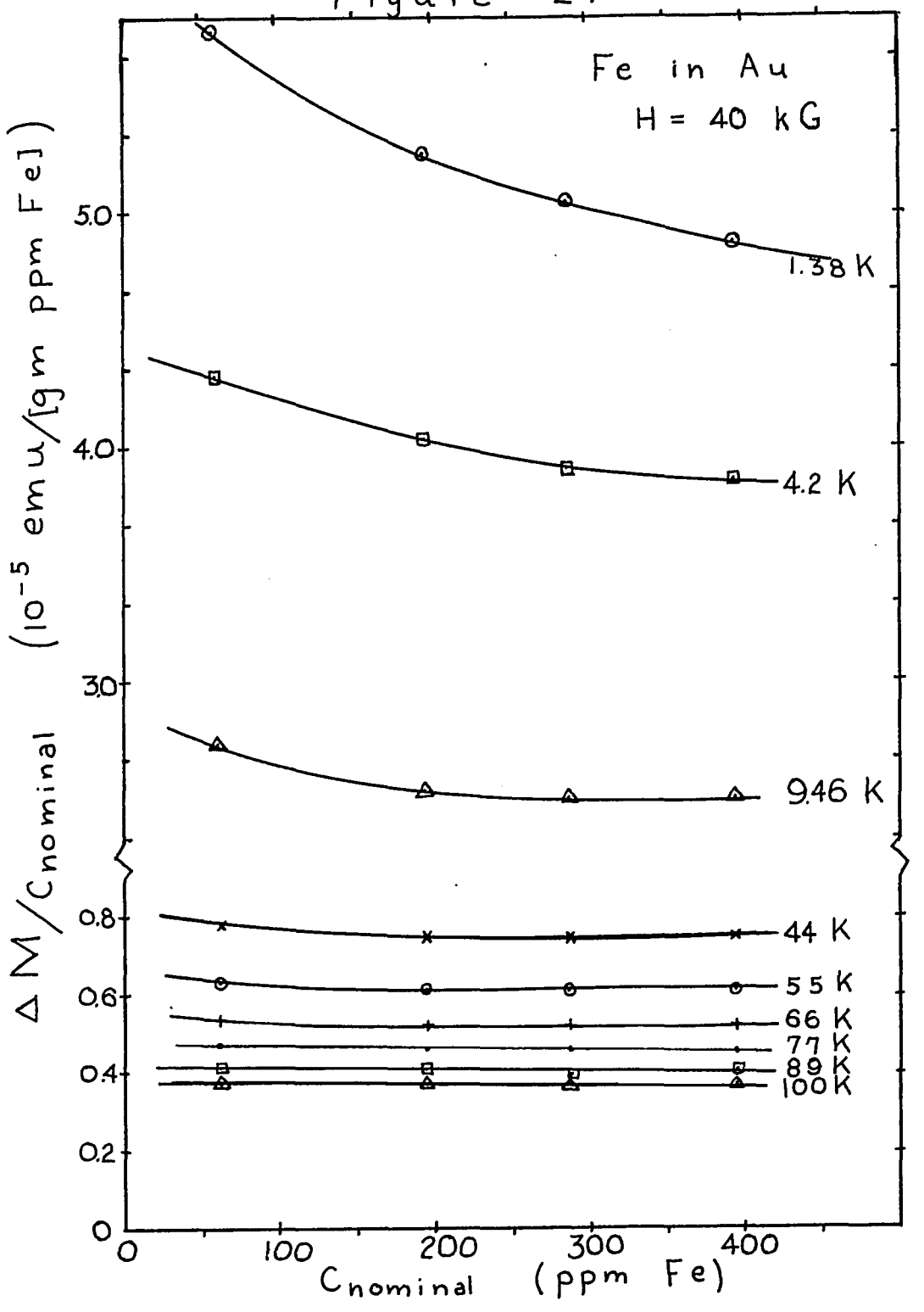
Fe in Au
H = 40 kG
1.38 K
4.2 K
9.46 K
44 K
55 K
66 K
77 K
89 K
100 K
ΔM/Cnominal (10⁻⁵ emu/gm ppm Fe)
Cnominal (ppm Fe)
0
0.2
0.4
0.6
0.8
3.0
4.0
5.0
100
200
300
400

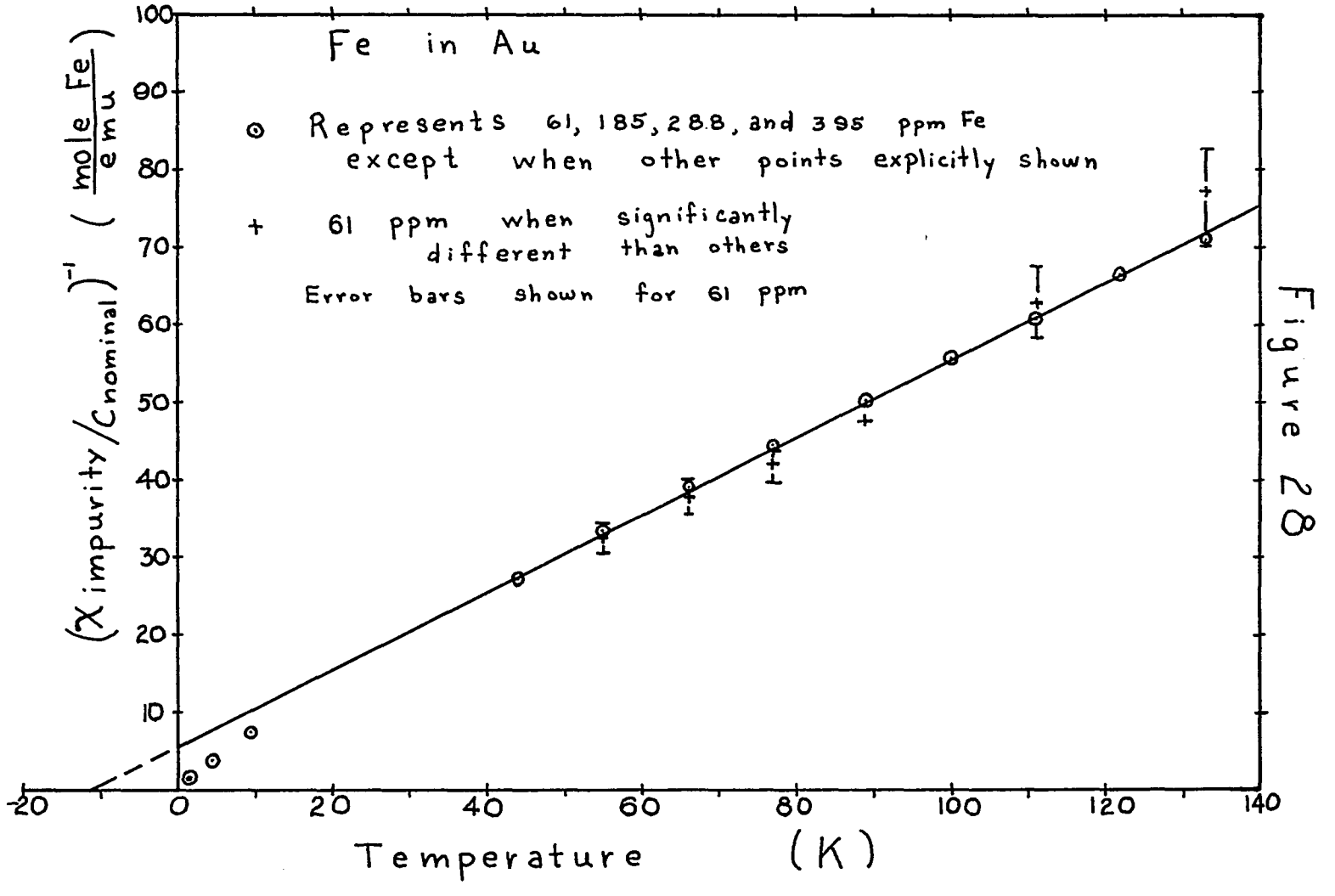
Fe in Au
⊙ Represents 61, 185, 288, and 395 ppm Fe except when other points explicitly shown
+ 61 ppm when significantly different than others
Error bars shown for 61 ppm
$(\chi_{impurity}/C_{nominal})^{-1}$ $\left(\frac{mole\ Fe}{emu}\right)$
Temperature (K)
100
90
80
70
60
50
40
30
20
10
-20
0
20
40
60
80
100
120
140

Figure 28

Figure 29

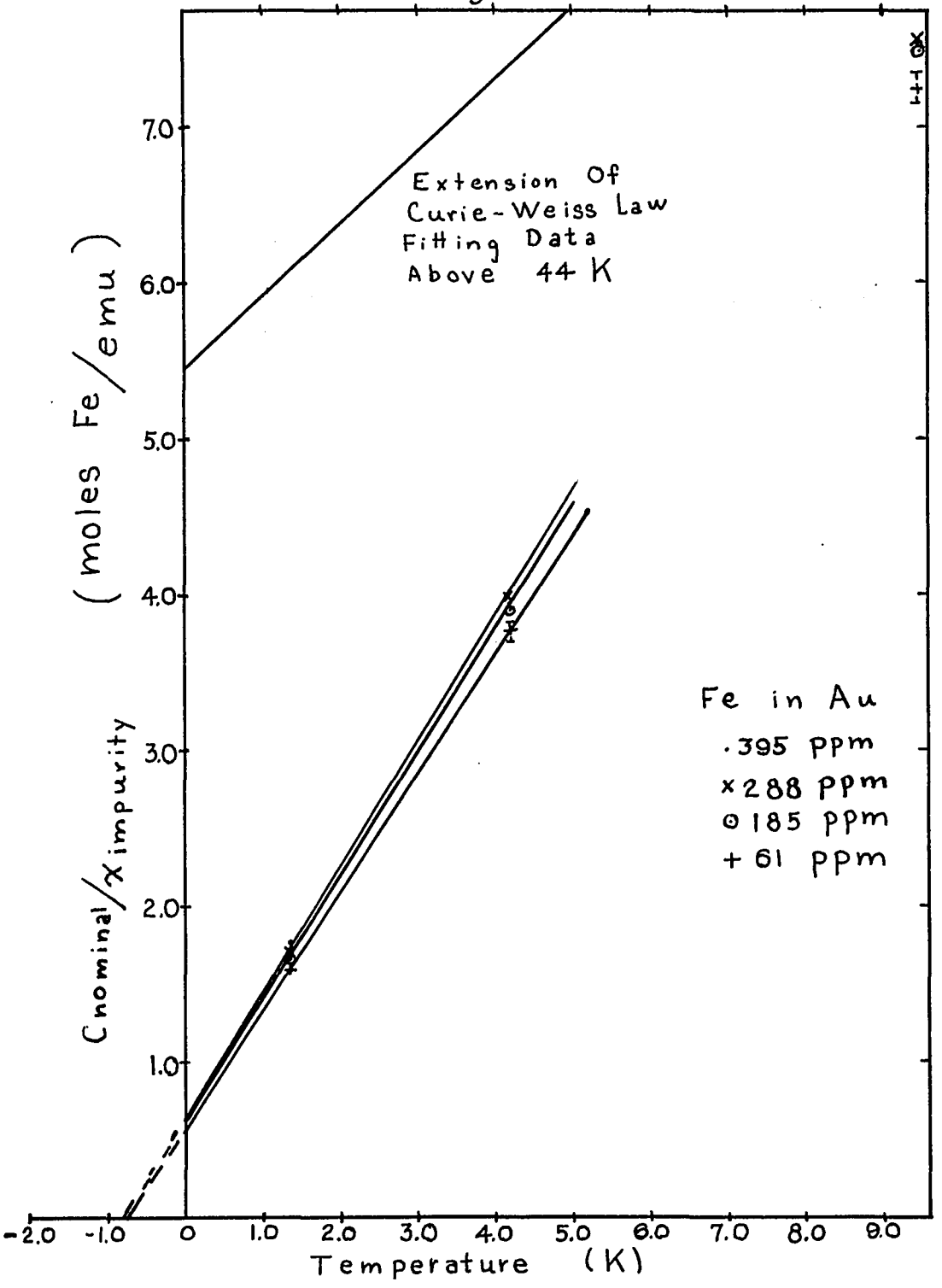
Extension Of
Curie-Weiss Law
Fitting Data
Above 44 K
Fe in Au
.395 ppm
×288 ppm
○185 ppm
+61 ppm
(moles Fe/emu)
Cnominal/χimpurity
Temperature (K)
-2.0
-1.0
0
1.0
2.0
3.0
4.0
5.0
6.0
7.0
8.0
9.0
1.0
2.0
3.0
4.0
5.0
6.0
7.0

Figure 34.

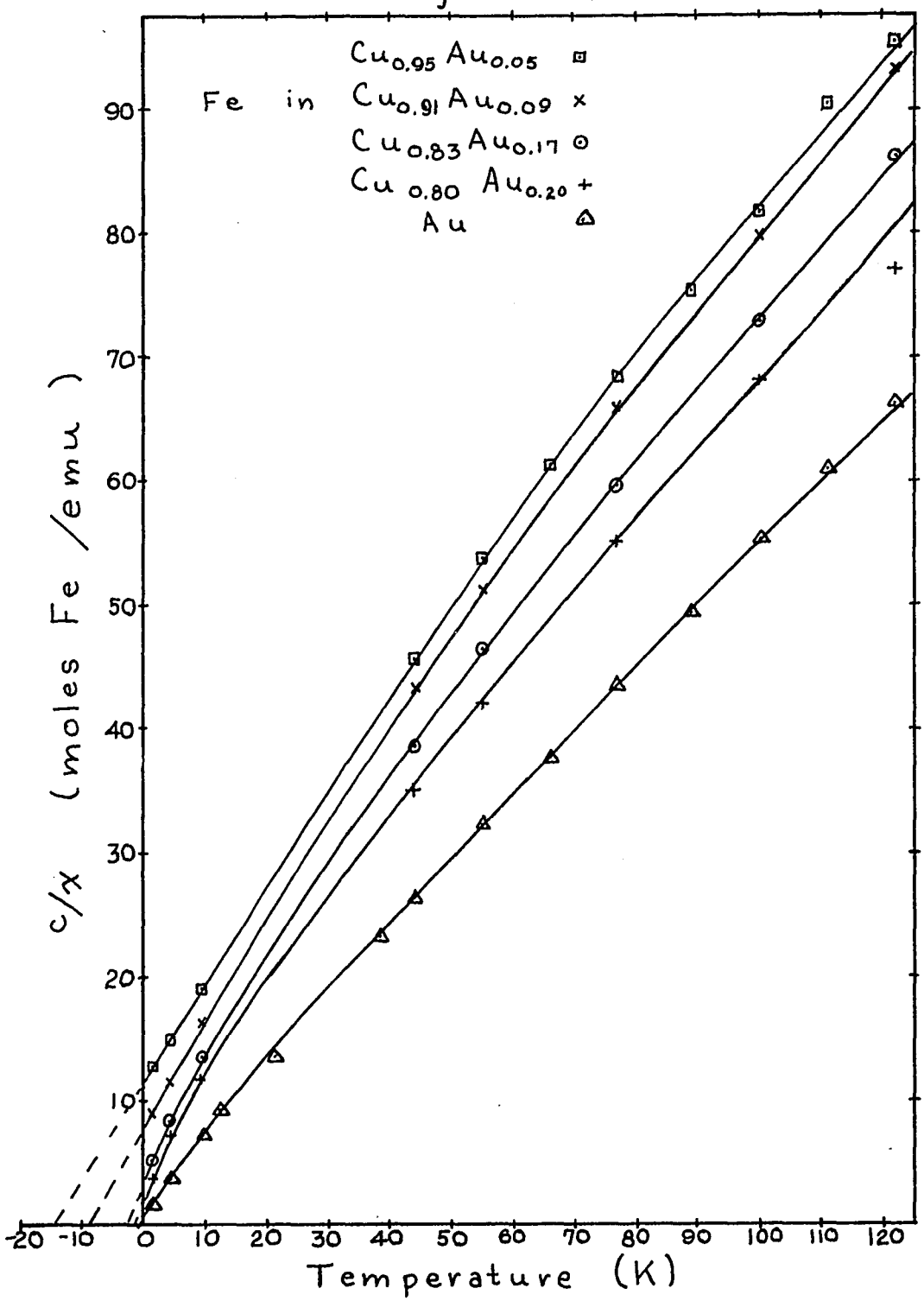
Fe in $Cu_{0.95}Au_{0.05}$
$Cu_{0.91}Au_{0.09}$
$Cu_{0.83}Au_{0.17}$
$Cu_{0.80}Au_{0.20}$
Au
c/χ (moles Fe /emu)
Temperature (K)
-20 -10 0 10 20 30 40 50 60 70 80 90 100 110 120
10 20 30 40 50 60 70 80 90

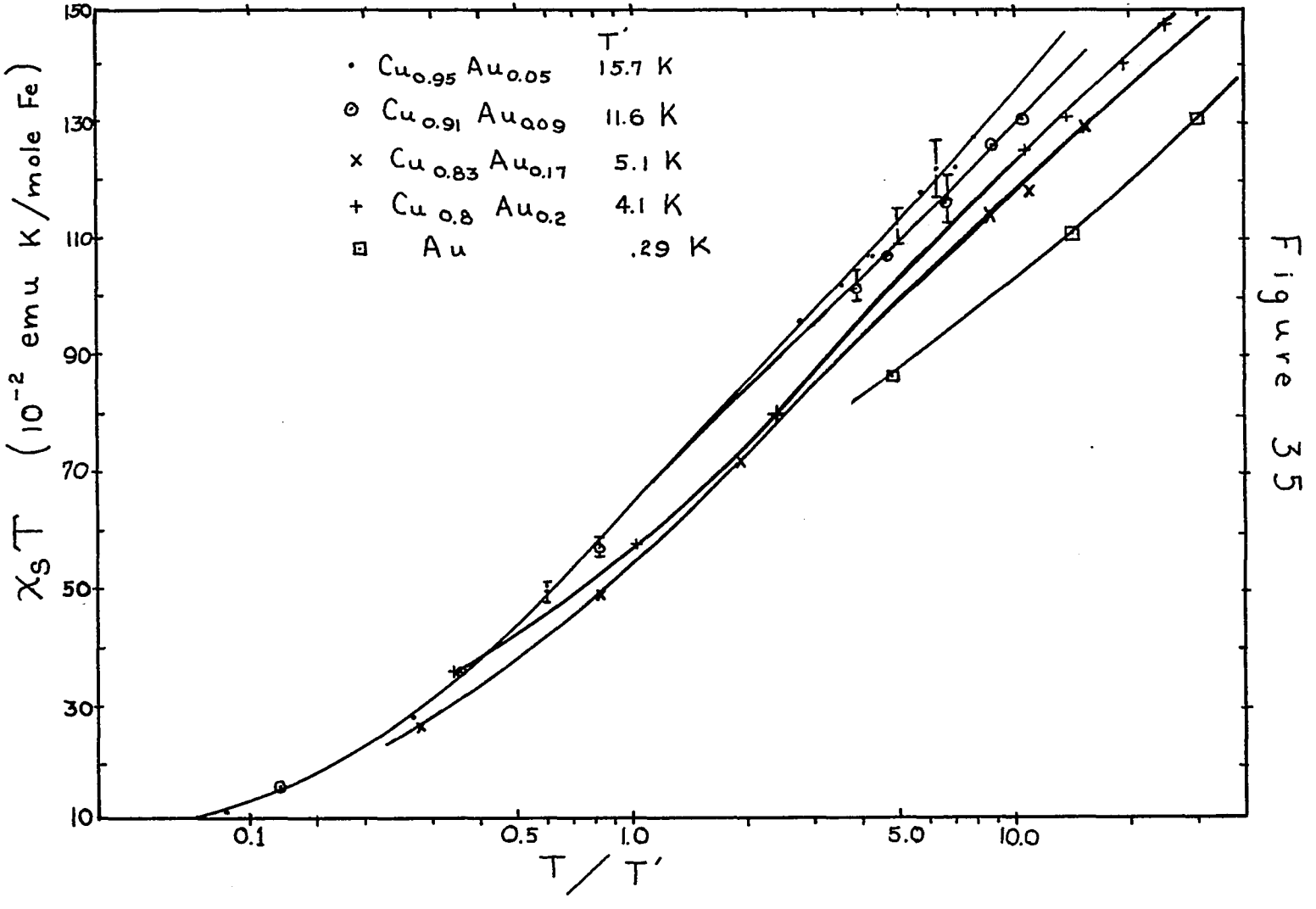
T'
• $Cu_{0.95}Au_{0.05}$ 15.7 K
⊙ $Cu_{0.91}Au_{0.09}$ 11.6 K
× $Cu_{0.83}Au_{0.17}$ 5.1 K
+ $Cu_{0.8}Au_{0.2}$ 4.1 K
⊡ Au .29 K
$\chi_S T$ (10^{-2} emu K/mole Fe)
150
130
110
90
70
50
30
10
0.1
0.5
1.0
5.0
10.0
T / T'

Figure 35

Figure 36

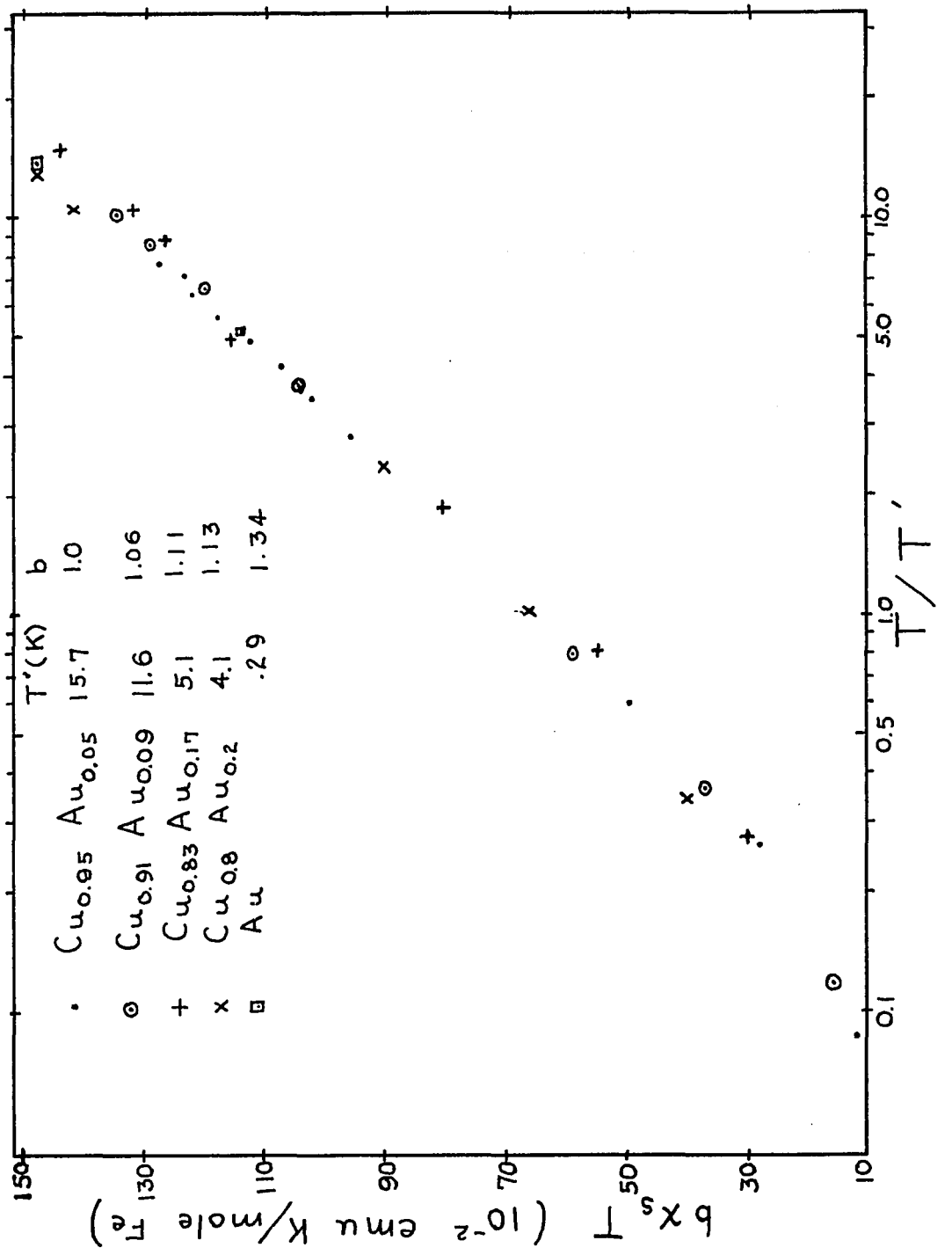
$b\chi_s T$ (10^{-2} emu K/mole Fe)
T/T'
T'(K) b
$Cu_{0.95}Au_{0.05}$ 15.7 1.0
$Cu_{0.91}Au_{0.09}$ 11.6 1.06
$Cu_{0.83}Au_{0.17}$ 5.1 1.11
$Cu_{0.8}Au_{0.2}$ 4.1 1.13
Au .29 1.34
150
130
110
90
70
50
30
10
0.1
0.5
1.0
5.0
10.0

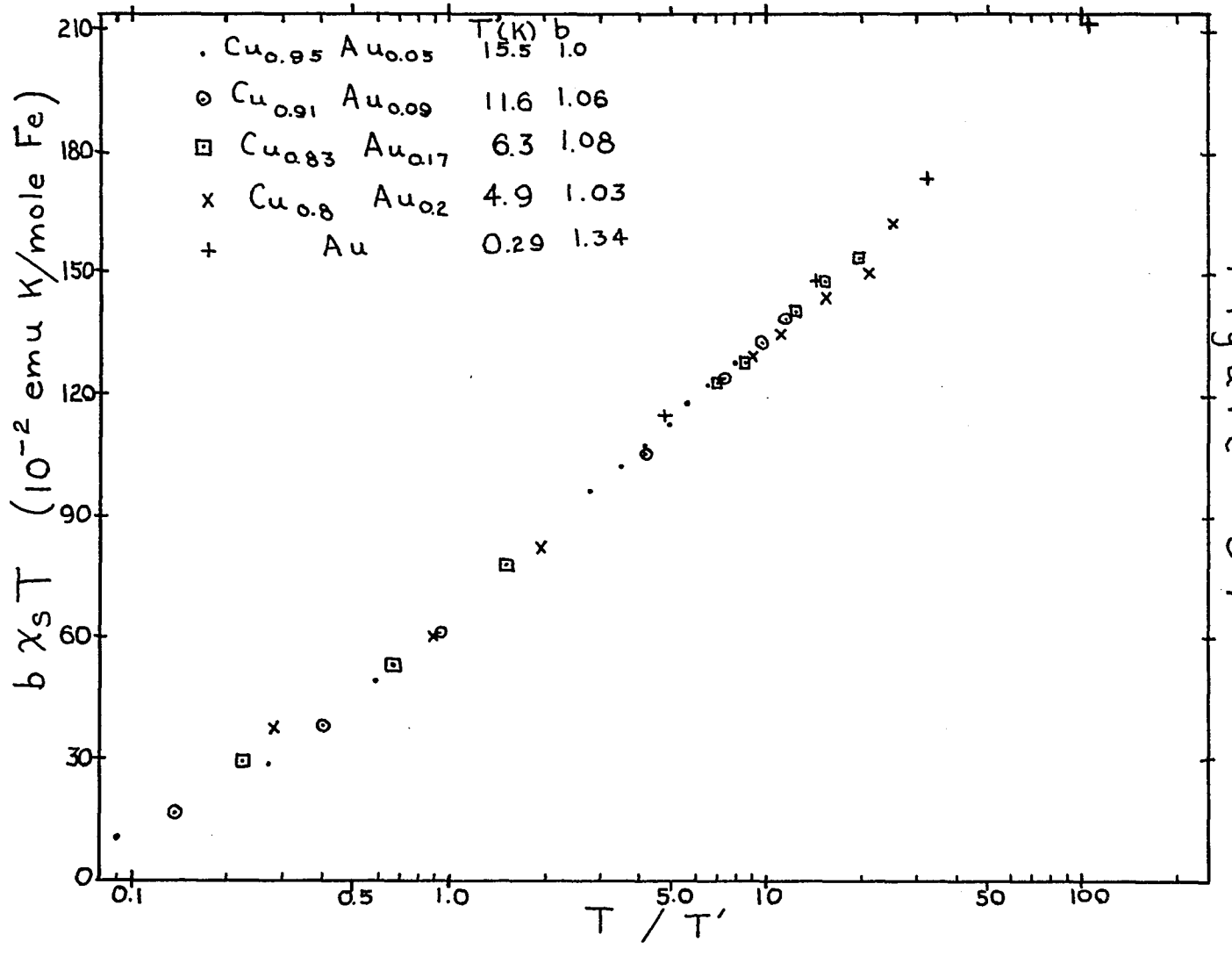
T'(K) b
. Cu0.95 Au0.05 15.5 1.0
⊙ Cu0.91 Au0.09 11.6 1.06
⊡ Cu0.83 Au0.17 6.3 1.08
x Cu0.8 Au0.2 4.9 1.03
+ Au 0.29 1.34
b χs T (10^-2 emu K/mole Fe)
210
180
150
120
90
60
30
0
0.1
0.5
1.0
5.0
10
50
100
T / T'

Figure 37

Figure 38

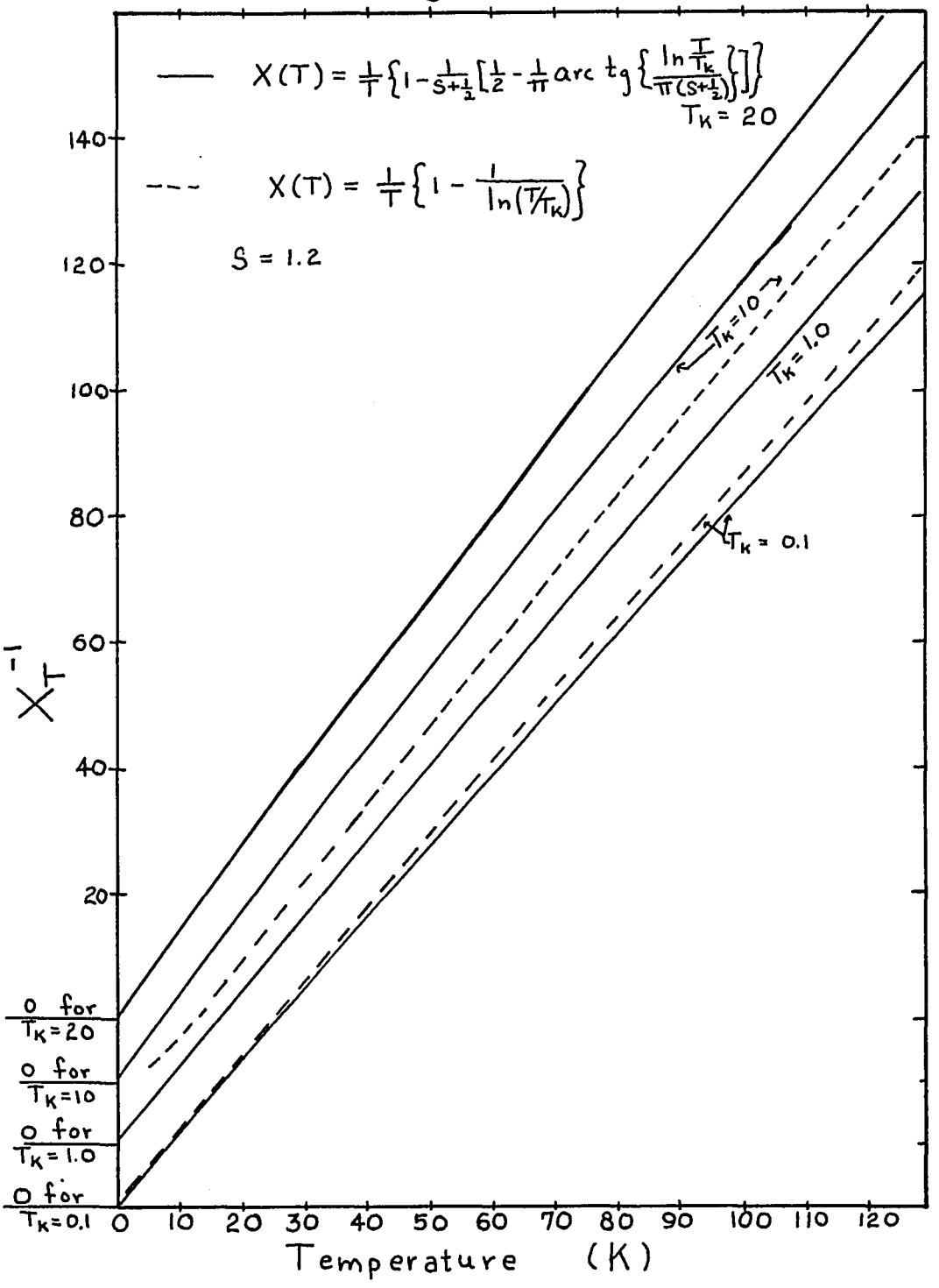
$X(T) = \frac{1}{T}\left\{1 - \frac{1}{S+\frac{1}{2}}\left[\frac{1}{2} - \frac{1}{\pi}\arctan\left\{\frac{\ln\frac{T}{T_K}}{\pi(S+\frac{1}{2})}\right\}\right]\right\}$
$T_K = 20$
$X(T) = \frac{1}{T}\left\{1 - \frac{1}{\ln(T/T_K)}\right\}$
$S = 1.2$
$T_K = 10$
$T_K = 1.0$
$T_K = 0.1$
$\bar{\chi}T$
140
120
100
80
60
40
20
0 for $T_K = 20$
0 for $T_K = 10$
0 for $T_K = 1.0$
0 for $T_K = 0.1$
0 10 20 30 40 50 60 70 80 90 100 110 120
Temperature (K)

Figure 39(a)

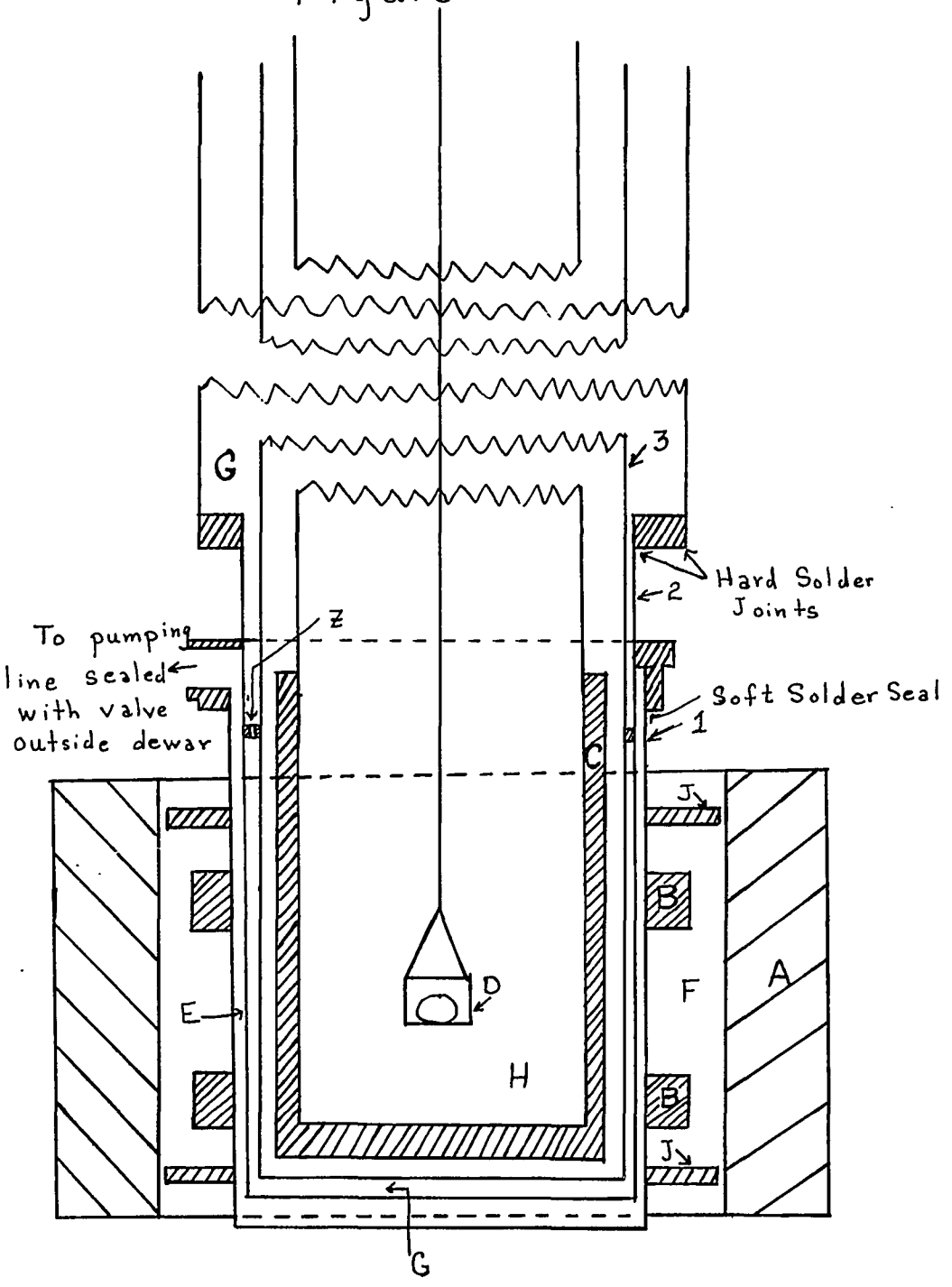
G
3
2
Hard Solder Joints
To pumping line sealed with valve outside dewar
Z
Soft Solder Seal
1
C
J
B
A
F
D
E
H
B
J
G

Figure 39 (b)

Flange R includes provisions for He transfer, level detection, and leads for magnet current.

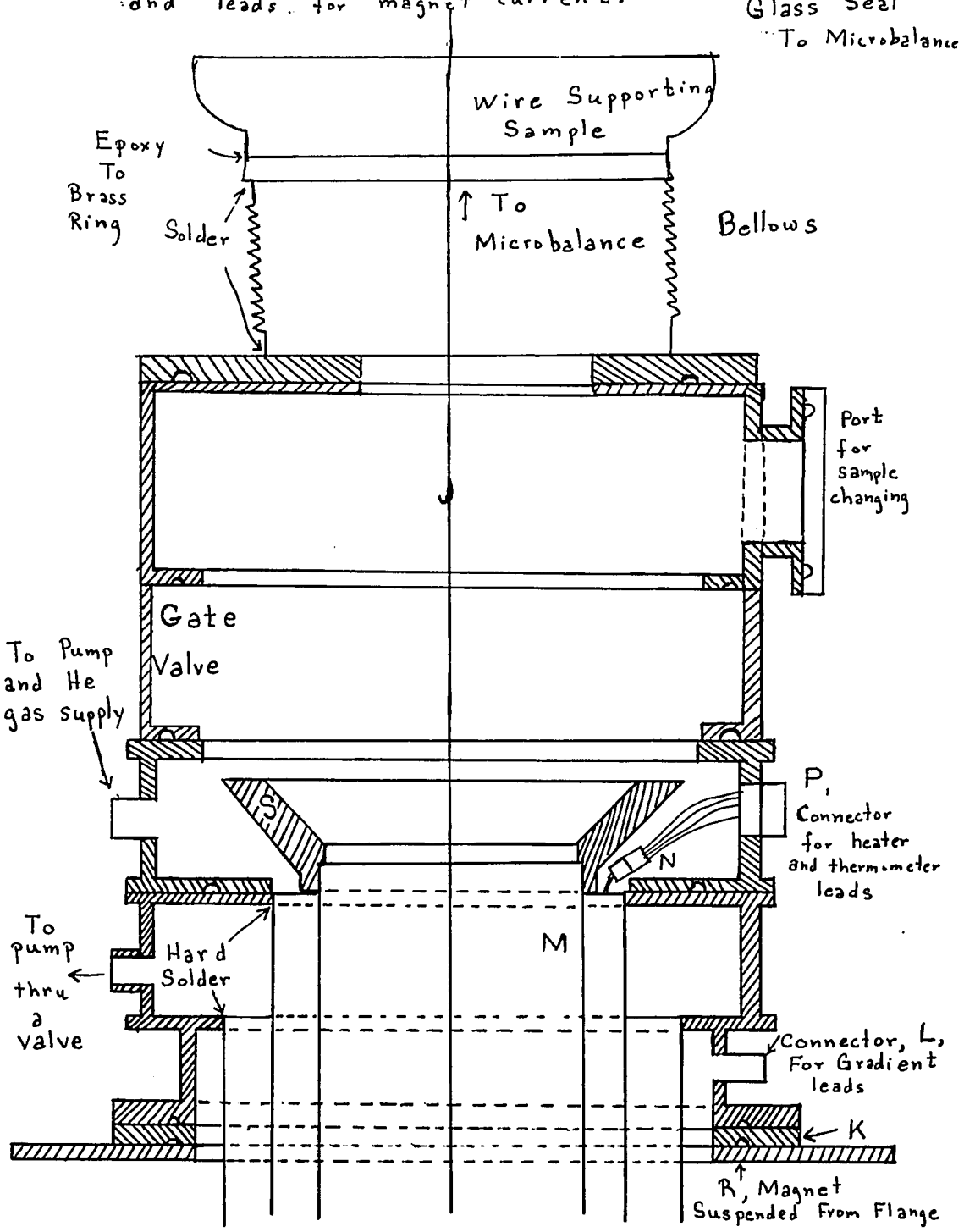

Figure 40

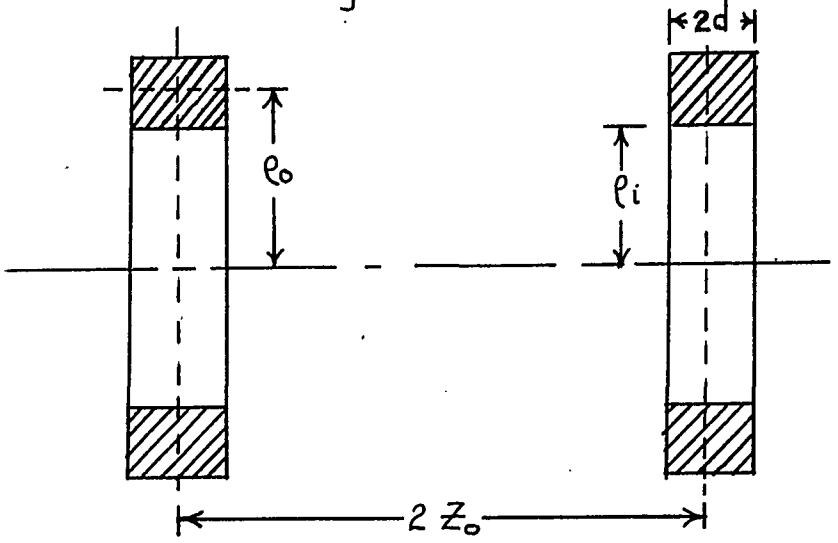

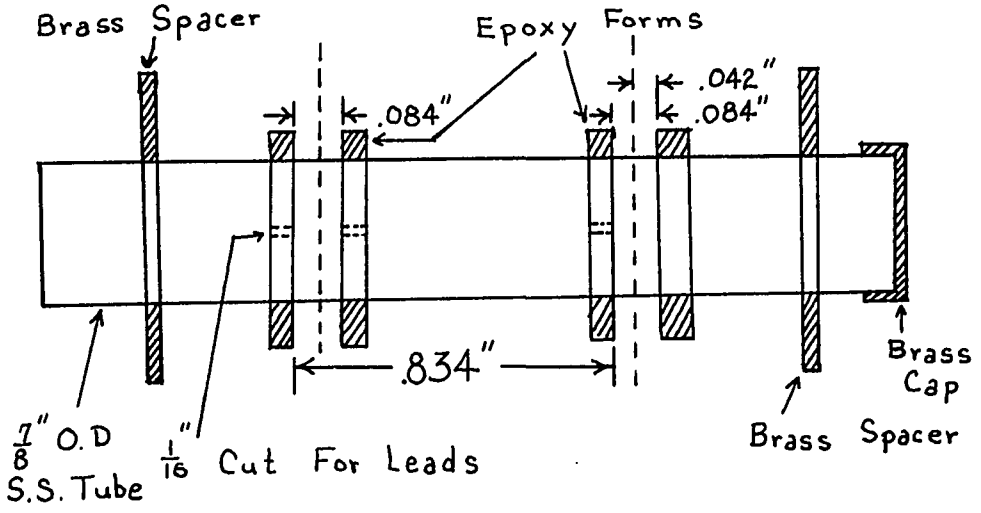

Figure 41

Figure 42

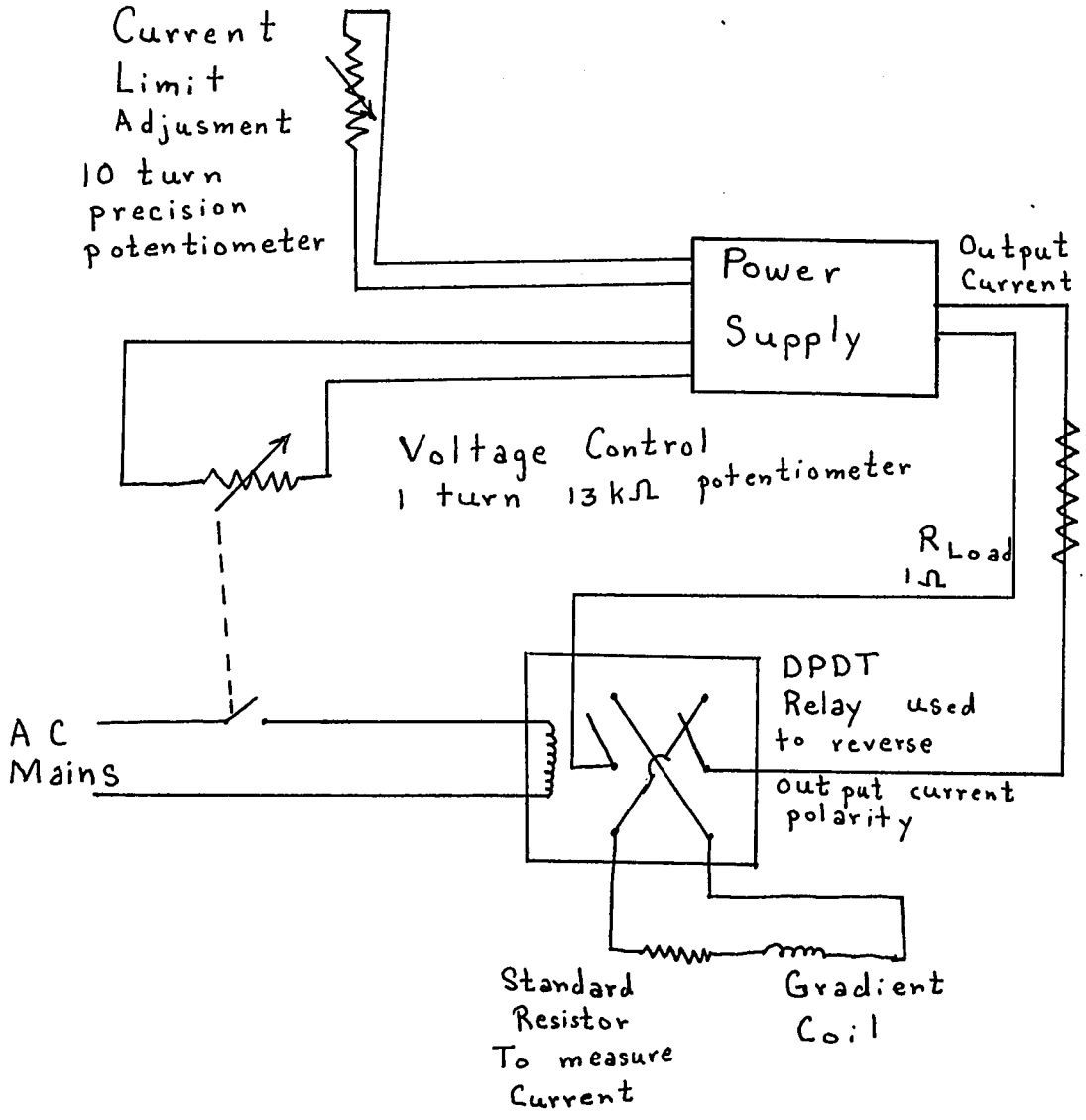
Current
Limit
Adjusment
10 turn
precision
potentiometer
Power
Supply
Output
Current
Voltage Control
1 turn 13 kΩ potentiometer
R Load
1Ω
DPDT
Relay used
to reverse
output current
polarity
A C
Mains
Standard
Resistor
To measure
Current
Gradient
Coil

Figure 43

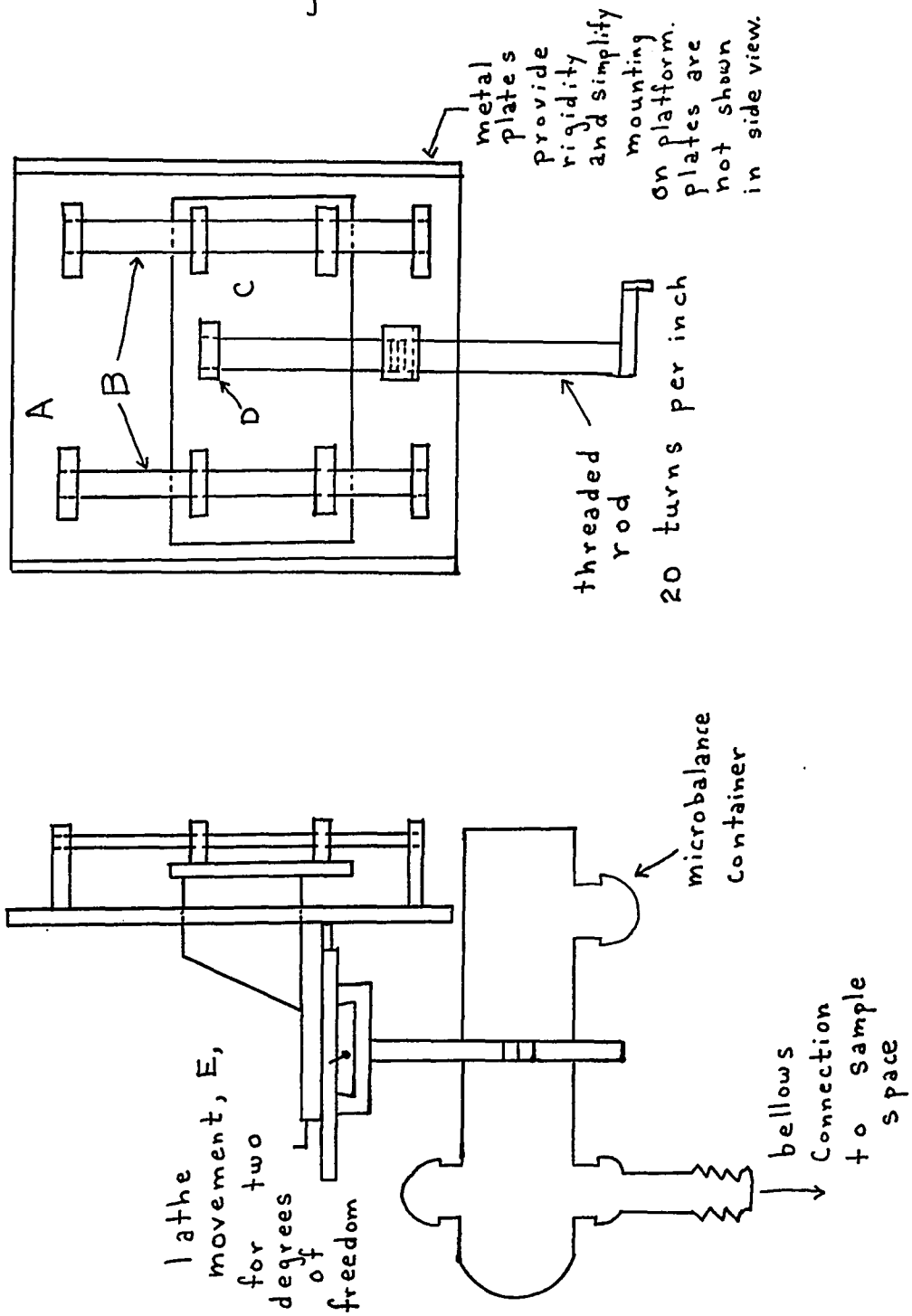
metal plates provide rigidity and simplify mounting on platform. plates are not shown in side view.
A
B
C
D
threaded rod
20 turns per inch
microbalance Container
bellows Connection to sample space
lathe movement, E, for two degrees of freedom

Figure 44

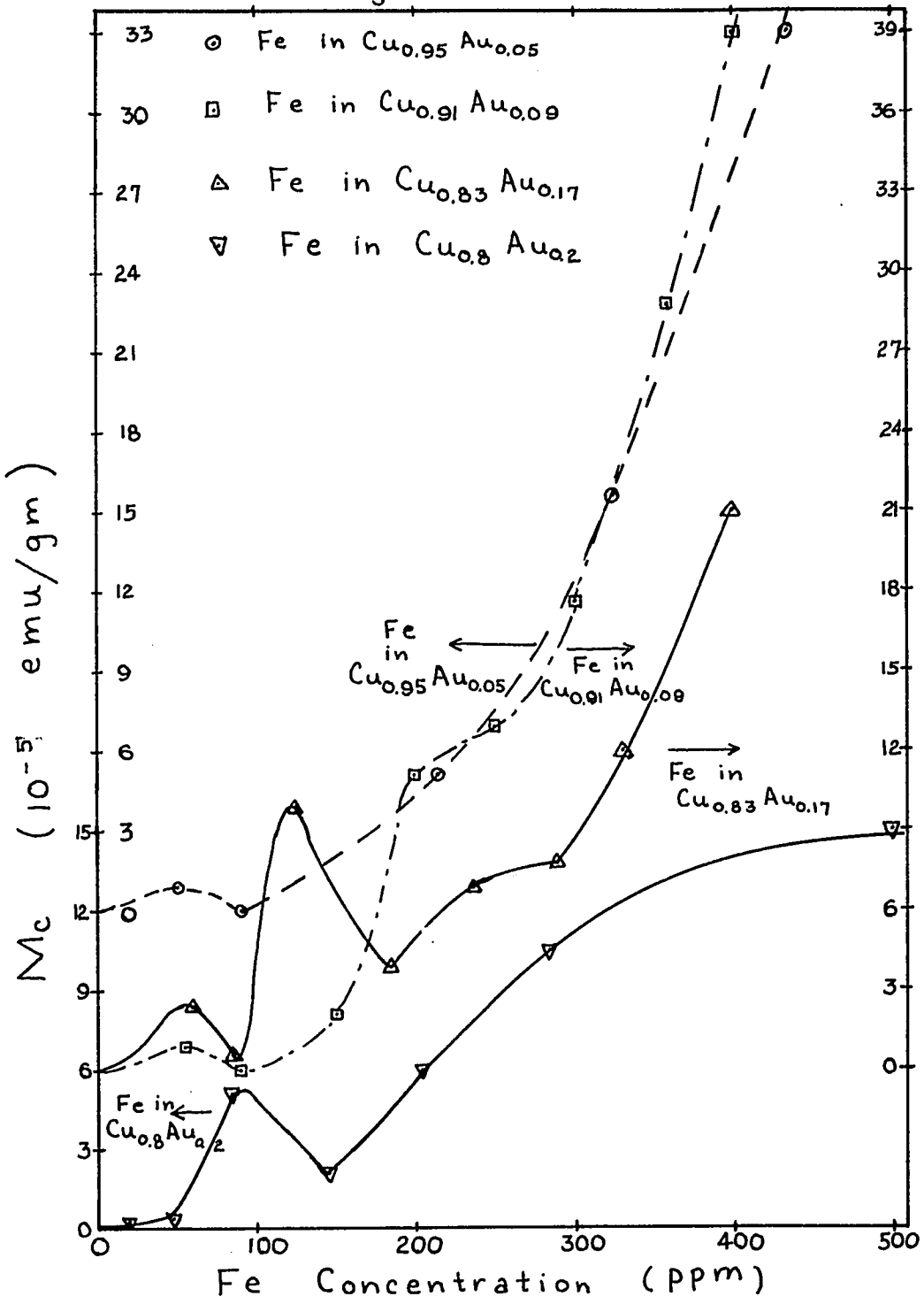
Fe in $Cu_{0.95}Au_{0.05}$
Fe in $Cu_{0.91}Au_{0.09}$
Fe in $Cu_{0.83}Au_{0.17}$
Fe in $Cu_{0.8}Au_{0.2}$
Fe in $Cu_{0.95}Au_{0.05}$
Fe in $Cu_{0.91}Au_{0.09}$
Fe in $Cu_{0.83}Au_{0.17}$
Fe in $Cu_{0.8}Au_{0.2}$
M_c (10^{-5} emu/gm)
Fe Concentration (ppm)
0
100
200
300
400
500

TABLE CAPTIONS

Table 1. A summary of some previous magnetization and susceptibility measurements on Cu(Fe).

Table 2. A summary of some previous magnetization and susceptibility measurements on Au(Fe).

Table 3. Magnetization and susceptibility of alloys of Fe in $Cu_{0.95}Au_{0.05}$ after correction for a contribution due to superparamagnetic clusters.

Table 4. Magnetization and susceptibility of alloys of Fe in $Cu_{0.91}Au_{0.09}$ after correction for a contribution due to superparamagnetic clusters.

Table 5. Magnetization and susceptibility of alloys of Fe in $Cu_{0.83}Au_{0.17}$ after correction for a contribution due to superparamagnetic clusters.

Table 6. Magnetization and susceptibility of alloys of Fe in $Cu_{0.8}Au_{0.2}$ after correction for a contribution due to superparamagnetic clusters.

Table 7. Magnetization and susceptibility of Au(Fe) alloys.

Table 8. Single impurity concentration for $Cu_{0.95}Au_{0.05}$(Fe) alloys as determined from high field susceptibility. Also shown are various contributions to the uncertainty in n_s.

Table 9. Single impurity concentration for $Cu_{0.91}Au_{0.09}$(Fe) alloys as determined from the high field susceptibility.

Table 10. Single impurity concentration for $Cu_{0.83}Au_{0.17}$(Fe) alloys as determined from the high field susceptibility.

Table 11. Single impurity concentration for $Cu_{0.8}Au_{0.2}$(Fe) alloys as determined from the high field susceptibility.

Tables 12 - 14. Coefficients M_o, M_1 and M_2 found from fits of the magnetization of $Cu_{0.95}Au_{0.05}$(Fe) alloys to $M_o+M_1n_s+M_2n_s^2$.

Also shown are χ_o, χ_1 and χ_2 found from $\chi = M/H$ and found from $\chi = \chi_o + \chi_1 n_s + \chi_2 n_s^2$.

Tables 15-17. Coefficients M_o, M_1 and M_2 found from fits of the magnetization of $Cu_{0.91}Au_{0.09}$(Fe) alloys to $M_o + M_1 n_s + M_2 n_s^2$. Also shown are χ_o, χ_1 and χ_2 found from $\chi = M/H$ and from $\chi = \chi_o + \chi_1 n_s + \chi_2 n_s^2$.

Tables 18-20. Same as tables 15-17, except data for second set of $Cu_{0.91}Au_{0.09}$(Fe) alloys was used in the fits.

Table 21. χ_o, C_s, Θ_s, C_p and Θ_p for $Cu_{0.95}Au_{0.05}$(Fe) alloys as determined from fits of $\chi = \chi_o + C_s/(T+\Theta_s) + C_p/(T+\Theta_p)$. For comparison similar parameters found from fits of M as a function of n_s are also shown.

Table 22. Same as table 21 except using data for $Cu_{0.91}Au_{0.09}$(Fe).

Table 23. Some parameters describing the pair term.

Tables 24-26. Same as tables 15-17 except data for the first set of $Cu_{0.83}Au_{0.17}$(Fe) was used in the fits.

Tables 27-29. Similar to tables 15-17 except data for the second set of $Cu_{0.83}Au_{0.17}$(Fe) alloys was used in the fits.

Table 30. χ_o, C_s, Θ_s, C_p, and Θ_p for $Cu_{0.83}Au_{0.17}$(Fe) alloys as determined by fitting $\chi = \chi_o + C_s/(T+\Theta_s) + C_p/(T+\Theta_p)$. For comparison, similar parameters derived from coefficients of $M = M_o + M_1 n_s + M_2 n_s^2$ are also shown.

Table 31. χ_o, C_1, Θ_1, C_2 and Θ_2 for $Cu_{0.8}Au_{0.2}$(Fe) alloys determined by fitting $\chi = \chi_o + C_1/(T+\Theta_1) + C_2/(T+\Theta_2)$.

Table 32. μ_{eff} and Θ found by numerically fitting susceptibility of Au(Fe) alloys at 1.38 and 4.2 K to a Curie-Weiss law. Values found using the host susceptibility and concentrations listed in Table 33 are also given.

Table 33. Host susceptibility and Curie constant for Au(Fe) alloys found by fitting susceptibility data above 44 K to $\chi=\chi_o+C/(T+10.5)$ Values of the concentration were found by assuming C=2.0 emu K/mole Fe.

Table 34. Comparison of Θ/Θ_{CuFe} using our values of Θ and Θ_{CuFe} from Tholence and Tournier[17] with $T_K/T_{K_{CuFe}}$ from resistivity measurements by Loram et al.[21] and specific heat measurements by Delinger et al.[22]

Table 35. Probability of having n Au nearest neighbors in random $Cu_{1-x}Au_x$(Fe) alloys.

Table 36. Bucket magnetization for various values of field and temperature.

Table 37. Saturation magnetization of the superparamagnetic clusters at several temperatures.

TABLE 1

Author, Comments	Temperature range (K)	Max. field (kG)	Concentration range (ppm)	$\frac{\mu_{eff}}{\mu_B}$	Θ or T_K (K)
Hurd[74], Fit Curie-Weiss law but there are systematic deviations above 170 K	15 -300	20	15-202	3.68	32 ± 2
Hurd[75], Same data fit to $\frac{\chi_{imp}}{C} = \frac{\mu^2_{eff}}{3kT}\left[1 - \frac{1}{\ln(T/T_K)}\right]$ [43, 44]				3.79	T_K = 3.8
Daybell and Steyert[9,10] At lowest temperatures observe different behavior in small applied field	0.04-40	1	54-330	At very low temperatures is independent of field and temperature	
	Using Hurd's $\mu_{eff} = 3.7\mu_B$			$T_K = \frac{\mu^2_{eff}}{3k}$ = 18	
Chaikin and Jensen[82], Observe a transition from the high temp. behavior, C/(T+32) to low temp. behavior, C/(T+16)	4 -30	11	30, 67, and 421		
Tholence and Tournier[17], Split magnetization into terms due to single impurities and pairs of ferromagnetically coupled Fe atoms. concentration of pairs is 130 c[2]	1.3-33	70	11-600	3.4	29±1
	spin of pairs is 2.7±0.1			Θ pairs is less than 5 K	

TABLE 1 (Continued)

Franz and Sellmyer[63], also observe pairs but concentration is $65c^2$ or 1/2 value of Tholence and Tournier — 1.6-50 | 95 | 440-6000 | 3.3-5.9 | 10.4 to -0.6
pair spin is 2.9

Hirschkoff et al.[69] Complicated behavior, most magnetization comes from the pairs — 0.01-0.4 | 200 gauss | 102-478

Ekström and Myers[64], Fit to terms due to single impurities and pairs

$$\chi = \chi_o + \frac{C_1}{T+\theta_1} + \frac{C_2}{T+\theta_2}$$

had evidence of clusters

			$\chi_o(10^{-4}\frac{emu}{mole})$	$C_1(\frac{emu}{mole\ Fe})$	C_2	1	2
1.7-300	8.5	304	11	1.167	0.24	26	1.7
		211	11.5	1.165	0.20	25	2.0
		143	14	1.14	0.22	26	4.5
		92	9	1.19	0.13	24	4

Mishra and Beck[83], Analyzed data of Tholence and Tournier[17] and Hirschkoff et al.[69] into contributions due to several types of moments

	$\chi_o(10^{-8})$	$\frac{\mu_1}{\mu_B}$	$\frac{\mu_2}{\mu_B}$	$\frac{\mu_3}{\mu_B}$	θ_1	θ_2	θ_3	C_1	C_2	C_3
T.T.(108 ppm)	0.48	2.7	5.3	10.6	20	17	14	40.4	5.5	2.7
Hirschkoff (112 ppm)	8.7	7.0	9.8	29.5	0.04	-.008	0	0.55	0.022	.003

TABLE 2

A Summary of Some Previous Measurements on Au(Fe)

Author, Comments	Temperature range (K)	Max. field (kG)	Concentration range (ppm Fe)	μ_{eff} / μ_B	or T_K(K)
Hurd[74], Fits to Curie-Weiss Law with large deviations above 160 K	6-300	20	6-220	3.5-3.8 mean 3.68± 0.22	mean 10± 2
Hurd[75], Same data fit to $\frac{\chi_{imp}}{c} = \frac{\mu_{eff}^2}{3kT}\left[1 - 1/\ln(T/T_K)\right]$ [43, 44]				3.8	T_K=1.0
Loram et al.[76] Fit magnetization data up to 120 K to a Brillouin function using $g = 2\left[1 - 0.5/\ln(T_{eff}/T)\right]$	1.5-4.2	60	29 54 99	3.10± 0.15 3.07± 0.08 3.12± 0.05	0.5± 0.15 0.4± 0.1 0.5± 0.05
Claus[78], Fit to $\chi = \frac{C_1}{T+\theta_1} + \frac{C_2}{T+\theta_2}$ measurements were not sensitive to find μ_2 and Θ_2 for the more dilute alloy	4 - 800	13	C_1 / C_2(10^{-2} emu/mole) 200 / 110 1000 / 140 / 53 c=0 limit	θ_1 / θ_2 0.5 1.5 / 40	
Tholence and Tournier[73], For c<100 ppm χ/c is independent of concentration even at 0.05 K. See effects of RKKY interaction above 100 ppm.	0.05-5	70	26-5000	3.25 ± 0.2	0.4+760c

TABLE 3

$M-M_c$ (10^{-3} emu/gm) for Fe in $Cu_{0.95}Au_{0.05}$

	M_c	0.0	0.009	0.0	0.05	0.155	0.340
	c_{nom}	0.0	54.9	89.8	206	324.6	436.3
T(K)	H(kG)						
	1	-0.096	-0.041	0.004	0.152		0.413
	2	-0.193	-0.074	0.008	0.290	0.610	0.961
	5	-0.480	-0.182	0.024	0.752	1.583	2.487
	10	-0.962	-0.364	0.046	1.488	3.127	4.882
4.2	20	-1.930	-0.752	0.051	2.838	5.951	9.236
	30	-2.903	-1.168	-0.003	4.012	8.425	13.00
	40	-3.874	-1.617	-0.132	5.013	10.57	16.23
	45	-4.366	-1.856	-0.202	5.447	11.53	17.68
	50	-4.857	-2.111	-0.306	5.840	12.42	19.03
	2	-0.186	-0.037	0.079	0.501	1.025	1.676
	5	-0.472	-0.095	0.180	1.225	2.508	4.038
	10	-0.944	-0.208	0.322	2.274	4.595	7.240
1.38	20	-1.891	-0.480	0.499	3.976	7.924	12.19
	30	-2.846	-0.817	0.563	5.336	10.61	16.10
	40	-3.796	-1.217	0.515	6.421	12.83	19.34
	45	-4.274	-1.441	0.457	6.879	13.78	20.75
	50	-4.753	-1.679	0.370	7.276	14.66	22.02
	2	-0.195	-0.103	-0.048		0.354	0.570
	5	-0.489	-0.267	-0.120	0.382	0.943	1.509
	10	-0.980	-0.534	-0.241	0.767	1.887	3.004
9.46	20	-1.963	-1.082	-0.497	1.507	3.697	5.897
	30	-2.945	-1.632	-0.767	2.193	5.415	8.639
	40	-3.931	-2.202	-1.064	2.819	7.018	11.19
	45						
	50		-2.789	-1.386	3.376		13.56
	2		-0.162	-0.136			0.074
	5	-0.494	-0.406	-0.346	-0.157	0.063	0.258
	10	-0.994	-0.810	-0.697	-0.308	0.127	0.522
44	20	-1.982	-1.621	-1.387	-0.605	0.246	1.044
	30	-2.977	-2.436	-2.085	-0.906	0.359	1.559
	40	-3.973	-3.250	-2.784	-1.206	0.478	2.083
	50	-4.971	-4.060	-3.476	-1.501		2.576

TABLE 3 (Continued)

T(K)	c_{nom} H(kG)	0.0	54.9	89.8	206.0	324.6	436.3
55	5		-0.422	-0.371	-0.212	-0.046	0.137
	10		-0.842	-0.744		-0.054	0.283
	20		-1.677	-1.481	-0.806	-0.105	0.578
	30		-2.520	-2.226		-0.169	0.841
	40	-3.976	-3.362	-2.970	-1.641	-0.230	1.117
66	5		-0.433		-0.239	-0.093	0.052
	10		-0.861		-0.477	-0.172	0.118
	20		-1.718		-0.956	-0.347	0.236
	30		-2.582	-2.320	-1.442	-0.527	0.341
	40	-3.979	-3.445	-3.103	-1.928	-0.709	0.457
77	5		-0.44	-0.400	-0.267	-0.138	-0.010
	10		-0.874	-0.798	-0.531	-0.259	-0.002
	20		-1.746	-1.593	-1.065	-0.519	-0.003
	30		-2.619	-2.392	-1.604	-0.786	-0.009
	40	-3.976	-3.499	-3.193	-2.143	-1.054	-0.015
88.9	5		-0.446		-0.293		
	10		-0.886		-0.577	-0.333	
	20		-1.769		-1.156		-0.202
	30		-2.659		-1.738	-1.004	
	40	-3.976	-3.547	-3.270	-2.322	-1.344	-0.415
100	5		-0.451		-0.310	-0.206	
	10		-0.896		-0.613	-0.391	
	20		-1.788		-1.227	-0.778	
	30		-2.684		-1.844	-1.172	
	40	-3.974	-3.578	-3.328	-2.461	-1.569	-0.719
111	30		-2.704				
	40	-3.970	-3.608	-3.374		-1.752	-0.975
122	5		-0.458		-0.338	-0.251	-0.168
	10		-0.909		-0.669	-0.477	-0.302
	20		-1.815		-1.332	-0.949	-0.590
	30		-2.724		-2.000	-1.425	-0.885
	40	-3.968	-3.631	-4.413	-2.668	-1.903	-1.176

TABLE 3 (Continued)

χ (10^{-8} emu/gm) for Fe in $Cu_{0.95}Au_{0.05}$

c_{nom}	0.0	54.9	89.8	206	324.6	436.3
T(K)						
1.389	-9.422	-1.85	3.80	25.0	51.3	83.8
4.2	-9.601	-3.608	0.482	15.12	31.81	49.81
9.46	-9.827	-5.34	-2.433	7.70	18.9	30.5
44	-9.944	-8.125	-6.959	-2.986	1.183	5.20
55	-9.964	-8.401	-7.422	-4.088	-0.545	2.795
66	-9.964	-8.606	-7.741	-4.827	-1.765	1.147
77	-9.964	-8.739	-7.978	-5.362	-2.625	-0.022
89	-9.964	-8.86	-8.175	-5.803	-3.344	-1.017
100	-9.964	-8.937	-8.319	-6.150	-3.900	-1.791
122	-9.944	-9.069	-8.533	-6.658	-4.729	-2.893

TABLE 4

$M-M_c$ (10^{-3} emu/gm) for Fe in $Cu_{0.91}Au_{0.09}$

	M_c	0.0	0.03	0.0	0.02	0.119	0.127	0.392		
	c_{nom}	0.0	55.2	89.7	151	197	252	260	352	468
T(K)	H(kG)									
	2	-0.200	-0.010	0.125	0.397	0.618	0.920	0.873	1.466	2.355
	5	-0.506	-0.025	0.286	0.968	1.510	2.250	2.199	3.554	5.593
	10	-1.009	-0.077	0.523	1.790	2.768	4.115	4.035	6.455	9.954
1.384	20	-2.026	-0.276	0.839	3.069	4.734	7.002	6.922	10.91	16.49
	30	-3.052	-0.599	0.956	3.963	6.166	9.149	9.106	14.27	21.42
	40	-4.082	-1.030	0.892	4.539	7.192	10.75	10.76	16.88	25.27
	45	-4.598	-1.282	0.805	4.731	7.581	11.38	11.42		26.89
	50	-5.122	-1.558	0.681	4.865	7.899		11.99		28.33
	1	-0.106	-0.042	0.005	0.090	0.140	0.216		0.344	
	2	-0.210	-0.071	0.016	0.195	0.323	0.494	0.498	0.803	1.264
	5	-0.517	-0.167	0.048	0.496	0.834	1.282	1.281	2.083	3.233
	10	-1.035	-0.336	0.094	0.972	1.633	2.524	2.488	4.098	6.344
4.2	20	-2.074	-0.711	0.142	1.821	3.077	4.766	4.756	7.749	11.92
	30	-3.113	-1.134	0.112	2.512	4.294	6.676	6.679	10.88	16.64
	40	-4.158	-1.609	-0.005	3.028	5.278	8.263	8.294	13.52	20.62
	45	-4.685	-1.867	-0.099	3.238		8.943	8.987		22.38
	50	-5.215	-2.143	-0.216	3.397		9.553	9.611	15.72	24.00
	2	-0.214	-0.116	-0.058	0.061	0.140	0.246	0.254	0.439	0.727
	5	-0.539	-0.283	-0.139	0.158	0.377	0.660	0.670	1.168	1.881
	10	-1.077	-0.571	-0.275	0.307	0.743	1.310	1.324	2.328	3.739
9.46	20	-2.152	-1.155	-0.561	0.580	1.436	2.552	2.575	4.565	7.324
	30	-3.224	-1.752	-0.863	0.815	2.073	3.718	3.755	6.674	10.71

TABLE 4 (Continued)

T(K)	H(kG)	$c_{nominal}$ 0.0	55.2	89.7	151	197	252	260	352	468
	40	-4.298	-2.366	-1.197	0.997	2.634	4.775	4.833	8.615	13.82
9.46	45	-4.827	-2.680	-1.378	1.067	2.884	5.261			
	50	-5.366	-3.007	-1.566	1.118	3.113	5.720			
	2	-0.210		-0.155			-0.063			0.107
	5	-0.536	-0.444	-0.391	-0.283	-0.197	-0.110	-0.095	0.075	0.319
	10	-1.074	-0.888	-0.783	-0.567	-0.407	-0.214	-0.196	0.156	0.634
44	20	-2.139	-1.772	-1.553	-1.131	-0.813	-0.426	-0.395	0.314	1.267
	30	-3.210	-2.663	-2.330	-1.701	-1.229	-0.644	-0.599	0.461	1.893
	40	-4.285	-3.553	-3.107	-2.271	-1.640	-0.858	-0.800	0.616	2.523
	45	-4.823	-4.000	-3.494	-2.555	-1.847	-0.966			
	50	-5.355	-4.443	-3.878	-2.835	-2.050	-1.074			
	2			-0.166						
	5	-0.537	-0.461	-0.416	-0.326	-0.258	-0.183			0.176
	10	-1.074	-0.920	-0.829	-0.649	-0.514	-0.355			0.358
55	20	-2.142	-1.834	-1.649	-1.293	-1.027	-0.706			0.710
	30	-3.217	-2.762	-2.746	-1.946	-1.550	-1.065	-1.024	-0.134	1.055
	40	-4.290	-3.677	-3.302	-2.600	-2.074	-1.424	-1.371	-0.184	1.398
	45	-4.826	-4.135	-3.712	-2.926	-2.333	-1.602			
	50	-5.366	-4.599	-4.128	-3.254	-2.596	-1.781			
	2			-0.180						
	5	-0.536	-0.481	-0.444	-0.376	-0.326	-0.270	-0.259	-0.147	0.007
	10	-1.072	-0.952	-0.884	-0.741	-0.640	-0.520	-0.506	-0.277	0.032
77	20	-2.142	-1.903	-1.761	-1.484	-1.280	-1.034	-1.012	-0.551	0.059
	30	-3.217	-2.858	-2.642	-2.230	-1.925	-1.553	-1.522	-0.832	0.082
	40	-4.289	-3.813	-3.523	-2.980	-2.571	-2.075	-2.031	-1.114	0.102

TABLE 4 (Continued)

T(K)	$c_{nominal}$ H(kG)	0.0	55.2	89.7	151	197	252	260	352	468
	45	-4.831	-4.294	-3.965	-3.354	-2.893	-2.335			
77	50	-5.368	-4.773	-4.403	-3.279	-3.215	-2.597			
	2			-0.185						
	5	-0.536	-0.495	-0.461	-0.407	-0.372	-0.326	-0.319		-0.096
	10	-1.071	-0.977	-0.917	-0.802	-0.720	-0.624	-0.617	-0.424	-0.171
100	20	-2.141	-1.947	-1.831	-1.602	-1.434	-1.238	-1.224	-0.841	-0.342
	30	-3.213	-2.920	-2.741	-2.405	-2.154	-1.856	-1.834	-1.263	-0.517
	40	-4.289	-3.899	-3.660	-3.212	-2.876	-2.480	-2.443	-1.688	-0.698
	45	-4.827	-4.386	-4.116	-3.613	-3.236	-2.790			
	50	-5.364	-4.875	-4.577	-4.014	-3.597	-3.101			
	5	-0.536	-0.505	-0.471	-0.427	-0.402	-0.366	-0.358		-0.164
	10	-1.070	-0.992	-0.940	-0.841	-0.775	-0.692	-0.690	-0.522	-0.305
122	20	-2.138	-1.973	-1.872	-1.676	-1.537	-1.371	-1.361	-1.030	-0.596
	30	-3.210	-2.959	-2.807	-2.517	-2.306	-2.054	-2.035	-1.545	-0.899
	40	-4.284	-3.953	-3.744	-3.360	-3.077	-2.740	-2.712	-2.059	-1.206
	45	-4.822	-4.446	-4.214	-3.781	-3.462	-3.082			
	50	-5.360	-4.941	-4.684	-4.203	-3.844	-3.426			

TABLE 4 (Continued)

χ (10^{-8} emu/gm) for Fe in $Cu_{0.91}Au_{0.09}$

$c_{nominal}$	0.0	55.2	89.7	151	197	252	260	352	468
T(K)									
1.38	-10.07	-0.519	6.10	19.4	31.0	44.92	44.1	73.81	115
4.2	-10.37	-3.316	1.038	10.1	16.64	25.75	26.0	41.9	64.9
9.46	-10.73	-5.751	-2.734	3.019	7.370	13.05	13.46	23.54	37.72
44	-10.71	-8.890	-7.751	-5.678	-4.118	-2.145	-2.015	1.540	6.296
55	-10.73	-9.194	-8.247	-6.508	-5.199	-3.559	-3.424	-0.452	3.488
77	-10.73	-9.539	-8.801	-7.459	-6.430	-5.178	-5.070	-2.770	0.264
100	-10.73	-9.737	-9.144	-8.026	-7.177	-6.177	-6.066	-4.216	-1.726
122	-10.73	-9.864	-9.358	-8.397	-7.662	-6.814	-6.728	-5.127	-2.980

TABLE 5

$M-M_c$ (10^{-3} emu/gm) for Fe in $Cu_{0.83}Au_{0.17}$

$c_{nominal}$		0.0	61.5	87.9	127.1	185.4	234.0	288.1	331.9	400.2
T(K)	H(kG)									
	2	-0.221	0.088	0.245	0.414	0.795	1.063	1.485	1.693	2.292
	5	-0.558	0.208	0.582	1.031	1.937	2.577	3.573	4.079	5.458
	10	-1.116	0.349	1.049		3.543		6.438	7.400	9.617
1.384	20	-2.247	0.372	1.569	3.088	5.814	7.852	10.53	12.20	15.71
	30	-3.402	0.085	1.641	3.667	7.158	9.822	13.18	15.40	19.73
	40	-4.573	-0.431	1.386	3.811	7.868	11.08	14.88	17.55	22.49
	45	-5.158	-0.750	1.172	3.764	8.054	11.48	15.49	18.35	23.54
	50	-5.744	-1.100	0.914	3.656	8.152	11.78	15.96	18.99	24.41
	1	-0.118	-0.031	0.017	0.047	0.227	0.235	0.318	0.384	0.510
	2	-0.235	-0.050	0.037	0.135	0.339	0.504	0.691	0.823	1.099
	5	-0.583	-0.115		0.373	0.864	1.259	1.755	2.085	2.787
	10	-1.157	-0.239	0.171	0.732	1.692	2.484	3.449	4.093	5.450
4.2	20	-2.315	-0.537	0.250	1.331	3.157	4.648	6.457	7.693	10.17
	30	-3.484	-0.923	0.200	1.749	4.322	6.437	8.933	10.69	14.07
	40	-4.657	-1.406	0.005	1.966	5.175	7.823	10.89	13.08	17.21
	45	-5.252	-1.688	-0.147	1.996	5.488	8.383	11.69	14.09	18.51
	50	-5.847	-1.996	-0.334	1.981	5.731	8.859	12.38	14.98	19.68
	2	-0.241	-0.125	-0.071	-0.013	0.107	0.205	0.311	0.397	0.550
	5	-0.596	-0.305		-0.004	0.286	0.532	0.813	1.025	1.421
	10	-1.189	-0.614		-0.011	0.565	1.053	1.619	2.036	2.819
9.46	20	-2.377	-1.242		-0.049	1.085	2.047	3.159	3.982	5.502
	30	-3.564	-1.885	-1.159	-0.126	1.542	2.959	4.584	5.794	7.926
	40	-4.762	-2.561	-1.618	-0.258	1.913	3.761	5.859	7.435	10.27

TABLE 5 (Continued)

	$c_{nominal}$	0.0	61.5	87.9	127.1	185.4	234.0	288.1	331.9	400.2
T(K)	H(kG)									
	45	-5.363	-2.907	-1.862	-0.357	2.063	4.116	6.434	8.190	11.32
9.46	50	-5.968	-3.266	-2.116	-0.454	2.187	4.439	6.943	8.982	12.31
	2	-0.244	-0.206		-0.177	-0.133		-0.067	-0.041	0.001
	5	-0.608	-0.509		-0.409	-0.317	-0.231	-0.143	-0.072	0.048
	10	-1.214	-1.019		-0.816	-0.629	-0.459	-0.281	-0.143	0.097
44	20	-2.422	-2.030		-1.624	-1.252	-0.919	-0.559	-0.282	0.192
	30	-3.639	-3.049		-2.440	-1.881	-1.380	-0.846	-0.427	0.280
	40	-4.855	-4.066		-3.257	-2.511	-1.840	-1.127	-0.566	0.375
	45	-5.465	-4.577		-3.676	-2.826	-2.069	-1.268	-0.637	0.423
	50	-6.078	-5.084		-4.066	-3.139	-2.300	-1.410	-0.704	0.473
	2	-0.242	-0.216		-0.197		-0.129		-0.081	-0.048
	5	-0.611	-0.524		-0.445		-0.296		-0.167	-0.066
	10	-1.218	-1.045		-0.883		-0.587		-0.324	-0.128
55	20	-2.429	-2.089		-1.760		-1.171		-0.645	-0.256
	30	-3.647	-3.141		-2.644		-1.763		-0.974	-0.394
	40	-4.867	-4.194		-3.531		-2.354		-1.299	-0.528
	45	-5.476	-4.726		-3.971		-2.646		-1.464	-0.596
	50	-6.080	-5.250		-4.415		-2.944		-1.628	-0.665
	2	-0.244	-0.227	-0.208	-0.217	-0.183		-0.142	-0.127	-0.110
	5	-0.610	-0.550	-0.520	-0.491	-0.429	-0.375	-0.318	-0.272	-0.203
	10	-1.218	-1.091	-1.041	-0.962	-0.845	-0.735	-0.622	-0.532	-0.387
77	20	-2.432	-2.176	-2.085	-1.917	-1.684	-1.466	-1.240	-1.062	-0.772
	30	-3.651	-3.266	-3.129	-2.879	-2.527	-2.202	-1.867	-1.597	-1.162
	40	-4.871	-4.359	-4.176	-3.841	-3.374	-2.938	-2.490	-2.134	-1.553

TABLE 5 (Continued)

	$c_{nominal}$	0.0	61.5	87.9	127.1	185.4	234.0	288.1	331.9	400.2
T(K)	H(kG)									
	45	-5.482	-4.902		-4.323	-3.798	-3.306	-2.804	-2.402	-1.749
77	50	-6.084	-5.446	-5.220	-4.807	-4.217	-3.678	-3.120	-2.671	-1.947
	2	-0.244	-0.236		-0.234		-0.189		-0.160	-0.149
	5	-0.611	-0.564				-0.423		-0.341	-0.286
	10	-1.219	-1.114		-1.012		-0.826		-0.663	-0.548
100	20	-2.433	-2.220		-2.012		-1.646		-1.319	-1.085
	30	-3.651	-3.331		-3.020		-2.467		-1.976	-1.630
	40	-4.871	-4.441		-4.030		-3.292		-2.640	-2.177
	45	-5.479	-5.000		-4.537		-3.705		-2.966	-2.453
	50	-6.090	-5.554		-5.041		-4.117		-3.300	-2.725
	2		-0.240						-0.182	-0.177
	5		-0.573						-0.386	-0.343
	10	-1.218	-1.128						-0.747	-0.654
122	20		-2.249		-2.075				-1.480	-1.289
	30		-3.371		-3.110				-2.222	-1.934
	40	-4.864	-4.498		-4.150				-2.963	-2.579
	45	-5.471	-5.061						-3.333	
	50	-6.090	-5.624		-5.191				-3.705	-3.228

TABLE 5 (Continued)

χ (10^{-8} emu/gm) for Fe in $Cu_{0.83}Au_{0.17}$

$c_{nominal}$	0.0	61.5	87.9	127.1	185.4	234.0	288.1	331.9	400.2
T(K)									
1.384	-11.16	4.40	12.3	20.5	39.8	53.2	74.3	84.7	114.6
4.2	-11.60	-2.729	1.832	7.555	17.35	25.37	35.30	41.82	55.92
9.46	-11.87	-6.10		-0.08	5.72	10.64	16.31	20.5	28.71
44	-12.16	-10.16		-8.144	-6.275	-4.599	-2.819	-1.407	0.937
55	-12.16	-10.51		-8.825		-5.887		-3.251	-1.335
77	-12.18	-10.89	-10.45	-9.597	-8.427	-7.344	-6.229	-5.337	-3.882
100	-12.18	-11.10		-10.08		-8.215		-6.579	-5.428
122	-12.17	-11.23		-10.39				-7.382	-6.417

TABLE 6

$M-M_c$ (10^{-3} emu/gm) for Fe in $Cu_{0.80}Au_{0.20}$

	$c_{nominal}$	0.0	18.5	42.8	92.7	156.9	206.9	246.3	289.1	512
T(K)	H(kG)									
	1	-0.128	-0.097	-0.058	0.014	0.136	0.202	0.244		0.710
	2	-0.246	-0.191	-0.114	0.046	0.260	0.430	0.543	0.711	1.483
	5	-0.603	-0.473	-0.282	0.125	0.659	1.089	1.397	1.794	3.738
	10	-1.203	-0.945	-0.563	0.229	1.286	2.128	2.739	3.509	7.301
4.2	20	-2.409	-1.910	-1.172	0.349	2.358	3.948	5.119	6.561	13.59
	30	-3.623	-2.913	-1.854	0.315	3.149	5.376	7.039	9.035	18.74
	40	-4.849	-3.957	-2.620	0.111	3.640	6.405	8.501	10.97	22.85
	45	-5.466	-4.497	-3.034	-0.054	3.779	6.773	9.074	11.74	
	50	-6.085	-5.047	-3.465	-0.262	3.852	7.061	9.548	12.38	26.14
	2	-0.228	-0.128	0.013	0.296	0.727		1.245	1.584	3.152
	5	-0.574	-0.327	0.016	0.718	1.746	2.571	3.025	3.802	7.405
	10	-1.148	-0.680	-0.031	1.292	3.157	4.629	5.484	6.827	13.01
1.384	20	-2.320	-1.513	-0.379	1.917	5.004	7.400	8.928	11.06	20.83
	30	-3.520	-2.488	-1.013	1.975	5.881	8.921	10.96	13.65	26.01
	40	-4.742	-3.560	-1.838	1.656	6.151	9.652	12.18	15.23	29.58
	45	-5.355	-4.115	-2.291	1.402	6.135	9.825	12.53	15.76	30.94
	50	-5.975	-4.683	-2.770	1.100	6.044		12.78	16.15	32.08
	2	-0.251	-0.220	-0.171	-0.076	0.049	0.146	0.217	0.315	0.756
	5	-0.623	-0.547	-0.429	-0.184	0.125	0.375	0.576	0.801	1.928
	10	-1.243	-1.093	-0.857	-0.377	0.239	0.738	1.138	1.580	3.836
9.46	20	-2.486	-2.191	-1.725	-0.775	0.440	1.419	2.202	3.071	7.502
	30	-3.730	-3.293	-2.606	-1.208	0.584	2.023	3.174	4.446	10.92
	40	-4.980	-4.406	-3.510	-1.683	0.651	2.517	4.021	5.672	14.02

TABLE 6 (Continued)

	$c_{nominal}$	0.0	18.5	42.8	92.7	156.9	206.9	246.3	289.1	512
T(K)	H(kG)									
	45	-5.606	-4.969	-3.973	-1.942	0.652				
9.46	50	-6.235	-5.538	-4.439	-2.212	0.631				
	2	-0.256	-0.180	-0.227	-0.198	-0.158		-0.104	-0.072	0.066
	5	-0.642	-0.620	-0.575	-0.491	-0.396	-0.321	-0.239	-0.172	0.183
	10	-1.285	-1.237	-1.152	-0.989	-0.795	-0.644	-0.484	-0.350	0.365
44	20	-2.562	-2.467	-2.297	-1.976	-1.588	-1.273	-0.972	-0.706	0.732
	30	-3.846	-3.705	-3.451	-2.970	-2.388	-1.928	-1.466	-1.065	1.096
	40	-5.133	-4.940	-4.603	-3.967	-3.186	-2.577	-1.959	-1.420	1.461
	45	-5.776	-5.557	-5.179	-4.463	-3.585	-2.894			
	50	-6.418	-6.177	-5.751	-4.958	-3.979	-3.215			
	2	-0.257	-0.250	-0.233	-0.212	-0.178				
	5	-0.644	-0.625	-0.588	-0.517	-0.439		-0.308	-0.251	
	10	-1.287	-1.248	-1.175	-1.037	-0.878		-0.614	-0.506	
55	20	-2.566	-2.494	-2.345	-2.075	-1.756		-1.236	-1.018	
	30	-3.852	-3.735	-3.520	-3.121	-2.640		-1.864	-1.535	0.256
	40	-5.142	-4.984	-4.696	-4.167	-3.523	-3.019	-2.492	-2.053	0.338
	45	-5.783	-5.609	-5.286	-4.691	-3.963				
	50	-6.429	-6.239	-5.875	-5.206	-4.407				
	2	-0.257	-0.253	-0.239	-0.228	-0.201				
	5	-0.645	-0.632	-0.600	-0.551	-0.490	-0.446	-0.386	-0.345	
	10	-1.287	-1.261	-1.199	-1.095	-0.974	-0.881	-0.765	-0.686	-0.230
77	20	-2.568	-2.518	-2.397	-2.193	-1.946	-1.761	-1.537	-1.376	-0.461
	30	-3.852	-3.774	-3.597	-3.290	-2.924	-2.643	-2.314	-2.073	-0.697
	40	-5.142	-5.032	-4.798	-4.393	-3.901	-3.529	-3.093	-2.770	-0.936

TABLE 6 (Continued)

$c_{nominal}$		0.0	18.5	42.8	92.7	156.9	206.9	246.3	289.1	512
T(K)	H(kG)									
	45	-5.788	-5.667	-5.405	-4.944	-4.392				
77	50	-6.431	-6.300	-6.005	-5.497	-4.880				
	2	-0.258	-0.255	-0.243	-0.237	-0.216				
	5	-0.645	-0.635	-0.609	-0.570	-0.521		-0.432	-0.402	
	10	-1.286	-1.266	-1.215	-1.132	-1.033		-0.856	-0.797	-0.424
100	20	-2.569	-2.529	-2.427	-2.261	-2.064		-1.720	-1.596	-0.848
	30	-3.852	-3.974	-3.642	-3.392	-3.096		-2.588	-2.400	-1.276
	40	-5.143	-5.062	-4.862	-4.527	-4.132	-3.834	-3.459	-3.203	-1.704
	45	-5.785	-5.693	-5.473	-5.098	-4.650				
	50	-6.430	-6.331	-6.083	-5.667	-5.169				
	5	-0.645						-0.463	-0.438	
	10	-1.286	-1.269	-1.227	-1.154	-1.070		-0.917	-0.868	-0.548
122	20	-2.565	-2.536	-2.446	-2.302	-2.136		-1.838	-1.736	-1.096
	30	-3.851	-3.804	-3.672	-3.457	-3.206		-2.763	-2.607	-1.645
	40	-5.133	-5.071	-4.897	-4.614	-4.277	-4.027	-3.691	-3.482	-2.196
	45	-5.782	-5.708	-5.515		-4.815				
	50	-6.430	-6.340	-6.123	-5.766	-5.350				

TABLE 6 (Continued)

χ (10^{-8} emu/gm) for Fe in $Cu_{0.80}Au_{0.20}$

$c_{nominal}$ T(K)	0.0	18.5	42.8	92.7	156.9	206.9	246.3	289.1	512
1.384	-11.46	-6.5	0.65	14.8	36.35	54.0	62.3	79.2	157.6
4.2	-12.02	-9.4	-5.60	2.50	13.18	21.8	28.0	35.88	74.8
9.46	-12.46	-10.91	-8.55	-3.68	2.50	7.50	11.52	16.02	38.6
44	-12.83	-12.35	-11.51	-9.90	-7.96	-6.439	-4.887	-3.53	3.652
55	-12.85	-12.46	-11.75	-10.43	-8.818	-7.548	-6.244	-5.150	0.85
77	-12.86	-12.58	-12.01	-11.00	-9.760	-8.812	-7.741	-6.932	-2.352
100	-12.85	-12.65	-12.17	-11.32	-10.33	-9.585	-8.651	-8.009	-4.269
122	-12.86	-12.68	-12.25	-11.53	-10.71	-10.07	-9.159	-8.644	-5.472

TABLE 7

$M-M_c$ (10^{-3} emu/gm) for Fe in Au

Sample Number		98	100	101	102	103	104	105
$c_{nominal}$		0.0	0.0	61	120	185	288	395
T(K)	H(kG)							
	2		-0.208	0.167	0.432	0.888	1.479	
	5	-0.558	-0.472	0.383	1.022	2.080	3.411	4.702
	10	-1.135	-0.979	0.563	1.709	3.514	5.744	7.865
1.384	20	-2.394	-2.194	0.277	2.137	4.859	8.290	11.58
	30	-3.744	-3.451	-0.533	1.811	5.021	9.259	13.39
	40	-5.143	-4.814	-1.641	1.110	4.571	9.375	14.14
	45	-5.839	-5.496	-2.239	0.688	4.215	9.241	14.26
	50	-6.550			0.224		9.012	14.25
	1	-0.132	-0.126	-0.053	0.015	0.104	0.230	0.369
	2	-0.262	-0.247	-0.098	0.038	0.213	0.473	0.751
	5	-0.649	-0.612	-0.237	0.102	0.542	1.189	1.894
	10	-1.294	-1.220	-0.479	0.190	1.046	2.304	3.663
4.2	20	-2.595	-2.454	-1.053	0.224	1.087	4.118	6.590
	30	-3.917	-3.722	-1.768	0.045	2.176	5.332	8.600
	40	-5.270	-5.027	-3.635	-0.354	2.171	6.000	9.944
	45	-5.952	-5.689	-3.121	-0.626	2.048	6.164	10.39
	50	-6.644	-6.366	-3.635	-0.938	1.856	6.230	10.60
	2	-0.274	-0.265					
	5	-0.683	-0.665	-0.469	-0.250	-0.057	0.291	
9.46	10	-1.364	-1.325	-0.936	-0.503	-0.117	0.573	1.308
	20	-2.725	-2.648	-1 880	-1.022	-0.266	1.082	2.521
	30	-4.090	-3.976	-2.884	-1.577	-0.482	1.483	3.575

TABLE 7 (Continued)

Sample Number		98	100	101	102	103	104	105
T(K)	H(kG)							
	40	-5.465	-5.312	-3.846	-2.183	-0.790	1.743	4.424
	45	-6.157						
9.46	50	-6.843	-6.666	-4.884	-2.767		1.845	
	2	-0.282			-0.212			
	5	-0.711	-0.706		-0.534	-0.539	-0.441	-0.341
	10	-1.421	-1.409	-1.303	-1.061	-1.076	-0.881	-0.680
44	20	-2.830	-2.807	-2.597	-2.103	-2.137	-1.756	-1.349
	30	-4.246	-4.210	-3.893	-3.150	-3.206	-2.632	-2.022
	40	-5.664	-5.614	-5.189	-4.192	-4.274	-3.509	-2.689
55	40	-5.680	-5.640	-5.295	-4.345	-4.547	-3.922	-3.264
66	40	-5.690	-5.655	-5.365	-4.454	-4.725	-4.193	-3.633
77	2		-0.284					
	5	-0.718	-0.712					-0.490
	10	-1.428	-1.420					-0.976
	20	-2.849	-2.831					-1.946
	30		-4.247					-2.918
	40	-5.702	-5.668	-5.413	-4.522	-4.850	-4.382	-3.889
89	40	-5.706	-5.675	-5.453	-4.570	-4.953	-4.559	-4.102
100	40	-5.712	-5.682	-5.483	-4.605	-5.030	-4.655	-4.259
111	40		-5.687	-5.508	-4.634	-5.093	-4.750	-4.391
122	40		-5.692	-5.529	-4.653	-5.146	-4.826	-4.496

TABLE 7 (Continued)

χ (10^{-8} emu/gm) for Fe in Au

Sample Number T(K)	98	100	101	102	103	104	105
1.384	-11.2	-9.44	8.35	21.6	44.4	73.95	103
4.2	-12.94	-12.10	-4.74	2.04	10.84	23.78	37.88
9.46	-13.63	-13.24	-9.36	-5.03	-1.14	5.82	13.08
12.2			-10.47		-4.0		
21.2			-11.70		-7.5		
38.4			-12.81		-10.23		
44	-14.16	-14.04	-12.99	-10.60	-10.69	-8.773	-6.723
55	-14.20	-14.10	-13.24	-10.86	-11.37	-9.805	-8.16
66	-14.23	-14.14	-13.41	-11.14	-11.81	-10.48	-9.083
77	-14.26	-14.17	-13.53	-11.31	-12.13	-10.96	-9.723
89	-14.27	-14.19	-13.63	-11.43	-12.38	-11.40	-10.26
100	-14.28	-14.21	-13.71	-11.51	-12.58	-11.64	-10.65
111		-14.22	-13.77	-11.59	-12.73	-11.88	-10.98
122		-14.23	-13.82	-11.63	-12.87	-12.07	-11.24
133		-14.24	-13.87		-12.98		
144		-14.25	-13.90		-13.07		
172		-14.26	-13.97		-13.25		

TABLE 8

Determination of n_s for $Cu_{0.95}Au_{0.05}$(Fe) alloys

$c_{nominal}$	0	54.9	89.8	206	324.6	436.3
$M_{50}-M_{45}$	-.482	-.240	-.087	.400	.88	1.28
.2% $(M'_{50}-M'_{45})$	.001	.001	.000	.001	.002	.003
.2% M'_{50}	.012	.007	.003	.014	.030	.047
.2% M_{Fe}		.001	.001	.001	.002	.003
ΔM_{Fe}		.242	.395	.882	1.362	1.762
$e_{\Delta M_{Fe}}$		.022	.017	.029	.047	.066
n_s-K		56.5 ± 5.1	92.3 ± 4.0	206 ± 6.8	318 ± 11	412 ± 15

Assuming $n_s-K=(\Delta M_{Fe}/\Delta M_{206})206$ ppm K≈4

TABLE 9

$Cu_{0.91}Au_{0.09}$(Fe)

$c_{nominal}$	55	90	150	197	252†	258	361*	500
n_s-K	57.8	93.6	154.0	197	251.7	255.1	353	459.5
e_{n_s-K}	±3.0	±1.9	±2.6	±3.5	±8	±5		±9

Assumed $n_s-K=(\Delta M_{Fe}/\Delta M_{197})197$ ppm K≈4.5 ppm †used $\Delta M=M_{45}-M_{40}$

* From data at 4.2 K

TABLE 10

$Cu_{0.83}Au_{0.17}$(Fe)

$c_{nominal}$	61.5	87.9	127.1	185.4	234.0	288.1	331.9	400.2
n_s-K	65.0	90.2	131.3	184.7	242.4	290.5	338.6	400.2
$e_{(n_s-K)}$	± 3	± 2.5	± 3	± 4.1	± 5	± 6.4	± 7.5	± 9

$K \approx 4$ Assumed $n_s - K = (\Delta M_{Fe} / \Delta M_{400.2}) 400.2$ ppm

TABLE 11

$Cu_{0.8}Au_{0.2}$(Fe)

$c_{nominal}$	18.5	42.8	92.7	156.9	206.9	246.3	289.1	512
n_s-K	15.4	42.1	94.3	156.9	206.4	256.3	299	520
e_{n_s-K}	±4	±3.3	±2.5	±3.9	±8.6	±6	±7	±12

$K \approx 5$ Assumed $n_s - K = (\Delta M_{Fe} / \Delta M_{156.9}) 156.9$

TABLE 12

$-M_o$ (10^{-3} emu/gm) from fits of $M=M_o+M_1n_s+M_2n_s^2$

Fe in $Cu_{0.95}Au_{0.05}$

T(K)	1.384	4.2	9.46	44	55	66	77	89	100	111	122
H(kG)											
1		0.107									
2	0.184	0.197	0.198								
5	0.474	0.493	0.501	0.501	0.489	0.505	0.505		0.509		0.505
10	0.966	0.990	1.006	1.006	1.003	1.005	1.006	1.005	1.006		1.002
20	1.960	1.991	2.019	2.008	1.998	2.002	2.005	2.001	2.001		1.999
30	2.964	3.000	3.027	3.016	2.996	3.010	3.002	3.011	3.004		2.999
40	3.960	4.012	4.044	4.025	4.019	4.021	4.014	4.012	4.006	4.000	3.997
45	4.458	4.519									
50	4.961	5.030	5.016	5.039							

$-\chi_o=M(40\ kG)/40\ kG$ (10^{-7} emu/gm)

0.990	1.003	1.011	1.006	1.005	1.005	1.004	1.003	1.002	1.000	0.999

$-\chi_o$ (10^{-7} emu/gm) from fits of $\chi=\chi_o+\chi_1n_s+\chi_2n_s^2$

0.956	0.987	1.017	1.008	1.007	1.006	1.005	1.005	1.004		1.001

TABLE 13

$M_1(10^{-6}$ emu/[gm ppm]) from fits of $M=M_o+M_1n_s+M_2n_s^2$

Fe in $Cu_{0.95}Au_{0.05}$

T(K) H(kG)	1.384	4.2	9.46	44	55	66	77	89	100	111	122
1		1.159									
2	1.979	1.832	1.416								
5	5.184	4.626	3.575	1.485	1.095	1.171	1.052		0.941		0.765
10	10.89	9.375	7.240	3.020	2.542	2.310	2.083	1.911	1.764		1.485
20	22.17	18.79	14.46	6.050	5.089	4.538	4.098	3.705	3.412		2.942
30	32.85	28.04	21.55	0.099	7.540	6.821	6.060	5.631	5.112		4.399
40	42.46	36.91	28.57	12.15	10.28	9.092	8.138	7.378	6.745	6.211	5.812
45	46.93	41.20									
50	51.26	45.31	35.09	15.39							

χ_1 from M/H (10^{-10} emu/[gm ppm])

10.95	9.37	7.20	3.029	2.54	2.273	2.05	1.86	1.72	1.55	1.47

χ_1 (10^{-10}emu/[gm ppm]) from fits of $\chi=\chi_o+\chi_1n_s+\chi_2n_s^2$

10.67	9.33	7.39	3.06	2.61	2.28	2.05	1.86	1.71		1.47

TABLE 14

M_2 (10^{-9} emu/[gm (ppm)^2]) from fits of $M=M_o+M_1 n_s+M_2 n_s^2$

Fe in $Cu_{0.95}Au_{0.05}$

T(K)	1.384	4.2	9.46	44	55	66	77	89	100	111	122
H(kG)											
1		0.206									
2	5.815	2.207	0.985								
5	13.24	5.904	2.916	0.791	0.945	0.380	0.307				0.092
10	20.64	11.03	5.571	1.520	1.271	0.893	0.753	0.559	0.461		0.449
20	27.58	19.03	10.58	2.970	2.542	1.933	1.638	1.421	1.223		1.012
30	30.12	24.15	15.02	4.376	3.900	2.833	2.611	1.899	1.821		1.557
40	31.34	27.15	18.59	5.843	4.744	3.834	3.381	2.905	2.641	2.433	2.213
45	31.53	28.05									
50	31.33	28.87	22.25	6.715							

χ_2 from M_2/H (10^{-13} emu/[gm (ppm)^2])

29.1	12.0	5.8	1.47	1.27	0.96	0.84	0.69	0.63	0.61	0.52

χ_2 (10^{-13} emu/[gm (ppm)^2]) from fits of $\chi=\chi_o+\chi_1 n_s+\chi_2 n_s^2$

24.2	11.7	5.61	1.40	1.12	0.94	0.83	0.71	0.61	0.55

TABLE 15

$-M_o(10^{-3}$ emu/gm) from fits of $M=M_o+M_1n_s+M_2n_s^2$

Fe in $Cu_{0.91}Au_{0.09}$

Set 1

T(K) / H(kG)	1.384	4.2	9.46	44	55	77	100	122
2	0.211	0.220	0.221					
5	0.530	0.538	0.553	0.543	0.543	0.541	0.541	0.542
10	1.059	1.074	1.104	1.086	1.085	1.081	1.080	1.078
20	2.130	2.154	2.207	2.163	2.163	2.159	2.157	2.152
30	3.205	3.234	3.307	3.251	3.250	3.241	3.234	3.229
40	4.276	4.315	4.408	4.333	4.331	4.321	4.318	4.310
45	4.812	4.874	4.952	4.878	4.871	4.868	4.859	4.851
50	5.386	5.423	5.505	5.415	5.416	5.409		5.392

$-\chi_o$=M(40kG)/40kG (10^{-7}emu/gm)

1.059	1.076	1.105	1.083	1.084	1.080	1.079	1.077

$-\chi_o(10^{-7}$ emu/gm) from fits of $\chi=\chi_o+\chi_1n_s+\chi_2n_s^2$

1.069	1.078	1.101	1.083	1.083	1.081	1.080	1.079

TABLE 16

$M_1(10^{-6}$ emu/(gm ppm Fe) from fits of $M=M_o+M_1n_s+M_2n_s^2$

Fe in $Cu_{0.91}Au_{0.09}$

Set 1

T(K)	1.384	4.2	9.46	44	55	77	100	122
H(kG)								
2	2.75	2.20	1.60					
5	6.78	5.328	3.95	1.515	1.26	0.961	0.785	0.700
10	13.6	10.59	7.85	2.954	2.50	1.963	1.608	1.361
20	26.84	21.05	15.58	5.895	5.00	3.891	3.218	2.774
30	38.6	31.0	23.13	8.859	7.47	5.827	4.829	4.165
40	48.6	40.3	30.5	11.8	9.93	7.74	6.438	5.553
45	53.2	45.2	34.0	13.3	11.18	8.756	7.279	6.256
50	58.9	49.5	37.5	14.78	12.41	9.741		6.972

χ_1 (10^{-10} emu/(gm ppm Fe) from M_1/H

13.6	10.6	7.90	2.95	2.50	1.94	1.609	1.388

χ_1 (10^{-10} emu/(gm ppm Fe) from fits of $=\chi_o+\chi_1n_s+\chi_2n_s^2$

14.12	10.76	7.767	2.943	2.481	1.933	1.617	1.408

TABLE 17

M_2 (10^{-9} emu/(gm [ppm Fe]^2)) from fits of $M=M_o+M_1n_s+M_2n_s^2$

Fe in $Cu_{0.91}Au_{0.09}$

T(K)	1.384	4.2	9.46	44	55	77	100	122
H(kG)								
2	6.87	2.52	1.00					
5	16.8	7.48	3.39	0.859	0.705	0.482	0.284	0.001
10	27.3	14.5	6.77	2.019	1.61	1.07	0.819	0.689
20	37.0	25.1	12.9	3.960	3.13	2.288	1.738	1.313
30	41.0	34.3	18.5	5.96	4.77	3.47	2.57	2.00
40	43.1	37.5	23.1	7.89	6.35	4.66	3.43	2.72
45	43.4	38.1	25.5	8.79	7.09	5.14	3.73	3.06
50	35.4	39.4	27.5	9.66	7.95	5.63		3.35

χ_2 (10^{-13} emu/(gm[ppm Fe]^2)) from M_2/H

34.4	15.0	6.78	2.01	1.59	1.15	0.86	0.67

χ_2 (10^{-13} emu/(gm [ppm Fe]^2)) from fits of $\chi=\chi_o+\chi_1n_s+\chi_2n_s^2$

31.7	14.7	7.25	1.97	1.59	1.19	0.86	0.68

TABLE 18

$-M_o$ (10^{-3} emu/gm) from fits of $M=M_o+M_1 n_s+M_2 n_s^2$

Fe in $Cu_{0.91}Au_{0.09}$

T(K)	1.384	4.2	9.46	44	55	77	100	122
H(kG)								
2	0.212	0.219	0.220					
5	0.537	0.543	0.556	0.543		0.540	0.539	0.539
10	1.075	1.085	1.112	1.088		1.081	1.078	1.076
20	2.154	2.173	2.222	2.166		2.160	2.157	2.150
30	3.233	3.260	3.329	3.251	3.252	3.244	3.235	3.229
40	4.309	4.349	4.436	4.340	4.336	4.326	4.319	4.309
50		5.445						

$-\chi_o$ from M_o/H (10^{-8} emu/gm)

10.76	10.86	11.11	10.85	10.84	10.81	10.78	10.76

$-\chi_o$ (10^{-8} emu/gm) from fits of $\chi=\chi_o+\chi_1 n_s+\chi_2 n_s^2$

10.77	10.87	11.08	10.87	10.73	10.82	10.80	10.79

TABLE 19

Cu Au9
Second Set of Samples

Results of Fits of M vs. n_s

$M_s(10^{-6}\ \frac{emu}{gm\ ppm})$

H	1.4	4.2	9.5	44	55	77	100	122
2	2.506	2.180	1.512					
5	7.165	5.618	4.026	1.536		.961	.717	.558
10	14.60	11.02	8.011	3.086		1.985	1.569	1.291
20	28.50	22.12	15.85	6.113	7.725	3.990	3.226	2.682
30	40.53	32.62	23.55	9.131		5.990	4.861	4.100
40	50.88	42.42	31.12	12.20	10.28	7.986	6.544	5.531
45								
50		51.23						

$\chi_1\ (10^{-10}\ \frac{emu}{gm\ ppm\ Fe})$ from $\chi_1 = \frac{M_1}{H}$

14.5	11.11	8.0	3.06	2.57	1.995	1.613	1.35

$\chi_1\ (10^{-10}\ \frac{emu}{gm\ ppm\ Fe})$ from fits of $\chi = \chi_o + \chi_1 + \chi_1 n_s + \chi_2 n_s^2$

14.14	11.47	8.087	3.045	2.582	2.008	1.659	1.419

TABLE 20

$Cu\,Au_9$
Second Set of Samples

Results of Fits of M

$$M_2(10^{-9}\,\frac{emu}{gm(ppm)^2})$$

H \ T	1.4	4.2	9.5	44	55	77	100	122
2	6.364	2.101	1.079					
5	12.66	5.226	2.513	.644		.445	.492	.519
10	19.14	10.39	5.015	1.264		.838	.792	.767
20	24.21	17.06	9.712	2.612		1.607	1.399	1.372
30	25.93	21.15	13.75	3.969	3.157	2.389	2.031	1.882
40	26.28	23.36	16.82	5.249	4.208	3.150	2.554	2.360
45								
50		24.95						

$\chi_2\ (10^{-13}\ \frac{emu}{gm\,(ppm\,Fe)^2}\ )$ from $\chi_2 = \frac{M_2}{H}$

31.8	10.5	5.03	1.31	1.052	.788	.64	.59

$\chi_2\ (10^{-13}\ \frac{emu}{gm\ (ppm\ Fe)^2}$ from $\chi = \chi_o + \chi_1 n_s + \chi_2 n_s^2$

27.32	10.06	4.986	1.32	1.029	.773	.597	.534

TABLE 21

$Cu_{0.95}Au_{0.05}$

Parameters Describing Impurity Susceptibility from Different Methods of Analysis

$$\chi_{imp} = \chi_o + \frac{C_s}{T+\Theta_s} + \frac{C_p}{T+\Theta_p}$$

Method of Analysis	χ_o	C_s	Θ_s	$\frac{C_p}{C}$	Θ_p
Fits of $\Delta M = M_1 n_s + M_2 n_s^2$					
$\chi_s = \chi_o + \frac{C_s}{T+\Theta_s}$ $\chi_2 = \frac{C_p/C}{T+\Theta_p}$	6.073×10^{-4} emu/mole Fe	$1.306 \pm .1$ emu/mole Fe	15.8	$(4.38 \pm .6) \times 10^{-4}$ emu/mole Fe ppm Fe	1.15
Fits of $\chi = \chi_o + \frac{C_s}{T+\Theta_s} + \frac{C_p}{T+\Theta_p}$					
using $\Theta_s = 15.8$ $\Theta_p = 1.15$					
C(ppm Fe)					
417	17.92×10^{-4}	1.155		5.504×10^{-4}	
320	13.15	1.227		4.991	
210	10.83	1.250		5.276	
96.3	6.924	1.298		6.0	
60.2	6.859	1.350		5.12	
4.0	-8.2	1.950		-.05	
Θ_s and Θ_p allowed to vary					
417	24.83×10^{-4}	1.151	12.0	3.215	0.5
320	21.93	1.101	15	5.964	1.5
210	19.71	1.096	15.8	8.318	2.0
96.3	17.82	1.076	16.0	17.4	3.4
60.2	17.19	1.114	15.8	28.2	5.0
4.0					

TABLE 22

$Cu_{0.91}Au_{0.09}$

Parameters Found for Different Analyses

$$\chi_{imp} = \chi_o + \frac{C_s}{T+\Theta_s} + \frac{C_p}{T+\Theta_p}$$

Method of Analysis		χ_o	C_s	Θ_s	C_p	Θ_p
From $M = M_s n_s + M_2 n_s^2$	Set 1	35.8×10^{-4} emu/mole Fe	1.046 emu/mole Fe	8.4	5.41×10^{-4} emu/mole Fe ppm Fe	.4
	Set 2	27.45	1.037	8.4	4.11	.4
Fits of using $\Theta_s = 8.4$ $\Theta_p = .4$						
	C(ppm Fe)					
	466.7	35.55	1.047	8.4	3.56	.4
	352.8	35.57	1.024		3.68	
	261	29.44	1.078		3.14	
	256	29.74	1.060		3.68	
	201	34.76	1.012		4.38	
	159	28.4	1.057		3.62	
	98	33.2	.997		4.41	
	62	29.6	1.047		3.85	
Θ_s and Θ_p allowed to vary						
	466.7	31.26	1.083	9.0	3.68	0.4
	352.8	29.53	1.064	9.5	4.29	0.5
	261	29.44	1.078	8.4	3.14	0.4
	256	29.80	1.021	9.0	5.35	0.8
	201	34.76	1.012	8.4	4.38	0.4
	159	28.4	1.057	8.4	3.62	0.4
	98	33.2	.997	8.4	4.41	0.4
	62	29.6	1.047	8.4	3.85	0.4

TABLE 23

Parameters Describing The Pair Term In $Cu_{1-x}Au_x(Fe)$

x		$M_{2\ Sat}$ $(10^{-9}\frac{emu}{gm(ppm\ Fe)}2)$	C_2 $(10^{-12}\frac{emu\ K}{gm(ppm\ Fe)}2)$	n_p	S	Θ_p
0.05		31.0 ± 2.0	6.17 ± 1.3	$(61 \pm 15)c^2$	3.3 ± 1.2	1.5
0.09	Set 1	43 ± 4.3	7.12 ± 1.2	$(86 \pm 20)c^2$	2.7 ± 0.9	0.7
	Set 2	25 ± 2.5	5.44 ± 0.9	$(36 \pm 15)c^2$	3.8 ± 1.5	0.4
0.17			2.52	$36\ c^2$	Assume 3	less than 1.3
0.0	Ref. 17			$130\ c^2$	2.7 0.1	$\Theta < 5$
	Ref. 63			$65\ c^2$	2.9	

TABLE 24

$Cu\,Au_{17}$
Set 1

Fits of M vs. n_s

$-M_o\ (10^{-3}\ \frac{emu}{gm})$

T / H	1.4	4.2	9.5	44	55	77	100	122
2	.241	.250	.249	.245	.244	.243	.245	
5	.610	.616	.617	.615	.616	.614	.615	
10	1.230	1.228	1.231	1.230	1.228	1.227	1.226	1.225
20	2.441	2.449	2.461	2.452	2.451	2.451	2.447	2.424
30	3.657	3.679	3.689	3.684	3.681	3.679	3.672	3.634
40	4.887	4.907	4.928	4.914	4.912	4.909	4.899	4.888
45	5.492	5.527	5.546	5.531	5.530	5.523	5.510	5.504
50	6.098	6.146	6.160	6.151	6.140	6.130	6.125	6.119

$-\chi_o\ (10^{-8}\ \frac{emu}{gm})$ from $\chi_o = \frac{M_o}{H}$

12.20	12.28	12.32	12.29	12.28	12.27	12.25	12.23

$-\chi_o\ (10^{-8}\ \frac{emu}{gm})$ from fits of $\chi = \chi_o + \chi_1 n_s + \chi_2 n_s^2$

12.08	12.04	12.29	12.30	12.28	12.27	12.25	12.22

TABLE 25

$Cu\,Au_{17}$
Set 1

$M_1\ (10^{-6}\ \frac{emu}{gm\ ppm\,Fe})$

H \ T	1.4	4.2	9.5	44	55	77	100	122
2	4.324	2.718	1.678	.466	.339	.127	.055	
5	10.99	6.874	4.314	1.477	1.252	.868	.715	
10	21.86	13.68	8.568	2.962	2.504	1.902	1.550	1.386
20	39.17	26.55	16.95	5.903	4.989	3.835	3.147	2.432
30	52.41	38.49	25.12	8.890	7.471	5.756	4.719	3.664
40	62.75	49.13	33.04	11.84	9.940	7.691	6.310	5.360
45	66.80	53.93	36.78	13.28	11.20	8.662	7.038	6.318
50	70.50	58.40	40.20	14.91	12.38	9.511	7.861	6.778

$\chi_1\ (10^{-10}\ \frac{emu}{gm\ ppm\,Fe})$ from $\chi_1 \equiv \frac{M_1}{H}$

22.0	13.8	8.62	2.957	2.490	1.920	1.572	1.36

$\chi_1\ (10^{-10}\ \frac{emu}{gm\ ppm\ Fe})$ from fits of $\chi = \chi_o + \chi_1 n_s + \chi_2 n_s^2$

22.33	13.54	8.473	2.978	2.478	1.931	1.577	1.334

TABLE 26

$Cu\,Au_{17}$
Set 1

$M_2(10^{-9}\ \frac{emu}{gm\ (ppmFe)^2})$

T / H	1.4	4.2	9.5	44	55	77	100	122
2	3.785	1.191	.589	.364	.414	.611	.058	
5	7.685	2.852	1.337	.300	.157	.375	.240	
10	9.417	5.226	2.710	.584	.361	.349	.258	.002
20	9.894	8.560	5.182	1.181	.758	.587	.382	.913
30	8.679	9.588	7.144	1.691	1.155	.865	.626	1.289
40	7.255	9.255	8.460	2.334	1.640	1.100	.745	.687
45	7.330	9.081	9.190	2.796	1.764	1.206	1.045	-.001
50	7.147	8.866	11.07	2.692	2.137	1.589	1.021	.697

$\chi_2\ (10^{-13}\ \frac{emu}{gm\ (ppm\ Fe)^2}$ from $\chi_2 \equiv \frac{M_2}{H}$

18.9	5.96	2.69	.584	.392	.29	.21	.14

$\chi_2\ (10^{-13}\ \frac{emu}{gm\ (ppm\ Fe)^2}\ )$ from fits of $\chi = \chi_o + \chi_1 n_s + \chi_2 n_s^2$

12.77	6.216	3.022	.550	.431	.249	.208	.211

TABLE 27

$Cu_{0.03}\,Au_{0.17}$

Set 2

$-M_o(10^{-3}\ \frac{emu}{gm})$

T / H	1.4	4.2	9.5	44	55	77	100	122
2	.243	.247	.247	.247		.245		
5	.619	.620	.618	.616		.614		
10		1.227	1.234	1.230		1.229		
20	2.459	2.453	2.468	2.454		2.455		
30	3.681	3.684	3.700	3.687		3.685		
40	4.901	4.911	4.932	4.919		4.917		
45	5.508	5.531	5.553	5.537		5.529		
50	6.113	6.148	6.171	6.158		6.142		

$-\chi_o\ (10^{-8}\ \frac{emu}{gm})$ from $\chi_o \equiv \frac{M_o}{H}$

	12.28	12.34	12.30		12.28

$-\chi_o\ (10^{-8}\ \frac{emu}{gm})$ from fits of $\chi = \chi_o + \chi_1 n_s + \chi_2 n_s^2$

12.96	12.04	12.31	12.32		12.30

TABLE 28

$Cu\,Au_{17}$
Set 2

$M_1(10^{-6}\ \frac{emu}{gm(ppmFe)})$

T / H	1.4	4.2	9.5	44	55	77	100	122
2	4.664	2.801	1.730	.582		.352		
5	11.77	7.022	4.352	1.475		.940		
10		13.97	8.697	2.987		1.930		
20	41.24	27.29	17.26	5.992		3.870		
30	54.87	39.50	25.92	9.008		5.804		
40	65.00	50.28	33.70	12.01		7.741		
45	69.15	55.22	37.56	13.52		8.726		
50	72.78	59.72	41.22	15.06		9.630		

$\chi_1\ (10^{-10}\ \frac{emu}{gm\ ppm\ Fe})$ from $\chi_1 \equiv \frac{M_1}{H}$

23.54	14.0	8.70	3.003		1.935

$\chi_1\ (10^{-10}\ \frac{emu}{gm\ ppm\ Fe})$ from fits of $\chi = \chi_o + \chi_1 n_s + \chi_2 n_s^2$

25.88	13.85	8.544	3.020		1.939

TABLE 29

$Cu\,Au_{17}$
Set 2

$M_2(10^{-9}\ \frac{emu}{gm(ppmFe)^2})$

H \ T	1.4	4.2	9.5	44	55	77	100	122
2	3.926	1.275	.573	.078		-.046		
5	7.964	3.407	1.670	.405		.184		
10		6.170	3.214	.713		.368		
20	8.857	9.502	5.919	1.334		.719		
30	7.114	10.60	6.851	1.935		1.061		
40	6.318	10.58	9.380	2.611		1.415		
45	6.192	10.07	10.01	2.938		1.506		
50	6.201	9.851	10.72	3.236		1.812		

$\chi_2\ (10^{-13}\ \frac{emu}{gm(ppm\ Fe)^2})$ from $\chi_2 \equiv \frac{M_2}{H}$

19.6	6.9	3.3	.653	.362	

$\chi_2\ (10^{-13}\ \frac{emu}{gm\ (ppm\ Fe)^2})$ from fits of $\chi = \chi_o + \chi_1 n_s + \chi_2 n_s^2$

5.181	7.196	3.876	.623	.349	

TABLE 30

Fe in $Cu_{0.83}Au_{0.17}$

Concentration	Θ_1	Θ_2	χ_o (10^{-3} $\frac{emu}{mole\ Fe}$)	C_1 ($\frac{emu\ K}{mole\ Fe}$)	$\frac{C_2}{n_s}$ ($\frac{10^{-4}\ emu\ K}{mole\ ppm\ Fe}$)
			Set 1		
From fits of M vs. n_s	3.3	0	6.065	.865	2.28
From fits of vs. n_s	2.9	1.3	6.97	.800	3.02
70.1	11	1.5	4.5	.692	60.3
136.5	20	2.0	2.42	.718	42.8
247.6	12	1.2	3.02	.792	17.5
343.8	11.5	1.9	2.60	.880	11.6
			Set 2		
From fits of M vs. n_s	2.6	0.15	8.64	.780	2.61
From fits of vs. n_s	1.8		10.3	.681	
193	14	1.2	2.43	.836	23.7
296	12	0.9	2.82	.859	14.5
405.4	10	0.6	2.38	.949	9.11

TABLE 31

$$\text{Fe in } Cu_{0.8}Au_{0.2} \quad \frac{(\chi - \chi_H)}{n_s} = \chi_o + \frac{C_1}{T+\theta_1} + \frac{C_2}{T+\theta_2}$$

$$\text{if } \chi_H = -12.86 \ \frac{\text{emu}}{\text{gm}}$$

Concentration	θ_1	θ_2	$\chi_o (10^{-3} \frac{\text{emu}}{\text{mole Fe}})$	$C_1 (\frac{\text{emu K}}{\text{mole Fe}})$	$C_2 (\frac{\text{emu K}}{\text{mole Fe}})$
5.0	3	0.2	-14.6	1.14	.019
20.4	4±0.5	0.2 ±0.1	-1.3	.95	.17
47.1	6.0±0.5	0.15±0.05	2.9	.91	.21
99.3	5.7	0.15	3.4	.95	.18
161.9	6.2	0.15	3.3	.93	.24
211.4	6.2	0.05	2.9	.96	.23
261.3	6.2	0.18	4.0	.93	.21
304	6.5	0.15	3.5	.94	.24
525	6.5	0.1	3.6	.94	.26

TABLE 32

Sample Number	Nominal Fe concentration (ppm Fe)	Θ (K)	Curie Constant (emu K/ mole Fe)	μ_{eff} / μ_B
Using $c_{nominal}$ and $\chi_{imp} = \chi_{Fe} - \chi_{sample}$ 98				
101	61	0.7	1.30	3.23
103	185	0.8	1.27	3.19
104	288	0.85	1.27	3.19
105	395	0.95	1.30	3.23
Using concentrations from Table 33				
98		1.0	1.21 ± 0.6	3.11 ± 1.5
100		1.05	1.29 ± 0.4	3.21 ± 1.1
101		0.7	1.29	3.21
103		0.75	1.31 ± .04	3.24
104		0.8	1.31 ± .04	3.24
105		1.0	1.38 ± .03	3.32

Uncertainty due to uncertainty in the determination of χ_{host} and concentration from data above 44 K.

TABLE 33

Sample Number	$-\chi_H(10^{-8}$ emu/ gm) From extrapolation to 1/(T+10) =0	C (10^{-8} emu K/ gm)	concentration (10^{-8} mole Fe/ gm alloy)	ppm
98	14.39 .08	13.0 6	6.23 3.1	12.3 6
100	14.35 .05	18.6 6	9.29 3.1	18.3 6
101	14.37	73.39	36.7	72.7
103	14.37 - 14.26	185.8 -196.0	92.9- 98.1	183-193
104	14.40 - 14.25	283.5 -300	142 - 150	279 -295
105	14.38 - 14.15	389 - 402	194 - 201	383 -395

TABLE 34

Values of Θ and T_k for $Cu_{1-x}Au_x$(Fe) Alloys Normalized To The Values Θ_o And T_{Ko} for Cu(Fe)

Type of measurement	x	
	0.05	0.54
Susceptibility	0.09	0.32
	0.17	0.11
	0.05	0.54
Resistivity Loram et al.[21]	0.10	0.36
Star et al.[89]	0.17	0.17
Specific heat	0.048	0.75
Delinger et al.[22]	0.108	0.5

TABLE 35

Probability of n nearest neighbors in various $Cu_{1-x}Au_x$ hosts

$$P = \frac{12!x^n (1-x)^n}{n!(12-n)!}$$

n ≡ number of Au nearest neighbors	$Cu_{0.95}Au_{0.05}$	$Cu_{0.91}Au_{0.09}$	$Cu_{0.8}Au_{0.2}$
0	.540	.322	.069
1	.341	.380	.21
2	.099	.208	.28
3	.017	.068	.24
4	.002	.015	.13
5	less than .002	less than 1%	.05
6			.02
			less than .01

TABLE 36

$-M_b$, Bucket Magnetization, (10^{-3} emu)

T(K) H(kG)	1.384	4.2	9.5	44	55	77	100	122
1		0.004						
2	0.024	0.030	0.035	0.042		0.040	0.040	0.040
5	0.099	0.124	0.130	0.137	0.137	0.137	0.137	0.137
10	0.244	0.287	0.294	0.304	0.306	0.309	0.309	0.309
20	0.552	0.613	0.625	0.651	0.653	0.653	0.653	0.653
30	0.870	0.946	0.962	0.993	0.995	0.997	0.997	0.997
40	1.195	1.281	1.297	1.338	1.340	1.343	1.343	1.343
45	1.361	1.449	1.465	1.511	1.512	1.517	1.517	1.517
50	1.526	1.617	1.633	1.685	1.687	1.692	1.692	1.692